

University of Groningen

Metabolic protein interactions in *Bacillus subtilis* studied at the single cell level

Detert Oude Weme, Ruud Gerardus Johannes

IMPORTANT NOTE: You are advised to consult the publisher's version (publisher's PDF) if you wish to cite from it. Please check the document version below.

Document Version

Publisher's PDF, also known as Version of record

Publication date:

2015

[Link to publication in University of Groningen/UMCG research database](#)

Citation for published version (APA):

Detert Oude Weme, R. G. J. (2015). *Metabolic protein interactions in Bacillus subtilis studied at the single cell level*. University of Groningen.

Copyright

Other than for strictly personal use, it is not permitted to download or to forward/distribute the text or part of it without the consent of the author(s) and/or copyright holder(s), unless the work is under an open content license (like Creative Commons).

The publication may also be distributed here under the terms of Article 25fa of the Dutch Copyright Act, indicated by the "Taverne" license. More information can be found on the University of Groningen website: <https://www.rug.nl/library/open-access/self-archiving-pure/taverne-amendment>.

Take-down policy

If you believe that this document breaches copyright please contact us providing details, and we will remove access to the work immediately and investigate your claim.

Downloaded from the University of Groningen/UMCG research database (Pure): <http://www.rug.nl/research/portal>. For technical reasons the number of authors shown on this cover page is limited to 10 maximum.

Metabolic protein interactions in *Bacillus subtilis* studied at the single cell level

Ruud Detert Oude Weme
2015



The work described in this thesis has been performed in the laboratory of Molecular Genetics of the Groningen Biomolecular Sciences and Biotechnology Institute at the Faculty of Mathematics and Natural Sciences of the University of Groningen, The Netherlands.

This research was funded by the Systems Biology of Microorganisms (SysMO) organization (European Union) through the Research Council of the Dutch Organization for Scientific Research (NWO-ALW; Aard- en Levenswetenschappen).

Publication of this thesis was financially supported by the Groningen Graduate School of Sciences and the University of Groningen.

Printed on FSC certified paper by Ipskamp Drukkers B.V., Enschede

Cover: Front: Artist impression of *Bacillus subtilis*. Designed by Katrin Beilharz. Back: on LB-agar medium: University logo drawn with red fluorescent *E. coli* cells and MolGen logo drawn with green fluorescent *E. coli* cells. By Ruud Detert Oude Weme.

© 2015. Ruud Detert Oude Weme, Groningen, The Netherlands.
All rights reserved.

ISBN: 978-90-367-8308-8



rijksuniversiteit
groningen

Metabolic protein interactions in *Bacillus subtilis* studied at the single cell level

Proefschrift

ter verkrijging van de graad van doctor aan de
Rijksuniversiteit Groningen
op gezag van de
rector magnificus prof. dr. E. Sterken
en volgens besluit van het College voor Promoties.

De openbare verdediging zal plaatsvinden op

vrijdag 11 december 2015 om 14.30 uur

door

Ruud Gerardus Johannes Detert Oude Weme

geboren op 9 maart 1986
te Weerselo

Promotor

Prof. dr. O. P. Kuipers

Beoordelingscommissie

Prof. dr. D. J. Slotboom

Prof. dr. I. van der Klei

Prof. dr. J. Stülke

Paranimfen

Jeroen Siebring

Ard Jan Grimbergen

Contents

Chapter 1

General introduction 1

Chapter 2

Benchmarking various GFP variants in *Bacillus subtilis* for live cell imaging 21

Chapter 3

Single cell FRET analysis for the identification of optimal FRET-pairs in *Bacillus subtilis* using a prototype MEM-FLIM system 35

Chapter 4

Probing the dynamics of CcpA HPr interactions in *Bacillus subtilis* by FRET 57

Chapter 5

Probing the regulatory effects of specific mutations in three major binding domains of the pleiotropic regulator CcpA of *Bacillus subtilis* 75

Chapter 6

An osmotic upshift to 0.6 M NaCl causes population heterogeneity and partial antibiotic resistance in *Bacillus subtilis* 97

Chapter 7

Summary and general discussion 111

References 120

Nederlandse Samenvatting voor de Leek 134

Dankwoord 141

Chapter 1

General introduction

Bacteria versus humans

“If you don't like bacteria, you're on the wrong planet.” Stewart Brand

Bacteria were most likely the first form of life on earth [240] and later during evolution a symbiosis of eukaryotic cells and a bacterium (alpha-proteobacteria) took place resulting in mitochondria in eukaryotic cells. Mitochondria have their own DNA, and the high similarity to bacterial DNA resulted in the discovery of this symbiosis [240].

The size of a bacterial genome varies from 580,000 to 13.6 million nucleotides and commonly consists of one circular piece of DNA. The human genome is roughly thousand times larger and comprises approximately 3 billion nucleotides that are divided over 23 chromosomes. The human genome was sequenced per chromosome (see [173] for a nice overview). The bacterial genome has roughly 600 to 6,000 protein coding regions (genes) and the human genome has around 24,000 protein coding regions. This enormous difference in genome length is partially because of the more complex form of life, the presence of introns (non-coding regions) in the human genome, and probably a more complex regulation mechanism for gene expression.

We have approximately 10x more bacterial cells in our body than human cells [14]. Bacteria in our gut are essential for our food digestion; they digest fibers and synthesize vitamins. Many researchers are currently examining the effect of our gut microorganisms on our immune system and general health [61].

Bacteria can be either beneficial or harmful to humans. However, most people only think of the harmful aspects of (a few) bacteria. Here, some examples of benefits from bacteria (and microorganisms like yeast) will be mentioned. Food fermentation by microorganisms was first used to prolong the shelf life of food products; the acidification by lactic acid bacteria or the ethanol formation by yeast are examples of food conservation. Nowadays these processes are better understood and extensively used. Food preservation is still important, but also the continuous availability of food, refrigerators, pasteurization, and better storage conditions are beneficial for safe food. Fermentation is now mainly done to change the texture, taste, and flavor of starting materials like milk into yogurt or cheese and cereals into bread or beer.

We can also benefit from microorganisms for enzyme production (for example enzymes for laundry detergent) and for the production of flavor compounds by bacteria instead of extracting them from plant-based material (like the molecule valencene for the orange taste). And microorganisms can help in the transition towards a more bio-based-economy (for example to produce starting materials to make bioplastics [192]).

Bacteria can harm us by means of food spoilage (*Bacillus cereus* for example) and via infectious disease (for example *Streptococcus pneumoniae* or *Staphylococcus aureus*). When bacteria are in the news it is most of the time in a negative context due to the growing resistance of pathogenic bacteria to antibiotics.

Bacteria in general

The first bacteria were discovered by the Dutch optician and biologist Antonie van Leeuwenhoek in the 1670's with his home-made microscope and he called them animalcules, beesjes, or cleijne schepsels [49]. Ehrenberg described the bacterium *Vibrio subtilis* in 1835, but Cohn renamed it to *Bacillus subtilis* in 1872 [49]. It was isolated by soaking hay in water and then boiling the water [11].

Robert Koch was the first to discover that a bacterium, *B. anthracis*, can cause a disease, reported already in 1877. He isolated bacteria from an animal that died due to anthrax and infected a mouse with these bacteria, causing anthrax as well. In fact, with his observation of the growth, division, and sporulation he was most probably the first to do a time-lapse microscopy experiment [49].

The size of bacteria ranges from 0.5 – 5 micrometer. Bacteria are classified into two types: Gram-positive and Gram-negative. The Gram-positive bacteria have a lipid bilayer as cell membrane and a thick cell wall consisting of peptidoglycan. The Gram stain (crystal violet dye) binds well; that is why they are called Gram-positive. The Gram-negative bacteria have a thin peptidoglycan layer and an additional outer membrane to which the Gram stain does not bind well.

Bacillus subtilis and *Escherichia coli*, which are Gram-positive and Gram-negative, respectively are used a lot to study cell biology and gene regulation. These bacteria are still used to study various biological processes. One advantage of using bacteria is that their cell division is fast (30-60 minutes). And many genes, for example for glucose metabolism and the tricarboxylic acid cycle, are conserved among species during evolution, so bacterial knowledge can be 'extrapolated' to larger organisms.

Brief *Bacillus* history

B. subtilis has been studied extensively as a Gram-positive model organism during the last 50 years [78,108]. It is a rod-shaped, aerobic, and endospore forming bacterium that is found in soil, water, human microbiota, and in the surrounding of plants. *B. subtilis* is Generally Recognized As Safe (GRAS). Many *Bacillus* species, in particular the closely related *B. licheniformis* and *B. amyloliquefaciens* have good protein secretion capacities and are

therefore widely used in industry for the production of enzymes (such as amylases and proteases).

The complete *B. subtilis* genome sequence of strain 168 consists of 4,241,810 nucleotides and about 4,100 protein-coding regions [108]. However a resequencing project yielded a *B. subtilis* genome with 4,215,606 nucleotides where small changes have been reported in 923 genes and 3323 genes were identical [11]. 271 genes were identified as essential when single gene knockout strains were grown on LB medium. Roughly half of the essential genes were involved in information processing, 20% in cell wall synthesis, cell shape and division, and 10% in energy production. Most of those genes were found in a wide range of bacteria and 70% of those genes were also found in Archaea and Eucarya [101]. Many wild isolates of *B. subtilis* also contain a plasmid, e.g. *B. subtilis* NCIB 3610 [104], which was isolated in Marburg, Germany around 1930 and is the undomesticated ancestor of *B. subtilis* 168 [236].

The main metabolism route of *B. subtilis* is the glycolytic pathway in combination with the tricarboxylic acid cycle [108]. The activity of the tricarboxylic acid cycle is low when glucose is present; glucose is metabolized to pyruvate and acetyl-CoA and secreted as acetate (see [139] for an extensive metabolomics overview). This is called overflow metabolism [139]. When glucose or glycolytic substrates are exhausted the cell can import acetate or intermediates of the tricarboxylic acid cycle and continue growth via the gluconeogenic pathway [195].

B. subtilis is capable of various ways of cellular differentiation: competence development, motility, and sporulation. Natural competence is the ability to take up extracellular DNA and integrate it into the chromosome and this ability makes genetic modification fairly easy. Motility and chemotaxis are mechanisms for the cells to move to a new environment where nutrients might be available again [108]. Sporulation is a last resort measure when the cells face starvation and when the secretion of proteases, amylases, and antibiotics or moving to another environment did not result in the availability of nutrients [57,108]. Sporulation of *B. subtilis* means the formation of heat- and stress-resistant dormant cells that wait for more favorable times.

Bacteria are unicellular organisms, but they can also behave like 'multicellular' organisms, e.g. when organized in biofilms. Biofilms have a complex structure, with a hydrophobic surface and differentiating cells: some cells produce exopolysaccharide and others do not produce this matrix compound [213,220].

A nice systematic overview of gene expression under many different conditions has been made recently [25,152].

Organization inside bacteria

Only since the last 15-20 years it is known that bacteria have a cytoskeleton, consisting of FtsZ (a tubulin homologue) and MreB (an actin homologue) [58,133]. This cytoskeleton has a ring-like structure which is located next to the membrane. Bacteria have been seen as homogeneous filled vesicles, but since the first reports on protein localization this view is rapidly changing. Protein localization in *Bacillus* has been shown for the first time for DNA replication proteins at mid-cell in *B. subtilis* where the DNA strand is pulled through the machinery [117]. The Soj protein for chromosome segregation showed dynamic localization [134]. During the exponential growth phase CcpA showed localization towards the nucleoid (chapter 4).

The different possibilities for cellular localization are: the mid-cell where the divisome is located, polar assemblies of chemotaxis proteins, cytoplasmic clusters which have been shown only in one bacterium for chemotaxis proteins, cytoskeletal elements or polymeric structures of FtsZ and MreB, and organelles like the periplasm in Gram-negative bacteria or the endospore in *B. subtilis* ([169]). It has been suggested that protein complexes might be the prokaryotic equivalent of organelles [96].

Protein localization is mainly realized via diffusion and capture where the protein diffuses through the cytoplasm until it adheres to its target protein. N-terminal tags on the proteins can also be important for localization, i.e. messenger signals to direct a protein to a certain location ref [169]. Another way of protein localization is via localized transcription and translation [119].

Lipid rafts have been discovered recently in bacteria and can localize a specific set of proteins in the membrane (an overview of lipid rafts is reviewed nicely [19]).

The cytoplasm of organisms is a crowded environment (Figure 1). 20 to 30% of the cytoplasm is occupied by macromolecules and the total concentration of RNA and proteins in *E. coli* ranges from 300-400 g/l [53]. One of the effects of crowding is that macromolecular associations are favored but diffusion rates decrease. In general, crowding is reducing the rates of biochemical reactions because those rates depend mostly on the speed at which the reaction components meet each other, i.e. they depend on the diffusion rate [53].

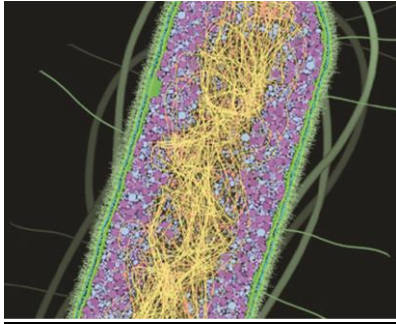


Figure 1. Artist impression of the Gram-negative bacterium *E. coli* representing the crowded cytoplasm [68]. In green the cell membrane is shown, in blue and purple the proteins in the cytoplasm are shown (mostly ribosomes; purple), and in yellow the DNA (nucleoid) is shown. The flagella are also shown in light green.

Protein-protein interactions

The main focus of this thesis is on protein-protein interaction studies. Furthermore gene expression in *ccpA* mutant strains and gene expression during osmotic upshift will be studied. Bacterial flagella are a well-known example of a protein complex. In total, flagella consist of approximately 580 protein copies comprising 35 different proteins plus approximately 2,000 copies of FliC for the tail [127]. The flagella structure has been shown by cryo-electron microscopy [239]. Protein complexes might be the prokaryotic equivalent of organelles [96,231] and in the described studies carboxysomes – carbon fixing protein complexes – were shown to exist in *Synechocystis spp* by using electron microscopy. Another example of protein-protein interactions is the metabolon, which has been suggested to be important for substrate channeling to prevent diffusion of intermediates, fast turnover of unstable or toxic intermediates, and continued flux of individual pathways. These metabolons might be transient in response to metabolic needs [38,143]. The crystal structure of the tryptophan synthase complex from *Salmonella typhimurium* shows the site for substrate channeling [87]. A glycolytic enzyme complex of 5 proteins in human red blood cells has been shown to exist by sequential use of antibodies and colocalization studies with fluorescence microscopy [26].

Most experimental evidences for protein complexes have been obtained via cross-linking studies and subsequent *in vitro* analysis. A glycosome in *B. subtilis* has been suggested to occur after cross-linking and bacterial-two-hybrid experiments, but this involved only 3 glycolytic enzymes [33]. In the same study a RNA-degradosome consisting of 5 RNase proteins has been shown and the authors also showed cross-interaction of the glycosome and the RNA-degradosome where Enolase (ENO) might play a role in RNA

metabolism [33]. A complex of three tricarboxylic acid (TCA) cycle proteins consisting of citrate synthase (CitZ), isocitrate dehydrogenase (Icd), and malate dehydrogenase (Mdh) has been found in *B. subtilis* [138]. The genes for those three enzymes are in one operon in *B. subtilis*. However, it is surprising that aconitase (CitB) was not found in this complex, but only as an interaction partner of Mdh [138]. In the TCA-cycle the enzymatic reaction of CitB is located between the reactions of CitZ and Icd. Recent work in mitochondria from beef heart showed a low-resolution crystal structure of a protein complex of Mdh, CitZ, and CitB, the possibility for substrate channeling is indicated there [230]. All three studies on these protein complexes suggest that these protein complexes facilitate substrate channeling [33,138,230].

Methods to study protein-protein interactions

There are various methods to determine protein-protein interactions (for an extensive review see [13]) and a distinction between *in vitro* and *in vivo* methods will be made here. The advantage of *in vivo* methods is that the dynamics of the interactions can be studied.

***In vitro* methods**

Crosslinking combined with pull down and mass spectrometry

A method to screen for all interaction-partners of a protein of interest is formaldehyde crosslinking combined with pull down and mass spectrometry (MS). It is an extended version of affinity chromatography which showed false positive and false negative results [83]. To pull down the protein of interest it is labeled with a tag (His or Strep), the strain is grown to the growth phase of interest and then the strain is incubated in a formaldehyde solution to crosslink the protein of interest with its interaction partners. Subsequently the strain is lysed and with affinity purification the protein and its interaction partners are purified from the cell free extract. By boiling the sample the formaldehyde crosslinking is reversed and the proteins will be loaded on SDS-PAGE followed by MS to identify the interaction partners [83]. The crosslinking method combined with MS is a nice starting point to identify interaction partners and the obtained information can be used for follow-up studies.

Co-immunoprecipitation

In a co-immunoprecipitation experiment the protein of interest can be purified with a specific antibody and subsequently precipitated. Proteins that interact with the protein of interest are also precipitated and can be identified by MS or Western blotting. However, this method can give false positive and false negative results, so control experiments are very important [13].

Far Western blotting

Far Western blotting is a modified version of normal Western blotting [30]. In normal Western blotting an antibody is used against the protein of interest which can be visualized using chemiluminescence. Far Western blotting can be used to show protein-protein interactions; first the protein of interest is loaded on SDS-PAGE, electrophoresis is done, the protein is transferred to a membrane and then the membrane is incubated with the potential interaction partner. This potential interaction partner must be purified first (for example via a His-tag). Visualization of the potential interaction partner can be done by radiolabeling that protein or by using a His-tag specific antibody. However, this is an indirect method because it must be shown that both proteins have migrated to the same position on the blot.

Surface Plasmon Resonance

Surface Plasmon Resonance (SPR) can be used to measure binding constants or to identify binding partners. For an SPR experiment the protein of interest has to be immobilized on a gold surface in a flow cell and the potential interacting proteins or substrates will be flown through the flow cell. The gold plasmons (gold electrons) are continuously oscillated at the same frequency as an incident light wave [8]. When proteins or metabolites interact with the immobilized protein then the oscillation frequency of the plasmons will change and thereby the refractive index of the incident light changes. The angle of light reflection is measured continuously and shown in a graph.

A method comparable to SPR is Isothermal Titration Calorimetry (ITC) which can also be used to study binding properties of protein-protein interactions; dissociation constants and the stoichiometry of a complex can be calculated from the obtained thermodynamic data (see for example [150]).

***In vivo* methods**

Bacterial-two-hybrid

The bacterial-two-hybrid method is derived from the yeast-two-hybrid method [209]. A bacterial-two-hybrid depends on the reconstruction of the adenylate cyclase enzyme which has been fused in two separate functional parts to the potential interaction partners [138]. When the two proteins of interest interact they will bring the two parts of the adenylate cyclase together which will become functional again. Adenylate cyclase synthesizes cAMP, and when the strain also contains a cAMP dependent promoter-LacZ fusion then a blue color can be easily observed on the colony level thereby proving the interaction [138]. However both bacterial-two-hybrid and yeast-two-hybrid are sometimes unreliable [67].

Bimolecular fluorescence complementation

Bimolecular fluorescence complementation (BiFC) is a kind of two-hybrid [65,93]. The gene coding for the fluorescent protein (FP) is split in two parts and fused to the genes coding for proteins that are potentially interacting. When the proteins of interest interact they are in close proximity, thereby bringing the two parts of the FP together. The two parts of the FP will assemble and become a functional FP; measuring fluorescence is a proof of interaction. The advantage of BiFC is that the signal-to-noise ratio is high because there is only fluorescence upon interaction and different protein-protein interactions can be studied at the same time when different color FPs are used [65]. Drawbacks of this method are that the maturation time of the FP is long, self-assembly of the two parts can occur which gives a false negative result, and the FP maturation is irreversible so dynamics of the interaction cannot be studied [65].

Förster Resonance Energy Transfer

Förster Resonance Energy Transfer (FRET) is preferred over BiFC to study protein-protein interactions, because the dynamics of the protein-protein interactions can be studied. FRET was first described by Theodor Förster in 1948 [200] and is applied in molecular biology since the widespread use of fluorescent proteins. FRET is the non-radiative energy transfer from an excited donor to an acceptor fluorophore. FRET has been a very important technique during this PhD-project and will be described in more detail below.

Fluorescent proteins

The Green Fluorescent Protein (GFP) was originally extracted and purified from the jellyfish *Aequorea victoria* by Osamu Shimomura in 1962 [187]. The first heterologous expression of *gfp* was reported by Martin Chalfie in 1994 and he showed that no cofactors are necessary for fluorescence [29]. Roger Tsien and members of his lab have done a great deal of protein engineering to make GFP brighter, faster maturing, and to change the absorbance and emission spectra yielding CFP and YFP among others and clone FP variants from other organisms [183,208]. For a nice overview of GFP variants and GFP related activities the reader is referred to table 1 and figure 1 in reference [39]. The impact of GFP and its variants on (molecular) biology has been enormous and resulted in the Nobel Prize in chemistry for Shimomura, Chalfie, and Tsien in 2008 (www.nobelprize.org).

Many variants are based on the GFP from the jellyfish *Aequorea victoria*. DsRed and variants like mCherry originate from the coral mushroom *Discosoma* [183]. tagRFP and variants originate from the sea anemone *Entacmaea quadricolor* [137].

Table 1. Characteristics of the fluorescent proteins used in chapter 3 [39]. Excitation (Ex) and Emission (Em) values are the wavelengths where excitation and emission are highest. ϵ is the molar extinction coefficient, the efficiency to absorb light and the quantum yield represents the percentage of absorbed photons that are emitted.

Protein	Ex (nm)	Em (nm)	ϵ ($M^{-1} cm^{-1}$)	Quantum yield	Quaternary structure
Cerulean	433	475	43,000	0.62	Monomer
GFP	488	507	56,000	0.60	Monomer
Venus	515	528	92,200	0.57	Monomer
tagRFP	555	584	100,000	0.48	Monomer
mCherry	587	610	72,000	0.22	Monomer
mKate2	588	633	62,500	0.40	Monomer

The large set of different FPs that is available nowadays brings a lot of possibilities for molecular biology like simultaneous labeling different proteins with different color FPs or FRET. The potential of FRET has been the motivation to engineer GFP [208]. FRET occurs in nature, in the jellyfish from which GFP has been isolated. In *A. victoria* the aequorin protein has a blue emission peak which is close to the excitation peak of GFP. Aequorin is a bioluminescent protein that needs Ca^{2+} to become luminescent [186]. GFP absorbs the blue emission from aequorin and emits the green light that is observed in the animal [208].

FRET to study protein-protein interactions

FRET is the non-radiative energy transfer from an excited donor fluorophore to an acceptor fluorophore. Many articles about FRET call it Fluorescence Resonance Energy Transfer [65,93,95,106,207,217], but the F in FRET stands for Förster [2,151]. The use of *Fluorescence* does not reflect the radiation free character of the energy transfer. Energy transfer during FRET is based on resonance, i.e. oscillation at the same frequency: when an object oscillates, then a second object in close proximity can oscillate at the same frequency (Figure 2A). FRET is a physical phenomenon that can be explained by a Jablonski diagram (Figure 2B). The ground states of both fluorophores are shown at the bottom of Figure 2B, the donor is shown on the left. Donor electrons are transferred to another electron shell away from the nucleus upon excitation and when the electron returns to the ground state a photon can be emitted. Due to vibration, part of the energy is lost and that is the reason why the wavelength of the emission is always longer than the wavelength of the excitation (longer wavelength means lower energy, as represented by the arrow lengths in Figure 2B). Instead of losing the energy via

the emission of a photon the donor can also transfer its energy by means of resonance to a neighboring acceptor fluorophore (the pink arrow in Figure 2B).

A nice overview of many FRET methods is given by Sun *et al.* and by Padilla-Para *et al.* [157,203].

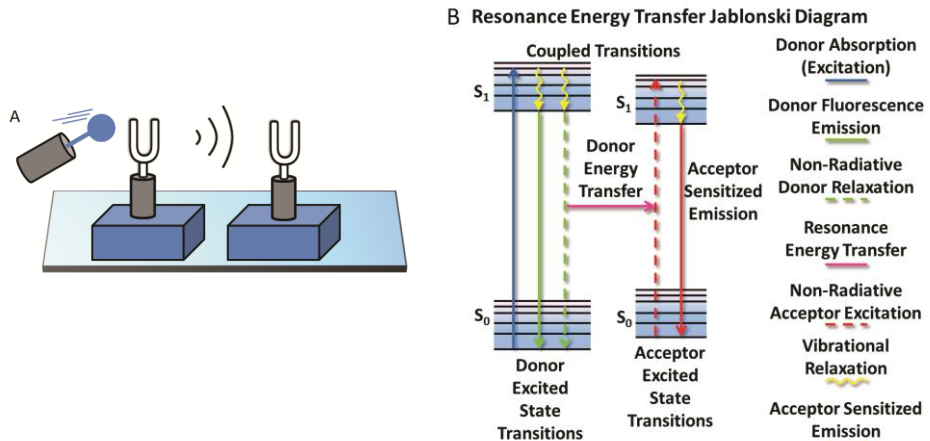


Figure 2. (A) The principle of resonance in FRET can be illustrated with tuning forks: when one fork is excited it will oscillate and a second fork in close proximity can oscillate at the same frequency; called resonance (figure adapted from: <http://www.photobiology.info/Experiments/Biolum-Expt.html>). **(B)** Jablonski diagram to explain the physical basis of FRET. The diagram for energy states of the donor fluorophore is shown on the left and the one of the acceptor on the right. Upon excitation of the donor electrons will move away from the nucleus (blue arrow). There are three options to return to the ground state: fall back and emit a photon (green arrow), fall back without emission (radiation free, dotted green arrow), or resonance energy transfer to a nearby acceptor (pink arrow). The acceptor can emit a photon of a longer wavelength (red arrow). Figure from <http://www.microscopyu.com/articles/fluorescence/fret/fretintro.html>.

There are three criteria for successful FRET. First, FRET can only occur when the donor and acceptor are in close proximity of each other (nanometer range). Second, the excitation spectrum of the donor should overlap with the absorbance spectrum of the acceptor. Third, the dipole-dipole orientation of the donor and acceptor should be aligned properly.

There is an inverse 6th power relation of the donor and acceptor distance to the energy transfer efficiency [114]. Every FRET pair has its own Förster radius R_0 which is defined as the distance between donor and acceptor where the energy transfer efficiency is 50%. R_0 is around 5.0 nm for many FRET pairs (see also **chapter 3**) and therefore FRET is also called a spectroscopic ruler [200].

The resolution in light microscopy is defined by the Abbe limit [81] and is approximately 250 nm for green light. That means that the resolution of FRET is roughly 50x higher than for normal fluorescence microscopy.

The distance requirement of FRET makes it a very useful tool to study protein-protein interactions: typical protein radii are around 2 nm for proteins up to 50 kDa [55]. However, when two fluorescent proteins are fused to two different proteins of interest and the FPs are located on opposite sides of those interacting proteins then their distance is around 8 nm which is larger than R_0 . Therefore, structural data on the proteins of interest can be helpful to choose whether N- or C-terminal protein-FP fusions are more likely to keep the FP distance as small as possible and thus increase the chance of a successful energy transfer (see figure 1A in **chapter 4** for an example).

Intra- and intermolecular FRET

There are two ways to utilize FRET: intramolecular FRET where both the donor and acceptor fluorophore are fused to the same protein or intermolecular FRET where the donor and acceptor fluorophore are fused to two different proteins (Figure 3).

Intramolecular FRET can be easily detected via a spectrum scan; an increase in acceptor fluorescence upon donor excitation between two different experimental conditions is the evidence that donor and acceptor interact in one of the experimental conditions. This change in acceptor fluorescence can be caused by a conformational change of the protein of interest which alters the distance between donor and acceptor. An altered distance results in an altered energy transfer efficiency. Biosensors are among the applications of intramolecular FRET, for example for intracellular calcium concentration measurements [207]. Another example is the conformational change of the glutamate transporter GltPh which has been shown at single molecule resolution [56]. The advantage of intramolecular FRET is that the ratio of donor and acceptor is always 1:1. That is beneficial because all donor and acceptor copies are in the same situation (interacting or not), so there is no need for control experiments.

Intermolecular FRET can be used to study protein-protein interactions and was the main method of interest during this PhD-project. However, a spectrum scan is not sufficient to determine the energy transfer efficiency in intermolecular FRET, because the acceptor fluorescence intensity does not directly reflect the interaction with the donor (a detailed explanation is given below in the sensitized emission section).

There are different ways to determine (intermolecular) FRET: FRET detection via sensitized emission, acceptor photo bleaching, and Fluorescence Lifetime Imaging Microscopy (FLIM).

Sensitized emission

FRET detection via sensitized emission was the main technique during this PhD-project. During FRET detected via sensitized emission the resonance energy transfer from an excited donor to the acceptor causes an increase in acceptor emission which can be measured [217](see the Jablonski diagram in Figure 2B and the representation in Figure 3). The spectra of donor and acceptor fluorophore must overlap to obtain successful energy transfer. However, because of this spectral overlap, the FRET efficiency is not a direct read-out from the sensitized emission experiment. Corrections have to be done for the spectral overlap of donor and acceptor: donor emission can contribute in the acceptor channel and acceptor can be excited directly by donor excitation light (bleed through). This need for corrections also causes noise in the final signals. The FRET efficiency in a sensitized emission experiment can be calculated from fluorescence images of three different strains; one strain with the protein of interest fused to the donor fluorophore, one strain with a second protein of interest fused to an acceptor fluorophore, and a third strain with both protein fusions present (**chapter 3 and 4**).

The most important advantage is that there is no specialized equipment needed: a fluorescence microscope, where different excitation and emission filters can be used sequentially, is sufficient.

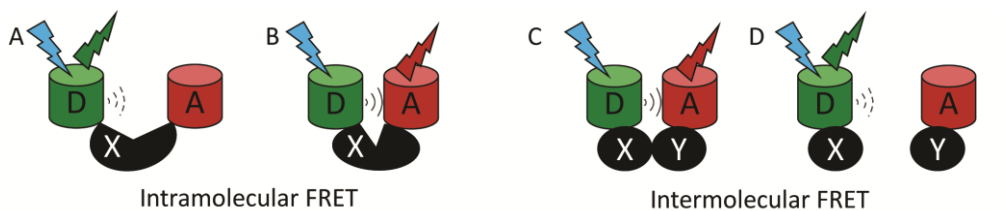


Figure 3. Schematic representation of FRET detected via sensitized emission. (A) Intramolecular FRET with a large distance between donor and acceptor; FRET efficiency is low. **(B)** Intramolecular FRET where the donor and acceptor are in close proximity after a conformational change of protein X, the donor can transfer its energy to the acceptor; FRET efficiency is high. **(C)** Intermolecular FRET with two proteins of interest fused to fluorescent proteins. When protein X and Y interact they bring the donor and acceptor in close proximity and thus FRET can occur. **(D)** Intermolecular FRET with two proteins of interest fused to fluorescent proteins. When protein X and Y do not interact then the donor and acceptor are not in close proximity and FRET cannot occur.

FRET detected via sensitized emission is the method of choice in this PhD-project to investigate protein-protein interactions.

FRET detected via sensitized emission has been used successfully to study protein-protein interactions. Protein kinase D fused to YFP was shown to associate transiently with the Na^+/H^+ exchanger regulatory factor 1 fused to CFP in live HeLa cells [107]. The anti-apoptotic protein Bcl-2 and the coiled-coil protein Beclin which regulates the activity of Bcl-2 are shown to interact in live COS cells (fibroblast cells) [69]. Proteins from the *E. coli* cell division machinery like FtsZ, FtsQ, ZapA, FtsN, FtsI, FtsW have been shown to interact by using FRET detected via sensitized emission [2], but that was done by a spectrum scan. The sensor for 2-oxoglutarate PII-PipX forms a complex when the level of 2-oxoglutarate is low. 2-oxoglutarate is an intermediate of the TCA-cycle and by using protein-FP fusions of PII-CFP and PipX-YFP the concentration of 2-oxoglutarate could be measured *in vivo* [31], however, this was done via a spectrum scan.

However, FRET detected via sensitized emission is challenging due to the three strains that are necessary for image acquisition. Post processing of those images to calculate FRET efficiencies results in noise [165]. Rajapakse *et al.* circumvent this problem by using Luminescence Resonance Energy Transfer (LRET) instead; they use a luminescent terbium complex as a donor. The advantage is that no corrections for spectral overlap are necessary but the terbium complex has to cross the cell membrane first and the terbium complex only had affinity to dihydrofolate reductase (from *E. coli*), which limits the use of LRET [165].

Acceptor photo bleaching

The donor fluorescence is quenched due to the interaction with an acceptor. When the acceptor is destroyed by photo bleaching it cannot quench the donor anymore. The resulting increase in donor fluorescence can be measured and used to calculate the FRET efficiency [95]. The disadvantage of acceptor photo bleaching is that it can only be used for a single time point because it is irreversible; once the acceptor is destroyed it cannot be used again. Therefore, acceptor photo bleaching is unsuitable to study the dynamics of protein-protein interactions, but it can be used to confirm sensitized emission data (**chapter 3**).

Fluorescence Lifetime Imaging Microscopy

The fluorescence lifetime is the time that a fluorophore resides in the excited state between excitation and emission. The fluorescence lifetime τ is defined as the time that is needed for the initial emission intensity of a population to decrease to $1/e$ ($\approx 37\%$) and is typically within the nanosecond

range [115]. The most important advantage of FLIM in comparison with sensitized emission is that it is intensity independent, but specialized equipment is necessary for FLIM measurements.

There are two ways to measure FLIM: via Time Domain (Figure 4A) or via Frequency Domain (Figure 4B) (see also chapter 4 and 5 in [112]).

In Time Domain FLIM the sample is excited with a short pulse (the duration of the pulse must be shorter than the fluorescence lifetime of the sample) and subsequently the emission of photons is recorded as a function of time. The emission of photons is summarized in a histogram (Figure 4A) and the fluorescence lifetime can be measured from the histogram. However, this method is time consuming because most Time Domain devices use time-correlated single photon counting (TCSPC) where only one photon per excitation pulse is counted and each point of the sample has to be excited sequentially [115].

In Frequency Domain FLIM the sample is continuously excited by an intensity modulated light source. Modulated means that the intensity of the excitation light follows a sinusoidal on/off pattern (black line in Figure 4B). The frequency is very high (40 MHz in chapter 3) to make sure that one period (dotted grey line in Figure 4B) is in the range of the fluorescence lifetime of the sample (grey line in Figure 4B). Excitation of the fluorescent sample with intensity modulated light means that the emission of the fluorescent sample will also occur with the same modulation frequency [113]. The fluorescence lifetime of the sample causes a delay in the fluorescence emission compared to the excitation (compare the black sinusoidal line (the excitation) with the dotted black sinusoidal line (the emission) in Figure 4B). This phase shift ϕ can be used to calculate the fluorescence lifetime.

Every donor fluorophore has a typical lifetime, which is influenced by its surrounding. The presence of an acceptor fluorophore in close proximity can quench the donor fluorescence, i.e. make the donor fluorescence lifetime shorter. When two proteins of interest are fused to a donor or an acceptor fluorophore (like in Figure 3C,D) then FRET-FLIM can be used to study their interaction; if the donor fluorescence lifetime in a donor-only sample is longer than in other samples where the acceptor is also present then that is an indication that the two proteins interact.

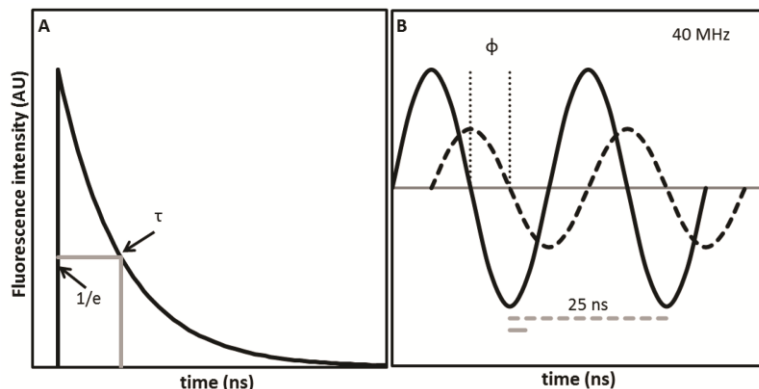


Figure 4. (A) Basic principle of Time Domain FLIM. The fluorescence intensity of the donor is measured as a function of time after a short excitation pulse. The fluorescence lifetime is defined as the time when the fluorescence intensity decreased to $1/e$ of the initial intensity, and can be read-out from the histogram. **(B) Basic principle of Frequency Domain FLIM.** The excitation light source (black sinusoidal line) is modulated at a frequency that is higher (ten times in this figure) than the lifetime of the fluorophore under investigation. Fluorescence emission (black dotted sinusoidal line) is delayed compared to the excitation light: this phase shift ϕ is used to calculate the fluorescence lifetime. The dotted grey line represents one period and the grey line represents the lifetime of the sample.

FLIM has proven its value for molecular biology. It has been used to study protein-protein interactions. A flavonoid metabolon in *Arabidopsis* protoplasts was shown by using FLIM. In that study it is suggested that loosely-organized enzyme complexes can dynamically reorganize to redistribute pathway flux to fine tune the plants response to environmental and developmental stimuli [38]. FLIM has also been used to show the binding of histone 2B to DNA in fixed HeLa cells, therefore the histone was fused to GFP and the fluorescent molecule Sytox Orange was added to fixed cells. Sytox Orange binds to DNA and was able to shorten the fluorescence lifetime of GFP, which proves that histone interacts with DNA [36]. The interaction of two cell cycle dependent kinases, Sic1 and Clb, has been shown in live *Saccharomyces cerevisiae* cells [175]. The Ato proteins for ammonium signaling in the yeast plasma membrane have been shown to interact with each other. However, photo-bleaching was used to show the difference in donor fluorescence lifetime instead of using a donor-only fusion [199]. The transcription factor C/EBP α was shown to dimerize in live mouse nuclei via the leucine zipper part of the protein [204]. The auto fluorescence of cells differs from healthy cells to some kinds of cancer cells. Sometimes FLIM can be used for diagnosis of these unhealthy cells, for example in melanoma [181]. FRET-FLIM can be used to screen potential drugs for its effectivity, as has been done for example for a

potential drug against pancreatic cancer in a mouse model [153], here a drug specific biosensor was used.

Next to the methodology presented in **chapters 2 and 3**, three biological systems in *B. subtilis* have been selected to be studied in detail. These biological systems are the interaction between CcpA and HPr (**chapter 4**), the function of individual amino acids in CcpA (**chapter 5**), and the response of *B. subtilis* upon osmotic upshift (**chapter 6**). These biological systems will be introduced in the sections below.

A case study: the interaction between CcpA and HPr studied with FRET

Bacteria can metabolize a large variety of carbon sources, but glucose is the preferred one. When glucose is present in the medium then the genes coding for enzymes for the metabolism of other carbon sources are repressed. This repression is necessary to ensure that cells use their energy efficient and thus to allow rapid growth. CcpA and HPr are responsible for the activation of genes related to glucose metabolism and the repression of other genes [70]. When HPr is phosphorylated on Serine46 by HPrK/P it forms a complex with CcpA. This complex formation induces a conformational change in CcpA which is necessary to bind to catabolite responsive elements (*cre* sites) on the DNA and thus to regulate gene expression (Figure 5, [70] and **chapter 4**). Here, we will study the dynamics of the interaction of CcpA and HPr in live *B. subtilis* cells by using FRET. Do CcpA and HPr interact only during a specific part of the cell cycle? Does the interaction between CcpA and HPr occur in all cells in a culture? With fluorescence microscopy we will be able to study this on the single cell level.

Recent work with fluorescently labeled LacZ showed quantitatively that *E. coli* cells which have more LacZ copies can grow faster, e.g. that metabolism is stochastic and causes phenotypic heterogeneity in the growth speed [97]. We will study whether there is also heterogeneity in the interaction between CcpA and HPr.

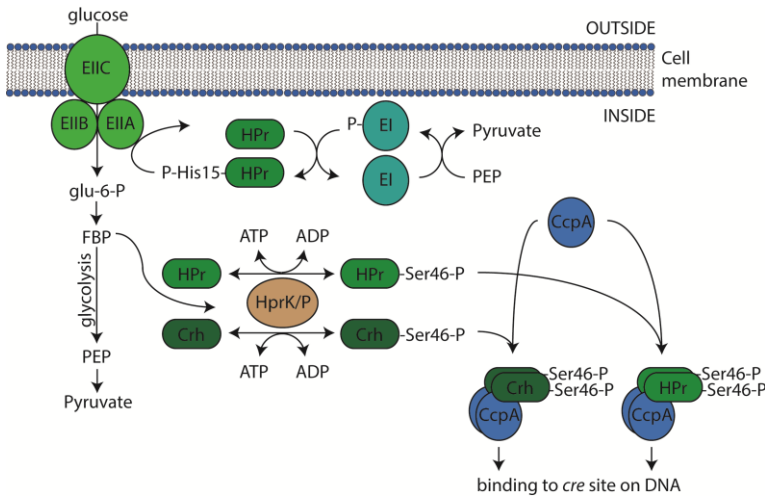


Figure 5. The mechanism of CCC. The intracellular concentration of fructose-1,6-bisphosphate (FBP) increases during glycolysis. HPr is phosphorylated on its serine46 by HPrK/P when the intracellular FBP concentration is high. HPr-Ser46-P can form a complex with CcpA which is necessary for CcpA to bind to the *cre* sites on DNA. Figure taken from thesis B.C. Marciniak (University of Groningen, 2012), which was inspired by [70].

Functional analysis of specific amino acids in CcpA

The gene regulation by CcpA will be studied in more detail at the transcriptome level (**chapter 5**). Therefore, the following three amino acids in different functional domains of CcpA will be mutated. The methionine on position 17 which is involved in DNA binding will be changed into the positive charged arginine, the threonine on position 62 which is necessary for the conformational change of CcpA upon HPr-Ser46-P binding is located in the core protein next to the hinge helix and will be changed into histidine, and the arginine on position 304 which is important to contact HPr-Ser46-P will be changed into tryptophan [176].

B. subtilis' response to osmotic stress studied at single cell level

The natural habitat of *B. subtilis* is the soil, where it faces different levels of osmolarity [21]. In this study, we will only focus on osmotic upshift. The most important mechanism to cope with osmotic upshift is the uptake of compatible solutes like glycine betaine, proline, and ectoine from the medium. Compatible solutes are small molecules which can be taken up at high concentrations in the cell to counteract the effect of water outflow due to salt stress. *B. subtilis* has high affinity membrane transporters like OpuA, B, C, D,

and E for compatible solutes [229]. Another mechanism is the synthesis of compatible solutes; glycine betaine can be synthesized by *B. subtilis* from the precursor choline, which has to be imported. Proline can be synthesized from glutamate, which is the most abundant amino acid in *B. subtilis*. A nice transcriptome, proteome, and fluxome overview of *B. subtilis* upon 1.2M NaCl osmotic upshift has been made recently [103]. The main finding there is that enzyme activity decreases upon osmotic upshift due to the increased amount of intracellular potassium, but cells compensate this by increasing the gene expression. The metabolite flux has been found to be very stable and the redirection towards increased proline biosynthesis is only a small part of the total flux [103]. However, results cannot be compared directly with this work, because the 1.2M NaCl osmotic upshift used in that study is much higher than the 0.5 to 0.7M NaCl used in this study.

In this study the heterogeneous response to osmotic upshift in an isogenic culture will be studied. Earlier work showed that the intracellular concentration of proline depends on the level of osmotic upshift and a large deviation was found at 0.6M NaCl [22]. We will study whether there is variation in the expression of the proline biosynthesis genes *proHJ* which are osmotically induced, upon different levels of osmotic upshift. Furthermore, we will examine whether the expression level of *proHJ* and thus the level of proline will influence the growth of *B. subtilis* (**chapter 6**).

It is already known that bacterial cells can enter a dormant state upon environmental stress [129]. Dormant cells are metabolically inactive and insensitive to antibiotics. Here we will study whether *B. subtilis* becomes dormant upon osmotic upshift.

Scope of the thesis

In this thesis we have used the recent knowledge of *B. subtilis* and of fluorescence microscopy to study protein-protein interactions in live single cells.

The use of Green Fluorescent Protein (GFP) has been very beneficial for molecular biology (to study gene expression and protein localization). Engineering of brighter GFP variants (**Chapter 2**) can be helpful to study the activity of weak promoters or low copy proteins.

FRET was chosen as a method to study protein-protein interactions and we first tested the suitability of different fluorescent proteins as FRET pairs (**Chapter 3**). The dynamics of the interaction between Catabolite Control Protein A (CcpA) and the phosphocarrier protein HPr were studied in live cells at the single cell level by using FRET (**Chapter 4**).

CcpA and HPr are the main regulators for the expression of genes involved in carbon metabolism. The favorite carbon source of *B. subtilis* is

Chapter 1

glucose and CcpA and HPr take care of gene activation or repression in a mechanism called carbon catabolite control; i.e. only the necessary genes are transcribed for efficient growth. Point mutations were made in CcpA to study the function of specific amino acids. The subsequent gene regulation by these CcpA variants was studied at the transcriptome level (**Chapter 5**).

The natural habitat of *B. subtilis* is the soil where it faces different levels of osmolarity during periods of rain or drought. Here we studied whether all cells in an isogenic culture respond in the same way or in a heterogeneous way to osmotic upshift (**Chapter 6**).

Chapter 2

Benchmarking various GFP variants in *Bacillus subtilis* for live cell imaging

This chapter is a modified version of:

Wout Overkamp, Katrin Beilharz*, Ruud Detert Oude Weme*, Ana Solopova*, Harma Karsens*, Ákos T. Kovács, Jan Kok, Oscar P. Kuipers, Jan-Willem Veening. (2013) Benchmarking various GFP variants in *Bacillus subtilis*, *Streptococcus pneumoniae* and *Lactococcus lactis* for live cell imaging. Applied Environmental Microbiology. 79: 6481-6490.

*These authors contributed equally.

W.O. and R.D.O.W. contributed equally to the *Bacillus subtilis* part of this article.

This work is also published in the thesis of Wout Overkamp, University of Groningen, 2015.

Abstract

Green fluorescent protein offers efficient ways of visualizing promoter activity and protein localization *in vivo* and many different variants are currently available to study bacterial cell biology. Which of these variants are best suited for a certain bacterial strain, goal or experimental condition is not clear. Here, we have designed and constructed two ‘superfolder’ GFPs with codon adaptation specifically for *Bacillus subtilis* and *Streptococcus pneumoniae* and have benchmarked them against five other previously available variants of GFP in *B. subtilis* using promoter-gfp fusions. Surprisingly, the best-performing GFP under our experimental conditions in *B. subtilis* was the one codon-optimized for *S. pneumoniae*. The data and tools described in this study will be useful for cell biology studies in low GC-rich Gram-positive bacteria.

Introduction

The use of *Aequorea victoria* green fluorescent protein (GFP) and its derivatives has tremendously increased our insights in bacterial cell biology [197,210]. Because of the possibilities to examine protein localization or gene expression in live cells new improved variants of GFP appear regularly. However, *in vivo* benchmarking to demonstrate which GFP variant is best suited for which experimental setup is scarce. Here, we benchmark a set of commonly used GFP variants to analyze gene expression in the low GC-rich Gram-positive model organism *Bacillus subtilis*.

B. subtilis is one of the best-studied micro-organisms that is able to differentiate into distinct cell types. It can form highly resistant spores, develop natural competence and motility, and secrete exoproteases [51,57,92,146,218]. Additionally it can form biofilms [20] for which, due to poor aeration, not all GFP variants might be suitable since maturation of GFP requires post-translational oxidation.

GFP offers efficient ways of visualizing gene expression and protein targeting. It exhibits intrinsic fluorescence and is commonly used as reporter gene in intact cells and organisms [29,197]. For *in vivo* studies of weakly expressed genes, a strong GFP fluorescence signal is crucial. Since the initial publication of *A. victoria* GFP and its application for molecular biology [29] many mutants of the protein have been described with either modified spectral properties, increased fluorescence intensity or improved folding properties [35,159,174,182]. The number of possible GFP variants has increased, but the most suitable candidate remains to be selected carefully for the particular research question at hand. The suitability of a certain GFP variant for a specific experiment strongly depends on factors such as

availability of oxygen, cultivation temperature, pH of the environment, photo stability, spectral overlap, toxicity and multimerization [182].

Methods to achieve the most optimal fluorescence signal are not limited to modifications on the protein level. Important factors influencing protein expression levels besides transcription rate are mRNA stability, translation signals and codon usage in the gene [121]. For instance, highly expressed prokaryotic genes have a pronounced codon usage bias, significantly different from genes expressed at low levels [145]. Adaptation of the *gfp* gene to the typical codon usage of the host could have a major impact on its translation, resulting in more efficient protein production and folding, resulting in higher net GFP expression and thus fluorescence signal [74]. *B. subtilis* has a small variation in codon usage compared to other bacteria and therefore a different *gfp* variant might be optimal in different bacterial species (Table S1). The GFP variants characterized in this chapter have all proven to be successful in molecular biology. However, knowing which GFP variant gives the most optimal fluorescence signal in *B. subtilis* would be very helpful in optimizing experimental set-ups.

In this work, we focused on benchmarking GFP for studying gene expression at the single-cell level. A previously characterized promoter and ribosome binding site were used to drive GFP expression. To assess gene activation accurately, it is important that the fluorescent signal appears immediately after induction. Therefore, we have also employed fast folding variants such as GFP+ [174] and superfolder GFP [159] and designed and generated vectors containing superfolder GFPs with codon usage adapted specifically for *B. subtilis* or *S. pneumoniae*. Interestingly, superfolder GFP did not give the highest fluorescence signals in *B. subtilis* liquid cultures, but was superior in both *S. pneumoniae* and *L. lactis* (these two bacterial species were also tested in the article, but their results are not shown in this chapter). More surprisingly was the finding that the *gfp* which was codon optimized for *S. pneumoniae* worked best in *B. subtilis*. Together, we provide a new GFP-toolbox and knowledge as to which GFP variant to use for single-cell gene expression analysis in *B. subtilis*.

Material and Methods

Bacterial strains, plasmids, media and growth conditions

Bacterial strains and plasmids used in this study are listed in Table 1. *B. subtilis* was grown at 37°C on Lysogeny Broth (LB) [171] solidified with 1.5% (w/v) agar, in liquid LB, or in Spizizen's minimal medium [3] with shaking at 200 rpm (see below). For induction of the P_{hyperspank} promoter, 0.1 mM isopropyl β-D-1-thiogalactopyranoside (IPTG) was used.

Escherichia coli DH5 α or EC1000 were used as host for cloning and grown in LB medium at 37°C with shaking or on LB medium solidified with 1.5% (w/v) agar. When required, the growth media were supplemented with the following antibiotics: 100 μ g/ml ampicillin (Amp) for *E. coli* or 100 μ g/ml spectinomycin (Spec) for *B. subtilis*.

Recombinant DNA techniques and oligonucleotides

Procedures for DNA isolation, restriction, ligation, agarose gel electrophoresis, and transformation of *E. coli* were performed as described earlier [171]. Plasmid DNA or PCR products were isolated and purified using the High Pure Plasmid Isolation Kit or the High Pure PCR purification kit, respectively (Roche Applied Science, Mannheim, Germany) according to the manufacturer's instructions. Enzymes were purchased from New England Biolabs (Ipswich, MA, USA) and Fermentas (Vilnius, Lithuania) and used as described by the manufacturer. For PCR amplification, Phusion- and Taq DNA polymerase (Fermentas) were used. *B. subtilis* was transformed as described before [77]. Oligonucleotides used in this study are listed in Table 2 and were purchased from Biolegio (Nijmegen, the Netherlands)

Codon optimization

To design a gene encoding superfolder GFP [159] that is codon-optimized for *S. pneumoniae*, we employed OPTIMIZER [163] using the genome of *S. pneumoniae* R6 as the reference and ensured that rare codons would never be used. Next, we ran simulations to generate more than 1000 solutions of superfolder *gfp* with the desired codon usage (similar codon usage to highly expressed genes). The variant with the lowest free energy (ΔG^0) value in mRNA secondary structure around the RBS was selected which potentially improves translation [42]. This gene was synthesized (Genscript USA Inc.; Piscataway, USA) and called *sfgfp(Sp)*. The sequence for a codon-optimized variant for *B. subtilis* was obtained from DSM Biotechnology Center (Delft, the Netherlands) and is called *sfgfp(Bs)* in this work. The DNA sequences of *sfgfp(Bs)* and *sfgfp(Sp)*, as well as the other, previously described *gfp* genes, are deposited at NCBI (accession number KF410612 - KF410618).

Construction of plasmids

Plasmid pDR111 was chosen to express the *gfp* variants in *B. subtilis*. To construct derivatives of pDR111 [24] for *B. subtilis*, each carrying a variant of the *gfp* gene, a PCR with the primers GFP_NheI_fw and GFP_SphI_rv was performed using the plasmids pKB01_gfpmut1, pKB01_gfp+, pKB01_gfp+htrA, pKB01_gfp(Sp), pKB01_sfgfp(Bs), pKB01_sfgfp(Sp) or pKB01_sfgfp(iGEM) as templates. The amplified fragments were purified and subsequently cleaved

with *NheI* and *SphI* and ligated separately in pDR111 digested with the same enzymes. This resulted in plasmids pDR111_gfpmut1, pDR111_gfp+, pDR111_gfp+htrA, pDR111_gfp(Sp), pDR111_sfgfp(Bs), pDR111_sfgfp(Sp) and pDR111_sfgfp(iGEM), respectively.

The construction of the pKB plasmids, with RBS and terminators surrounding *gfp*, is described in the article corresponding to this chapter [155]. An IPTG inducible promoter is already present in pDR111.

Construction of strains

B. subtilis strains 168_gfpmut1, 168_gfp+, 168_gfp+htrA, 168_gfp(Sp), 168_sfgfp(Bs), 168_sfgfp(Sp) and 168_sfgfp(iGEM) were obtained by double crossover recombination events between the chromosomal *amyE* gene of *B. subtilis* 168 [108] and the *amyE* regions in the plasmids pDR111_gfpmut1, pDR111_gfp+, pDR111_gfp+htrA, pDR111_gfp(Sp), pDR111_sfgfp(Bs), pDR111_sfgfp(Sp) and pDR111_sfgfp(iGEM), respectively. Transformants were selected on LB agar plates containing spectinomycin after overnight incubation at 37°C. Correct integration in the *amyE* gene was confirmed by lack of amylase activity upon growth of the strains on LB plates with 1% starch.

B. subtilis growth and *gfp* expression

gfp expression in *B. subtilis* was monitored as follows. LB medium with 100 µg/ml spectinomycin was inoculated with one of the *B. subtilis amyE::gfp* strains directly from the -80°C glycerol stock and grown at 37°C while shaking at 200 rpm for 16 hours. The overnight cultures were diluted 1:50 to an approximate OD₆₀₀ of 0.06 in 10 ml fresh Spizizen's minimal medium without antibiotics. After growth for 2 hours at 37°C, expression of *gfp* was induced by adding 0.1 mM isopropyl β-D-1-thiogalactopyranoside (IPTG). After another 2 hours of growth, the culture was washed with PBS and fluorescence intensity was measured both in a microtiter plate reader and by fluorescence microscopy (see description below). For the latter, cells were concentrated ten times by centrifugation after which 0.5 µL of cell suspension was spotted onto a microscope slide for the analysis. The slide carried a thin layer of 1% agarose (w/v) in PBS covered by a coverslip.

Microtiter plate assays

Cultures of *B. subtilis* were grown and prepared as described above. Growth and fluorescence was monitored in microtiter plates at 37°C with the following equipment and settings: Infinite 200 plate reader (Tecan Group Ltd.) with I-control™ 1.7.1.12 software (Tecan Group Ltd.), GFP filter set (Chroma, excitation at 485/20 nm, emission at 535/25 nm); GFP signals were collected as top readings with a gain setting of 70. GFP values were corrected for

background fluorescence, OD₆₀₀ and negative controls (values of the wild type strains). The OD₆₀₀ levels used were corrected for the background value of the corresponding medium that was used for growth. The calculation used to resolve the relative GFP intensities of the cultures is depicted by equation 1.

$$\left(\frac{GFP_{reporter} - GFP_{medium}}{OD_{reporter} - OD_{medium}} \right) - \left(\frac{GFP_{wt} - GFP_{medium}}{OD_{wt} - OD_{medium}} \right) \quad \text{equation 1}$$

Microscopy

Cultures of *B. subtilis* were grown and prepared as described above. Images were taken with an Olympus IX71 Microscope (Personal DV, Applied Precision) using CoolSNAP HQ2 camera (Princeton Instruments, Trenton, USA) with a 100× phase-contrast objective. Fluorescence filter sets (excitation, 450 to 490 nm; emission, 500 to 550 nm) used to visualize GFP were from Chroma Technology Corporation (Bellows Falls, USA). Excitation was done with an exposure time of 0.2 s and 32% transmission from a xenon light source (300 W). Softworx 3.6.0 (Applied Precision, Washington, USA) software was used for image capturing. Cell segmentation in phase-contrast images was done with MicrobeTracker [190]. MicrobeTracker was also used to extract fluorescence intensity values from the fluorescent images. Cell-length distributions and fluorescence signal intensities were plotted using MATLAB R2011a. Fluorescence levels were corrected for background fluorescence of the medium. Calculation of phenotypic noise strength was done as described in [156].

Table 1. Bacterial strains and plasmids.

Strains and plasmids	Relevant properties	Source or reference
Strains		
<i>E. coli</i> DH5α	F ⁻ , <i>araD139</i> , Δ(<i>ara-leu</i>)7696, Δ(<i>lac</i>)X74, <i>galU</i> , <i>galk</i> , <i>hsdR2</i> , <i>mcrA</i> , <i>mcrB1</i> , <i>rspL</i>	Laboratory stock
<i>B. subtilis</i>		
168	<i>trpC2</i>	[108]
168_gfpmut1	168, <i>amyE</i> ::P _{hyperspank} - <i>gfpmut1</i> , Spec ^r	This study
168_gfp+	168, <i>amyE</i> ::P _{hyperspank} - <i>gfp+</i> , Spec ^r	This study
168_gfp+htrA	168, <i>amyE</i> ::P _{hyperspank} - <i>gfp</i> (<i>htrA</i>), Spec ^r	This study
168_gfp(Sp)	168, <i>amyE</i> ::P _{hyperspank} - <i>gfp</i> (<i>Sp</i>), Spec ^r	This study
168_sfgfp(Bs)	168, <i>amyE</i> ::P _{hyperspank} - <i>sfgfp</i> (<i>Bs</i>), Spec ^r	This study
168_sfgfp(Sp)	168, <i>amyE</i> ::P _{hyperspank} - <i>sfgfp</i> (<i>Sp</i>), Spec ^r	This study
168_sfgfp(iGEM)	168, <i>amyE</i> ::P _{hyperspank} - <i>sfgfp</i> (<i>iGEM</i>), Spec ^r	This study
Plasmids		
pDR111	<i>bla</i> , <i>amyE</i> ' _{hyperspank} , <i>spec</i> ^r , <i>lacl</i> , ' <i>amyE</i>	Gift of D. Rudner

pDR111_gfpmut1	<i>bla</i> , <i>amyE'</i> , $P_{hyperspank}$ - <i>gfpmut1</i> , <i>spec^r</i> , <i>lacI</i> , ' <i>amyE</i>	This study
pDR111_gfp+	<i>bla</i> , <i>amyE'</i> , $P_{hyperspank}$ - <i>gfp+</i> , <i>spec^r</i> , <i>lacI</i> , ' <i>amyE</i>	This study
pDR111_gfp+htrA	<i>bla</i> , <i>amyE'</i> , $P_{hyperspank}$ - <i>gfp+(htrA)</i> , <i>spec^r</i> , <i>lacI</i> , ' <i>amyE</i>	This study
pDR111_gfp(Sp)	<i>bla</i> , <i>amyE'</i> , $P_{hyperspank}$ - <i>gfp(Sp)</i> , <i>spec^r</i> , <i>lacI</i> , ' <i>amyE</i>	This study
pDR111_sfGFP(Bs)	<i>bla</i> , <i>amyE'</i> , $P_{hyperspank}$ - <i>sfGFP(Bs)</i> , <i>spec^r</i> , <i>lacI</i> , ' <i>amyE</i>	This study
pDR111_sfGFP(Sp)	<i>bla</i> , <i>amyE'</i> , $P_{hyperspank}$ - <i>sfGFP(Sp)</i> , <i>spec^r</i> , <i>lacI</i> , ' <i>amyE</i>	This study
pDR111_sfGFP(iGEM)	<i>bla</i> , <i>amyE'</i> , $P_{hyperspank}$ - <i>sfGFP(iGEM)</i> , <i>spec^r</i> , <i>lacI</i> , ' <i>amyE</i>	This study

Table 2. Oligonucleotides used in this study. Restriction sites are underlined.

Primers	Sequence (5' to 3')
GFP_NheI_fw	CCGCGCTAGCTGATTA <u>ACTAATAAGGAGGACAAAC</u>
GFP_SphI_rv	GCAAGCATGCA <u>AAAGAATCTTGCTTGGCAAGGTT</u> C

Results and Discussion

Selection and design of codon optimized *gfp* genes

Green fluorescent proteins used in molecular biology are variants of the *Aequorea victoria* GFP protein with improved characteristics. Optimizations include codon adaptation of the *gfp* gene to the organism of interest, or amino acid modifications to alter the folding properties of the protein or to change the chromophore (Table 3). For this study, we selected or generated the following GFP's: GFPmut1, GFP+, GFP+(htrA), GFP(Sp), sfGFP(Bs), sfGFP(Sp) and sfGFP(iGEM). A widely used GFP variant for use in bacteria is GFPmut1 [35]. Mutations in the chromophore of this protein result in a red-shift of the excitation maximum to 488 nm and a 35-fold higher fluorescence signal compared to the original GFP excited at 488 nm. Folding and maturation of the chromophore are also improved compared to the original GFP and fluorescence can be detected earlier after induction. The *gfp+* gene [174] has an *E. coli* codon usage while the encoded protein carries chromophore and folding mutations, yielding 130-fold increased fluorescence compared to *A. victoria* GFP. In *gfp+(htrA)* an additional region upstream of *gfp+* is added which encodes the first three amino acid residues of the *S. pneumoniae* HtrA protein which probably improves ribosome accessibility. GFP+(htrA) was shown to work as a robust reporter for protein fusions and to significantly improve heterologous protein production in *S. pneumoniae*

[52,76]. The *S. pneumoniae* codon-optimized *gfp(sp)* variant specifies a protein with chromophore and folding mutations similar to those in GFPmut2 [135]. Dimerization of this GFP at higher concentrations is prevented by the dimer interface-breaking A206K mutation [235], making it very suitable for protein fusions meant to assess intracellular localization. Superfolder (sf) GFP is especially useful for translational fusions, since it rapidly folds and matures even when it is fused to poorly folding peptides [141,159]. Furthermore, sfGFP might be particularly suitable for gene expression studies since the emergence of fluorescence closely matches induction of transcription. We employ three sfGFP variants: sfGFP(iGEM), sfGFP(Bs), and sfGFP(Sp), originating from the *sfgfp* sequences created by Pédélecq et al. [159]. sfGFP(iGEM) is a previously characterized variant; the gene is designed for the International Genetically Engineered Machine competition (iGEM) by the University of Cambridge team 2008 and its codon usage is a compromise for optimum expression in *E. coli* and *B. subtilis* [141]. In addition, sfGFP(iGEM) carries the mutations S2R and S72A from GFPmut3* [4]. No phenotypic effects have been reported for S2R, while the S72A mutation close to the chromophore enhances fluorescence [4]. For optimal use of sfGFP in *B. subtilis* and *S. pneumoniae* we designed and synthesized codon-optimized genes for sfGFP variants: respectively *sfgfp(Bs)* and *sfgfp(Sp)* (see Materials and Methods). With the design of two new *sfgfp* genes, the total number of GFP variants benchmarked in this study is seven.

Table 3. GFP variants benchmarked in this study.

Name	Changes to <i>A. victoria</i> GFP	Properties	Gene codon optimization method	Reference
GFPmut1	F64L, S65T, L195S	35 fold brighter than wt GFP	Original codon adaptation from <i>A. victoria</i>	[35]
GFP+	F64L, S65T, Q80R, F99S, M153T, V163A	130 fold brighter than wt GFP	<i>E. coli</i>	[174]
GFP+(<i>htrA</i>)	M1MKHL, F64L, S65T, Q80R, F99S, M153T, V163A	Improved translation efficiency in <i>S. pneumoniae</i>	<i>E. coli</i>	[52]
GFP(<i>Sp</i>)	M1MV, S65A, V68L, S72A, A206K	Based on GFPmut2, Monomer	<i>S. pneumoniae</i> using OptimumGene™	[135]
sfGFP(<i>Bs</i>)	S30R, Y39N, F64L, S65T, Q80R, F99S, N105T, Y145F, M153T, V163A, I171V, A206V	Superfolder GFP, [159]	<i>B. subtilis</i> using dual codon method	this study

sfGFP(<i>Sp</i>)	S30R, Y39N, F64L, S65T, Q80R, F99S, N105T, Y145F, M153T, V163A, I171V, A206V	Superfolder GFP, [159]	<i>S. pneumoniae</i> using OPTIMIZER, [163]	this study
sfGFP(iGE M)	S2R, S30R, Y39N, F64L, S65T, S72A, F99S, N105T, Y145F, M153T, V163A, I171V, A206V	Superfolder GFP, additional mut3* mutations	<i>E. coli</i> and <i>B. subtilis</i>	[141]

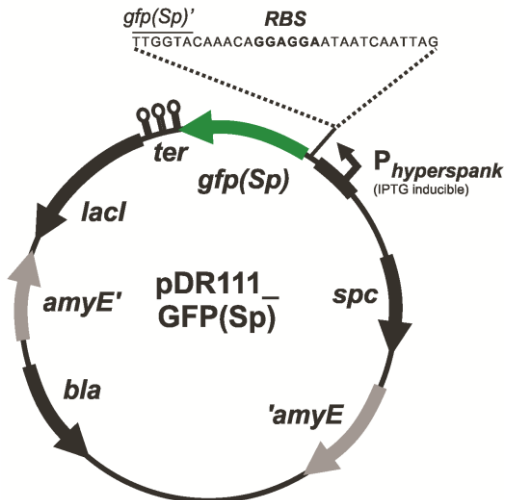


Figure 1. GFP expression vector for *B. subtilis*. Plasmid pDR111_gfp(*Sp*) integrates in the *B. subtilis* genome at the *amyE* gene locus by double cross-over and allows IPTG inducible expression of *gfp*(*Sp*).

Construction of new *gfp* vectors for *B. subtilis*

To evaluate the seven GFP's for their production and fluorescence properties, we constructed new *gfp* vectors for integration into the chromosome of *B. subtilis*. It is important to note that for each *gfp* variant the same promoter and RBS were used, allowing direct comparison. For *B. subtilis* plasmid pDR111 (kind gift from David Rudner) was used as the replicon. This vector is a derivative of the $P_{\text{spac-hy}}$ plasmid pJQ43 [164], which achieves better repression in the absence of the inducer IPTG due to an extra LacO operator site [24]. PCR fragments carrying *gfp* constructs were cloned downstream of the $P_{\text{hyperspank}}$ promoter region. The PCR fragments included three stop codons in the three different reading frames, a RBS upstream of the *gfp* gene, and three terminators downstream of the *gfp* gene to terminate transcription and prevent read-through transcription from downstream genes. The regions of the *amyE* gene flanking the *gfp* gene in pDR111 facilitate integration at the

amyE locus in the *B. subtilis* chromosome. Ampicillin and spectinomycin resistance cassettes are present to allow selection in *E. coli* and *B. subtilis*, respectively. The set up chosen guarantees that each of the seven *gfp* genes is located in exactly the same genetic surrounding.

Characterization of GFP intensity at the population level

Strains of *B. subtilis* were cultured in 96-well microtiter plates and examined for GFP fluorescence (Figure 2A).

Strikingly, in *B. subtilis*, *gfp(Sp)* carrying codon-optimizations for *S. pneumoniae* exhibited the strongest fluorescence signal; the average signals were approximately 5 fold higher than when the widely used GFPmut1 was expressed [35,120] (Figure 2A). The fluorescent proteins sfGFP(Sp), GFP+(htrA) and GFP+ also exhibited a signal stronger than that of GFPmut1. Different to what was expected, the sfGFP(Bs) performed worst in the host for which the gene was codon optimized, *B. subtilis*. While the protein sequences of sfGFP(Bs) and sfGFP(Sp) are identical, the fluorescence level of the latter is 6- to 7 fold higher in *B. subtilis*. At the DNA level sfGFP(Bs) and sfGFP(Sp) show 85% sequence identity illustrating the impact of codon usage on heterologous protein production.

Altogether these results demonstrate that for the conditions tested, a GFP with a strong fluorescence at the population level can be selected: GFP(Sp) for *B. subtilis*.

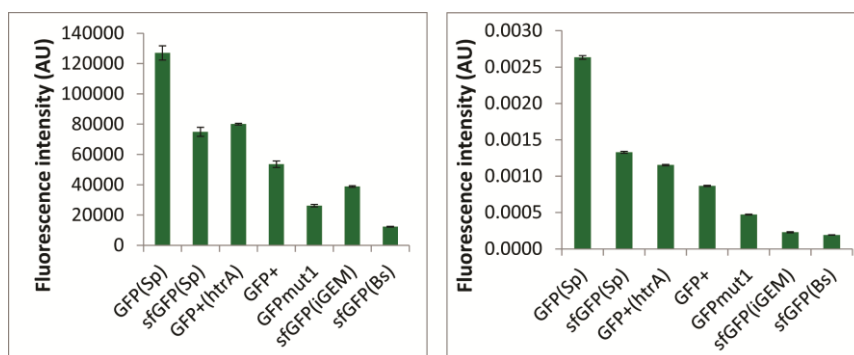


Figure 2. Fluorescence quantification of GFP variants in *B. subtilis*. (Left) population-level GFP signals recorded using microtiter plate readings. Fluorescence intensities are corrected for background fluorescence, OD₆₀₀ and wild type strain (no GFP) values. Error bars indicate the standard error of mean (n≥3). Simultaneously, single-cell fluorescence was measured in the same cultures with fluorescence microscopy (right). Fluorescence intensities are normalized for background fluorescence, cell area and wild type strain values. Error bars indicate the standard error of mean (n≥200). Note that fluorescence values from both methods are in arbitrary units and are not directly comparable.

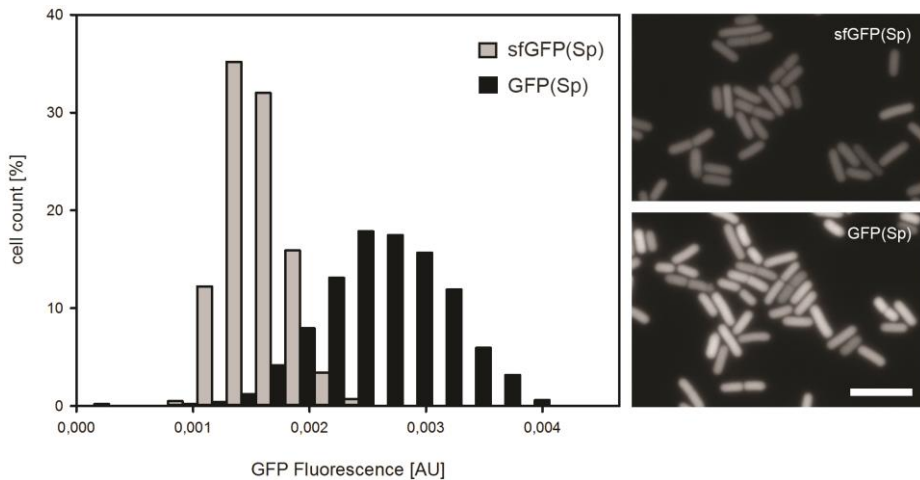


Figure 3. GFP fluorescence signal distribution. (left) The fluorescence intensity frequencies of GFP(Sp) (black bars) and sfGFP(Sp) (grey bars) in *B. subtilis* are plotted. While the mean signal of GFP(Sp) is higher, it is distributed over a wider range of intensities than sfGFP(Sp). (right) Micrograph examples of the two strains. Scale bar, 5 μm .

Characterization of GFP expression at the single-cell level

Fluorescence microscopy was performed to examine the signal of each GFP reporter at the single-cell level. Single-cell GFP signals were quantified using MicrobeTracker [190]. Simultaneously, population-level GFP signals were recorded on the same cultures using microtiter plate readings. Results are shown in Figure 2. In general, the average fluorescence observed in the single-cell assays correlated well with the population-wide data from the microtiter plate assays. The only GFP that deviates from the trend found in the microtiter plate assays is sfGFP(iGEM) (Figure 2B). Its fluorescence signal is twice lower than that of GFPmut1, making it, together with sfGFP(Bs), the GFP with the lowest fluorescence. The GFP variant generating the highest fluorescence signal is, again, GFP(Sp) with an average fluorescence almost two-fold above sfGFP(Sp), the second best GFP.

Not in every case do the data obtained from bulk cultures reflect the situation at the single-cell level. When plotted as a histogram it becomes evident that the fluorescence signal is not equal in all cells and that the amount of signal-variation among cells differs per GFP variant. From the histograms of *B. subtilis* GFP(Sp) and sfGFP(Sp) for example, it is clear that the GFP(Sp) signal is much broader than that of sfGFP(Sp) (Figure 3). See Figure S1 for all GFP signal distributions.

Phenotypic noise

As observed above in the single-cell analyses, GFP signals may vary among individual cells. In some experimental setups it is crucial that the GFP fluorescence signal is homogeneous, for example when studying phenotypic heterogeneity using promoter-*gfp* fusions as reporters for gene expression. In those cases one needs to be confident that variation in fluorescence signal originates from promoter activity, not from an intrinsic property of the GFP employed.

Thus, we quantified the spread in a population of expression levels of the various GFPs studied here. The distribution of gene expression of a single gene can be described by a mean value of expression (as measured by GFP signal) denoted $\langle p \rangle$ with a standard deviation σ_p . The phenotypic noise strength ($\sigma_p^2 / \langle p \rangle$) is a commonly used measure of noise [92,156,206]. This is because the relative standard deviation changes as the mean value changes, whereas the phenotypic noise strength is less sensitive to changes in the mean value. The phenotypic noise strength is thus a noise measure that allows relative comparison of gene-expression distributions among populations [92,156,206].

The general trend for the GFPs benchmarked in this study is that phenotypic noise strength is proportional to fluorescence signal (Table 4). The GFP generating the highest fluorescence signal, GFP(*Sp*), shows the most heterogeneous fluorescence at the single-cell level.

The sources for the observed differences in phenotypic noise are unclear but might involve cell-to-cell variability in protein synthesis (transcription, translation), mRNA stability, GFP maturation and/or -folding and are thus of crucial importance to take into account when examining single-cell gene expression patterns.

Table 4. Phenotypic noise strength in *B. subtilis*; Calculations done according to Ozbudak *et al.* [156].

GFP	*
GFPmut1	0.33
GFP+	0.87
GFP+(<i>htrA</i>)	1.26
GFP(<i>Sp</i>)	7.24
sfGFP(<i>Bs</i>)	0.16
sfGFP(<i>Sp</i>)	2.24
sfGFP(iGEM)	0.38

*Values are multiplied by 10^5

Concluding remarks

Seven GFP variants have been benchmarked with respect to their fluorescence signal strength in *B. subtilis*, both on the population level and on the single cell level. To this end a new *gfp* vector for genomic integration was constructed. Our results allow a clear ranking of the GFPs based on their fluorescence signals. The GFP generating the highest fluorescence signal for *B. subtilis* is GFP(Sp). It is important to note that this ranking is likely influenced by the choice of the RBS and each gene might be expressed differently with a different RBS [42,170]. The importance of the 5' end of the transcript for total protein production is well known. For instance, without the need to completely codon optimize the entire gene, expression of fluorescent protein production could be tremendously improved by adding a few codons of a gene of a well expressed protein to the 5' end of the gene encoding the fluorescent protein in *B. subtilis*, which likely improves ribosome accessibility to the RBS thus improving translation [219].

In general, the underlying molecular mechanisms for the large differences in GFP signals between the seven GFP variants is unclear at this moment and lies outside the scope of this work. Besides the specific mutations in the various GFPs, they might be related to mRNA stability, translation efficiency, GFP-folding efficiency, chromophore maturation and protein stability. Nevertheless, this work provides a good basis for selecting a proper GFP variant for the Gram-positive model bacterium *B. subtilis*.

Acknowledgements

We thank David Rudner for the kind gift of plasmid pDR111 and Nathalie Campo for kindly providing plasmid pUC57-gfp(opt). We thank Hans Roubos (DSM) for kindly providing the sfgfp(Bs) sequence. Ruud Detert Oude Weme is funded by a SysMO2 grant (NWO-ALW Earth and Life Science) to OPK.

Supplementary info

<http://aem.asm.org/content/suppl/2013/09/19/AEM.02033-13.DCSupplemental.html>

Chapter 3

Single cell FRET analysis for the identification of optimal FRET-pairs in *Bacillus subtilis* using a prototype MEM-FLIM system

Ruud G.J. Detert Oude Weme, Ákos T. Kovács, Sander J.G. de Jong, Jan-Willem Veening, Jeroen Siebring, Oscar P. Kuipers.

This chapter was published in: Single Cell FRET Analysis for the Identification of Optimal FRET-Pairs in *Bacillus subtilis* Using a Prototype MEM-FLIM System. PLoS ONE. 2015. 10(4):e0123239.

Abstract

Protein-protein interactions can be studied *in vitro*, e.g. with bacterial or yeast two-hybrid systems or surface plasmon resonance. In contrast to *in vitro* techniques, *in vivo* studies of protein-protein interactions allow examination of spatial and temporal behavior of such interactions in their native environment. One approach to study protein-protein interactions *in vivo* is via Förster Resonance Energy Transfer (FRET). Here, FRET efficiency of selected FRET-pairs was studied at the single cell level using sensitized emission and Frequency Domain-Fluorescence Lifetime Imaging Microscopy (FD-FLIM). For FRET-FLIM, a prototype Modulated Electron-Multiplied FLIM system was used, which is, to the best of our knowledge, the first account of Frequency Domain FLIM to analyze FRET in single bacterial cells. To perform FRET-FLIM, we first determined and benchmarked the best fluorescent protein-pair for FRET in *Bacillus subtilis* using a novel BglBrick-compatible integration vector. We show that GFP-tagRFP is an excellent donor-acceptor pair for *B. subtilis* *in vivo* FRET studies. As a proof of concept, selected donor and acceptor fluorescent proteins were fused using a linker that contained a tobacco etch virus (TEV)-protease recognition sequence. Induction of TEV-protease results in loss of FRET efficiency and increase in fluorescence lifetime. The loss of FRET efficiency after TEV induction can be followed in time in single cells via time-lapse microscopy. This work will facilitate future studies of *in vivo* dynamics of protein complexes in single *B. subtilis* cells.

Introduction

Bacteria have long been regarded as vesicles filled with proteins without any internal organization. However, the cytosol of bacterial cells is densely crowded [140], so a high level of organization is expected to ensure proper functioning of cellular processes. Recently, there has been growing interest in elucidating potential spatial organization inside bacterial cells. A large body of work in bacteria has now revealed spatial organization for DNA-protein interactions, protein localization, and protein-protein interactions [131,169,184,222]. Protein-protein interactions during cell division, regulatory interactions, and metabolic processes are increasingly studied.

Previously, techniques for studying protein-protein interactions were either indirect (e.g. yeast- or bacterial two hybrid) or *in vitro* methods (e.g. Surface Plasmon Resonance). These techniques are practical for screening potential interaction partners or to study binding affinities. In order to gain insight into the *in vivo* dynamics of these interactions, the *in vivo* method needs to produce time-resolved information. Förster Resonance Energy Transfer (FRET) allows time-resolved inspection of protein-protein

interactions. Single cell FRET analysis allows for the investigation of individual differences of protein-protein interactions, rather than studying an average FRET efficiency of a population.

Fluorescence microscopy only allows identification of protein co-localization due to its limited resolution. FRET is the non-radiative energy transfer from an excited donor fluorophore to an acceptor fluorophore that can only occur when donor and acceptor are in very close vicinity of each other (<10 nm). FRET is therefore a useful tool for proving interactions via excitation of the donor fluorophore and measuring emission of the acceptor molecule [69,149,217].

FRET was first described by Förster [60,112,200] and found widespread use in molecular biology [37,166] ever since the introduction of various fluorescent proteins (FPs)[182]. FRET has been successfully applied to demonstrate interactions between proteins, e.g. to study the assembly of the divisome in *Escherichia coli* [2], and the composition of the *Bacillus subtilis* competence machinery [106]. For a successful FRET experiment there are three requirements. First, the donor and acceptor fluorophores are within 1-10 nm from each other. Second, the donor emission spectrum overlaps with the acceptor excitation spectrum, and third, the fluorophores have similar orientation of the dipoles [112]. While the spectral overlap is necessary, it is also a disadvantage, because the acceptor can be excited by the light used to excite the donor instead of getting excited by non-radiative energy transfer. Also the donor emission can pass the acceptor emission filter. The potential of donor and acceptor bleedthrough demands corrections via imaging of samples with only a donor or acceptor fluorophore [217]. Another way to overcome the bleedthrough problems caused by spectral overlap is measuring the fluorescence lifetime of the donor fluorophore in presence or absence of an acceptor. A population of excited fluorophores displays a characteristic decay of spontaneous emission.

In this study the FRET efficiency was determined in two ways: the first method is via the detection of sensitized emission [217]: the measurement of the acceptor emission that originates from the resonance energy transfer from the excited donor. The second method is by measuring fluorescence lifetime, which is defined as the time needed for the fluorescence intensity to decrease to $1/e$ (approx. 37%) of the initial intensity immediately after excitation [113] and is commonly in the nanosecond range. Anything that quenches fluorescence – offers (more) non-radiative decay options, such as FRET does – will decrease the fluorescence lifetime [147].

Frequency Domain Fluorescence Lifetime Imaging Microscopy (FD-FLIM) [112,113,147,216] allows wide-field fluorescence lifetime determination via phase modulation [113]. For FD-FLIM the excitation light is modulated,

consequently resulting in a modulated emission signal. The lifetime of the fluorophore studied causes a delay in the phase of the modulated emission compared to the phase of the modulated excitation. By modulating the sensitivity of the detector at the same frequency as the excitation signal, the phase delay between emission and excitation can be measured and a fluorescence lifetime can be calculated in every pixel of the image. FD-FLIM allows fast wide-field fluorescence lifetime acquisitions and is highly suitable for time-lapse microscopy and thus time resolved FRET analysis. See Zhao *et al.* [238] and the textbook of Lakowicz [113] for a detailed explanation of FD-FLIM.

Here, we investigated which FRET couple is best suited for dynamic protein-protein interaction studies in single cells of the Gram-positive model bacterium *B. subtilis* [108]. Several genes coding for fluorescent proteins with potential good FRET properties were cloned pairwise, integrated at the *amyE* locus, expressed, and tested for FRET properties. The FPs were covalently linked with a linker containing a TEV protease recognition sequence. An inducible TEV protease gene was co-cloned with the FRET-pair allowing conditional high/low FRET efficiency situations. FRET efficiency was determined via sensitized emission and via a prototype MEM-FLIM system. The currently available FD-FLIM systems make use of an image intensifier, of which the photocathode is modulated at high frequencies (MHz). The image intensifier is typically the limiting factor for the spatial resolution, and is susceptible to damage by high light intensities. Therefore, FLIM recording is difficult to automate and is vulnerable. The prototype MEM-FLIM system used here modulates the CCD-sensor of the detector directly at the pixel level [238] resulting in a wide-field FLIM system that can easily be integrated in automated microscopy set-ups for time-lapse microscopy to study dynamics of protein-protein interactions. Furthermore, and more importantly, the increased spatial resolution is sufficient for single bacterial cell FRET-FLIM. To our knowledge this is the first study that incorporates single bacterial cell FD-FLIM analysis on a wide-field microscope.

Materials and Methods

Bacterial strains, plasmids, oligonucleotides, and growth conditions.

The strains, plasmids, and oligonucleotides used in this study are listed in Table 1, Table 2, and Table 3 respectively. *Escherichia coli* MC1061 was used for cloning. All strains were cultivated on LB (Lysogeny Broth) medium at 37°C, supplemented with 100 µg/ml ampicillin or 100 µg/ml spectinomycin when appropriate. For the time-lapse experiment a chemically defined medium was used.

Recombinant DNA techniques

DNA purification, restriction and ligation were done as described before [171]. Fast Digest Restriction enzymes, Phusion DNA polymerase and T4 DNA ligase were obtained from Fermentas (St. Leon-Rot, Germany). Synthetic DNA was ordered from Mr. Gene (Regensburg, Germany).

Plasmid construction

In this study, a new *B. subtilis* integration vector, pDOW01, was constructed by modifying pDR111 (kind gift of David Rudner). Both vectors integrate chromosomally in the *amyE* locus. The BglBrick assembly standard [5] was introduced into pDR111 resulting in pDOW01 to facilitate easy cloning of biological parts.

Further, a TEV protease recognition site (ENLYFQG) coding sequence was inserted as a linker in the middle of the BglBrick cloning site. The BglBrick cloning site, with *EcoRI*, *BglII*, *BamHI* and *XhoI* restriction sites, always remains present during cloning to realize up- or downstream insertion of a new part into an existing construct. The BglBrick cloning strategy is adapted from the BioBrick cloning method [100].

To create pDOW01 from pDR111 the following changes were made: the ORI for *E. coli* was replaced with the ORI for *E. coli* from pUC18 to remove the *BglII* and *XhoI* restriction sites, the Amp^R was removed, the BglBrick [5] restriction sites are introduced for cloning, and a TEV-protease recognition site was introduced in the middle of the BglBrick cloning site.

The homologous regions of the *amyE* gene and the spectinomycin marker from pDR111 (from 115-4707) and the *E. coli* origin of replication (1888-2583) from the pUC18 vector were PCR amplified including the *NcoI* and *SpeI* restriction sites in the primer sequences to combine the fragments into a pDR-pUC-hybrid (see Table 3 for the primers). Subsequently, Quikchange PCR (Agilent) was used to remove the *BamHI* site at position 745, with primers pDR111_quikchange_FW and pDR111_quikchange_REV. The part between 2100-2528 bp in the original pDR111 vector was redesigned *in silico* and ordered from Mr. Gene (Regensburg, Germany), with the following changes. The *XhoI*, *BglII* and *EcoRI* sites were removed by point mutation. The *Sall* site was removed and in the upstream direction a RBS with a seven bp spacer to the start codon was inserted. The start codon was followed by the BglBrick prefix, the TEV-protease recognition site, the BglBrick suffix, two stop codons, and a strong terminator sequence. The IPTG-inducible P_{hyperspank} promoter from pDR111 remained unchanged. The synthetic DNA was inserted into the pDR-pUC-hybrid by replacing the original 422 bp between the *SphI*- and *PstI*-sites with the 529 bp synthetic DNA via restriction and ligation. This final cloning step resulted in our basic cloning vector, pDOW01 (Figure 1). The newly

constructed plasmid was fully re-sequenced and the plasmid sequence has been submitted to the Genbank database under accession number KM009065.

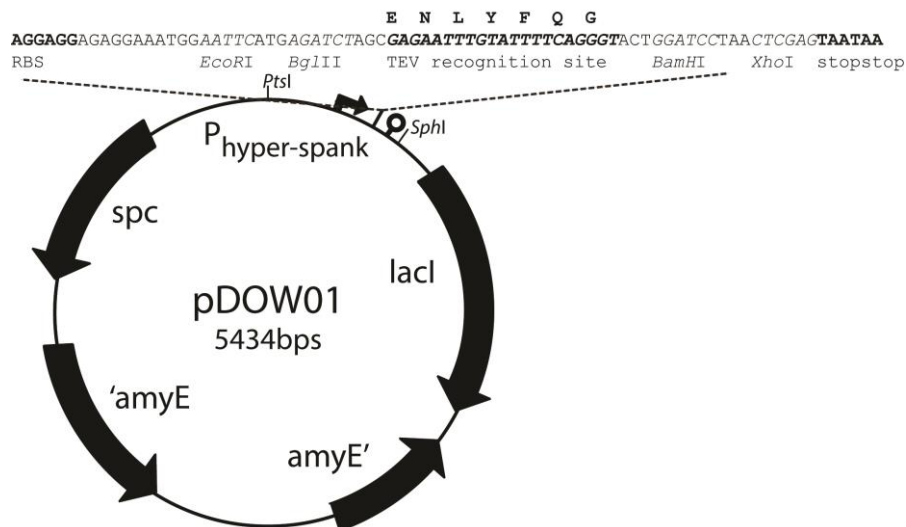


Figure 1. Map of the *amyE* integration vector pDOW01 with BglBrick cloning site, *EcoRI*, *BglIII*, *BamHI* and *XhoI* indicated in italics. Indicated in bold are the RBS (AGGAGG), the TEV-protease recognition site (GAGAATTTGTATTTTCAGGGT; amino acid sequence ENLYFQG) and the two stop codons (TAATAA).

Plasmid construction – fluorophore insertion

The fluorescent proteins used in this study are: Cerulean (a cyan FP [167]), Venus (a yellow FP [148]), sfGFP(Sp) [155], mCherry (a red FP [183], which is codon optimized by DSM as described before [155]), mKate2 (a far-red FP, Evrogen) and tagRFP (a red-orange FP, Evrogen). Codon optimization was done for sfGFP, mCherry, mKate2 and tagRFP as described before [155].

pDOW01 was used as basic vector to construct the following FRET pairs and their donor and acceptor only counterparts: Cerulean-Venus, GFP-mCherry, GFP-mKate2, GFP-tagRFP, and Venus-mCherry. Cerulean and Venus are improved versions of CFP and YFP [148,167]. The pairs were selected for use as a FRET pair based on the spectral properties [39] (see also: <http://www.microscopyu.com/>).

All genes encoding for fluorescent proteins were amplified by PCR with the BglBrick prefix (*EcoRI*, *BglIII*) in the forward primer and the BglBrick suffix (*BamHI*, *XhoI*) in the reverse primer for insertion into pDOW01 (see Table 3). Sequencing was used to verify the construct sequences.

Two fluorophores were linked to each other with a linker peptide containing a TEV-protease recognition site. The TEV-protease recognition site is ENLYFQ-G [48,161], with the cleavage site between the glutamine and glycine amino acids. The *B. subtilis* DOW01 strain used here contains an inducible TEV-protease (Table 1). The TEV-protease gene under control of the xylose inducible P_{xyI} promoter was amplified from BSG104 (primers constructTEV_FW & constructTEV_REV), inserted in pDG1664 and integrated in the *thrC* locus of the *B. subtilis* genome [71].

After cloning of the fluorophores into pDOW01, the resulting constructs were transformed and integrated in the *amyE* locus of *B. subtilis*. To facilitate transformation, *B. subtilis* was made naturally competent as described before [77]. Single copy, double recombination of the constructs was verified by the lack of (alpha)-amylase activity on LB starch plates.

Table 1. The strains used in this study.

Strain	Genotype	Source or reference
<i>E. coli</i>		
MC1061	F ⁻ <i>araD139</i> Δ(<i>ara-leu</i>)7696 <i>galE15 galK16</i> Δ(<i>lac</i>)X74 <i>hsdR2</i> (r _K ⁻ m _K ⁺) <i>mcrA mcrB1 rpsL</i> (Str ^r)	Laboratory stock
<i>B. subtilis</i>		
BSG1004	<i>B. subtilis</i> Δ <i>scpA</i> and <i>thrC</i> ::TEV-protease	[71]
168	<i>trpC2</i>	Bacillus Genetic Stock Center
DOW01	168 with <i>thrC</i> ::P _{xyI} -TEV-protease <i>ery-linc</i> ^r	This study
DOW03	DOW01 with <i>amyE</i> ::P _{hyperspank} -Cerulean Spec ^r	This study
DOW05	DOW01 with <i>amyE</i> ::P _{hyperspank} -GFP Spec ^r	This study
DOW09	DOW01 with <i>amyE</i> ::P _{hyperspank} -Venus Spec ^r	This study
DOW10	DOW01 with <i>amyE</i> ::P _{hyperspank} -mCherry Spec ^r	This study
DOW13	DOW01 with <i>amyE</i> ::P _{hyperspank} -tagRFP Spec ^r	This study
DOW14	DOW01 with <i>amyE</i> ::P _{hyperspank} -mKate2 Spec ^r	This study
DOW16	DOW01 with <i>amyE</i> ::P _{hyperspank} -Cerulean-Venus Spec ^r	This study
DOW21	DOW01 with <i>amyE</i> ::P _{hyperspank} -GFP-mCherry Spec ^r	This study
DOW23	DOW01 with <i>amyE</i> ::P _{hyperspank} -GFP-tagRFP Spec ^r	This study
DOW24	DOW01 with <i>amyE</i> ::P _{hyperspank} -GFP-mKate2 Spec ^r	This study
DOW26	DOW01 with <i>amyE</i> ::P _{hyperspank} -Venus-mCherry Spec ^r	This study

Table 2. The plasmids used in this study.

Plasmid	Genotype	Source or reference
pUC18	Amp ^r <i>lacZ'</i>	NCBI accession L09136
pDG1664	Amp ^r ' <i>thrC Ery</i> ^r <i>-linc</i> ^r <i>thrC</i> '	[73]
pDR111	Amp ^r <i>amyE</i> ' Spec ^r <i>lacI</i> P _{hyperspank} <i>amyE</i>	D. Rudner

pDOW01	<i>amyE'</i> <i>Spec^r</i> <i>lacI</i> <i>P_{hyperspank}</i> <i>amyE</i>	This study
pDOW03	<i>amyE'</i> <i>Spec^r</i> <i>lacI</i> <i>P_{hyperspank}</i> - <i>Cerulean amyE</i>	This study
pDOW05	<i>amyE'</i> <i>Spec^r</i> <i>lacI</i> <i>P_{hyperspank}</i> - <i>GFP amyE</i>	This study
pDOW09	<i>amyE'</i> <i>Spec^r</i> <i>lacI</i> <i>P_{hyperspank}</i> - <i>Venus amyE</i>	This study
pDOW10	<i>amyE'</i> <i>Spec^r</i> <i>lacI</i> <i>P_{hyperspank}</i> - <i>mCherry amyE</i>	This study
pDOW13	<i>amyE'</i> <i>Spec^r</i> <i>lacI</i> <i>P_{hyperspank}</i> - <i>tagRFP amyE</i>	This study
pDOW14	<i>amyE'</i> <i>Spec^r</i> <i>lacI</i> <i>P_{hyperspank}</i> - <i>mKate2 amyE</i>	This study
pDOW16	<i>amyE'</i> <i>Spec^r</i> <i>lacI</i> <i>P_{hyperspank}</i> - <i>Cerulean-Venus amyE</i>	This study
pDOW21	<i>amyE'</i> <i>Spec^r</i> <i>lacI</i> <i>P_{hyperspank}</i> - <i>GFP-mCherry amyE</i>	This study
pDOW23	<i>amyE'</i> <i>Spec^r</i> <i>lacI</i> <i>P_{hyperspank}</i> - <i>GFP-tagRFP amyE</i>	This study
pDOW24	<i>amyE'</i> <i>Spec^r</i> <i>lacI</i> <i>P_{hyperspank}</i> - <i>GFP-mKate2 amyE</i>	This study
pDOW26	<i>amyE'</i> <i>Spec^r</i> <i>lacI</i> <i>P_{hyperspank}</i> - <i>Venus-mCherry amyE</i>	This study

Table 3. The oligonucleotides used in this study. Restriction sites are shown in italics. BglBrick prefix in forward (FW) primer and suffix in reverse (REV) primer are underlined.

Oligonucleotide	Sequence (5' -> 3')
pDR111_ <i>amyE</i> _FW <i>NcoI</i>	TGATGCCATGGAATCAAATAAGGAGTGTCAAGAATG
pDR111_ <i>amyE</i> _REV <i>SpeI</i>	TTGCTACTAGTCGTCTAGCCTTGCCCTCAATG
pUC18_ORI_FW <i>SpeI</i>	TGAGGACTAGTGTAACCCCGTAGAAAAGATCAAAG
pUC18_ORI_REV <i>NcoI</i>	GGATACCATGGCTCGGGATAACGCAGGAAAGAAC
pDR111_ quikchange_FW	GACCGGCGCTCAGAATCCTAACTCAC
pDR111_ quikchange_REV	GTGAGTTAGGATTCTGAGCGCCGGTC
pDOW_seq1	CATGGCTCGGGATAACGCAGGAAAG
pDOW_seq2	CTGATTCTGACCGGGCACTTGGG
pDOW_seq3	CAAATAAAGCACTCCCGCGATC
pDOW_seq4	GATCTGTCAATGGTTCAGATAC
pDOW_seq5	TCTAGAGCTGCCTGCCGCGTTTCG
pDOW_seq6	ACGCGCCGTCGCAAATTGTC
pDOW_seq7	AATCAGCTGTTGCCGTCTCAC
pDOW_seqINSERT_FW	CTACAAGGTGTGGCATAATGTG
pDOW_seqINSERT_REV	AGCTTGATGCGGCTAGCTG
Cerulean/Venus_FW_BglBrick	GAGCTCGAATTCATGAGATCTATGTCAAAGGAGAAGA ACTTTTTAC
Cerulean/Venus_REV_BglBrick	GTCGAGCTCGAGTAAGGATCCCTTTATAAAGTTCGTCAT ACC
sfGFP_FW_BglBrick	GAGCTCGAATTCATGAGATCTATGTCAAAGGAGAAGA ATTG
sfGFP_REV_BglBrick	GTCGAGCTCGAGTAAGGATCCCTTTATAAAGTTCATCCAT TCCGTGTGTGATTC
mCherryDSM_FW_BglBrick	GAGCTCGAATTCATGAGATCTATGAGCAAAGGAGAAGA AG
mCherryDSM_REV_BglBrick	GTCGAGCTCGAGTAAGGATCCCTTTGTAAAGCTCATCCAT TC
tagRFP_FW_BglBrick	GAGCTCGAATTCATGAGATCTATGTGAGAACTTATCAAG

	GAAAATATG
tagRFP_REV BglBrick	GTCGAGCTCGAGTAAGGATCCTTTATGTCCCAATTTACT AGG
mKate2_FW BglBrick	GAGCTCGAATTCATGAGATCTATGTCAGAACTTATCAAG GAAAATATG
mKate2_REV BglBrick	GTCGAGCTCGAGTAAGGATCCACGGTGTCCCAATTTAC
constructTEV-FW+EcoRI	GCTGTCAAACATGAGAATTC
constructTEV-REV+BglII	CGCGAGATCTGGATTTCTTACGCGAAATACG

Western Blotting

An overnight culture of *B. subtilis* was diluted in fresh medium to an approximate OD₆₀₀ of 0.03 and grown for 2h at 37°C, while shaking at 225 rpm. After induction with 0.1 mM IPTG, the cultures were split into two equal volumes, and 1% (w/v) xylose was added to one part to induce the TEV-protease. Cells were grown for 2 more hours at 37°C and 2 ml of cell culture was centrifuged (1 min, 10.000 rpm) and resuspended in 200 µL 50 mM Tris-Cl pH 7.4. Cell lysis was achieved by adding a small spatula tip of glass beads (<106 microns, Sigma) to the mix, followed by two times one minute mini-bead beating (Mini-Beadbeater-16, Biospec products). After centrifugation (2 min, 10.000 rpm) the supernatant was carefully transferred to clean tubes and stored at -20°C. 30 µl supernatant supplemented with SDS-loading buffer was boiled at 80°C for 10 minutes and loaded on a 12% SDS-PAGE gel. After completion of electrophoresis the gel was transferred to a PVDF Western Blotting membrane (Roche. One hour at 80 mA), followed by blocking with 5% (w/v) skim milk (Oxoid) in PBST (58 mM Na₂HPO₄, 17 mM NaH₂PO₄, 68 mM NaCl, 0.1% (v/v) Tween20, pH 7.3) overnight at 4°C. The PVDF-membrane was washed three times 15 minutes in PBST and incubated with PBST with 5% skim milk and a 1:10.000 dilution of anti-GFP (rabbit serum, Invitrogen Molecular Probes) for two hours at room temperature. The membrane was washed three times 15 minutes in PBST and incubated with PBST supplemented with 1:5.000 goat-anti-rabbit Ig-Horseradish Peroxidase (Amersham Biosciences) for 1.5 hour at room temperature. Subsequently, the membrane was washed three times, gently dried with tissue papers and incubated for two minutes with 2 ml of ECL detection reagent (GE Healthcare). Signal visualization was done with a Molecular Imager ChemiDoc XRS+ (Bio-Rad).

Fluorescence microscopy

Microscope specification

Microscope imaging for sensitized emission experiments was done using a Personal DeltaVision microscope system (Applied Precision, Issaquah, USA), with Softworx 3.6.0 software. The microscope was equipped with an Olympus IX71 inverted microscope body, a 100x phase contrast objective (Olympus PlanApo 1.40 NA), a CoolSNAP HQ2 camera (Princeton Instruments), a 300W Xenon light source, and filters for imaging of CFP (ex. 430/24 nm; em. 472/30nm), GFP (ex. 470/40 nm; em. 525/50 nm), and mCherry (ex. 572/35 nm; em. 632/60 nm) from Chroma. For Cerulean and Venus the CFP/YFP/mCherry polychroic mirror was used (Chroma, 460-500, 525-575, 590-680 nm range) and for GFP, mCherry, mKate2, and tagRFP the GFP/mCherry polychroic mirror was used (Chroma, 400-470, 490-570, 580-630 and 640-730 nm range). Images were captured using 0.2s light exposure with 32% light transmission for every combination of filters. The FRET channel was set in the software by using the CFP or GFP excitation filter and the GFP or mCherry emission filter.

Strain preparation and protein overexpression

LB medium was inoculated from -80°C *B. subtilis* stocks and grown overnight at 37°C. The next morning the cultures were diluted 1 to 50 to an approximate OD₆₀₀ of 0.03 in fresh LB medium and grown for two hours at 37°C at 225 rpm. The cells were induced with 0.1 mM IPTG and one part of the culture containing the two fluorophores was transferred into a new bottle containing 1% (w/v) xylose to induce the TEV-protease. After an additional two hours of incubation, cells were transferred to a microscope slide containing 1% (w/v) agarose to immobilize the cells and fluorescence intensity was measured with the wide-field microscope described above for FRET detection via sensitized emission. The same sample preparation method was applied for the FLIM experiments described below.

Sensitized emission – Strain preparation for time-lapse

Time-lapse microscopy was done as described previously [40]. Briefly, LB medium was inoculated from -80°C stocks and grown for 8 hours at 37°C and 225 rpm. Subsequently, the culture was diluted 100 times in chemically defined medium (CDM; supplemented Spizizen's salt [3], per liter: 2 g (NH₄)₂SO₄, 14 g K₂HPO₄, 6 g KH₂PO₄, 1 g Na₃citrate.2H₂O, 0.27 g MgSO₄.7H₂O, 20 mg casamino acids (Formedium), 20 mg L-tryptophan and 5 g D-fructose) and grown overnight at 37°C, 225 rpm. The next morning the culture was diluted to an OD₆₀₀ of 0.08 in fresh CDM, grown for 5-7 hours at 37°C and 225

rpm to an OD_{600} of approximately 0.7. Now $(0.35/OD)*250 = 125 \mu\text{l}$ of cells were diluted in 500 μl fresh medium and 2 μl was transferred to a slide with 1.5% low-melting point agarose (Sigma) in CDM and 0.1 mM IPTG. When the TEV-protease gene should be expressed 1% (w/v) xylose was added to the slide medium as well. To make sure that the fluorophores were present right from the start of the time-lapse experiment, IPTG (final concentration 0.1 mM) was added to the liquid culture one hour before transfer to the agarose slide. And in case the TEV-protease should be expressed also 1% (w/v) xylose was added to the liquid medium. The agarose slide was divided in three columns, separated by air cavities; one for *B. subtilis* DOW5 (GFP only), one for *B. subtilis* DOW13 (tagRFP only), and one for *B. subtilis* DOW23 (GFP-tagRFP).

Time-lapse was done for 16 hours with a 15 minute interval. Of every strain the same four pictures were taken: phase contrast (GFP transmission light), FRET (GFP excitation, mCherry emission), donor (GFP excitation and emission), and acceptor (mCherry excitation and emission). In all cases the light exposure time was 0.2s and the light transmission was 32%. The microscope setup was the same as above except for the light source, which was now solid state TruLight Illumination (Applied Precision, Issaquah, USA). The microscope had a software-controlled stage to visit selected points routinely during a time-lapse experiment and the DeltaVision UltimateFocus was used to keep cells in focus.

Sensitized emission – Data analysis

Three biologically independent samples were used to obtain a total of eight images, necessary to do the FRET detection via sensitized emission and its corrections [217]: *B. subtilis* cells with only the donor, only the acceptor and with the donor and acceptor (Table 4). These samples with only one of the fluorophores are necessary to calculate the correction factor for the donor in the acceptor channel and vice versa, and to correct for bleedthrough (i.e. non-specific excitation and emission events in the partner fluorophore filter channels).

Here, FRET was performed with fluorescent proteins that were linked to each other by a TEV-protease cleavage site. Induction of the TEV-protease will cleave the fluorophores apart and is expected to result in a lower FRET efficiency.

ImageJ (<http://rsb.info.nih.gov/ij/index.html>) was used to measure the pixel intensities of the *B. subtilis* cells and Microsoft Excel to process the data. First, the background pixel intensity was subtracted from the cellular pixel intensity and four correction factors were calculated to correct for the spectral overlap (equation 1-4). The letters in equation 1 to 6 [217] refer to the symbols in Table 4.

$$\text{Equation 1.} \quad \alpha = d2/d$$

$$\text{Equation 2.} \quad \gamma = c/d$$

$$\text{Equation 3.} \quad \delta = d2/c$$

$$\text{Equation 4.} \quad \beta = b/a$$

α corrects for the acceptor fluorescence in the donor channel, γ is the correction for the acceptor excitation efficiency by donor excitation light, δ corrects for the sensitized emission back into the donor channel and β is the correction for the donor fluorescence in the acceptor channel [217]. These factors were used to correct for bleedthrough of the fluorophores.

The FRET was calculated with equation 5 [217] from the sensitized emission of the acceptor fluorophore in image S (Table 4). Subtraction of βD from S removes the donor contribution to the acceptor channel, subtraction of $(\gamma - \alpha\beta)A$ is necessary to correct for direct acceptor excitation, and the image is scaled by dividing by $1 - \beta\delta$.

$$\text{Equation 5.} \quad \text{FRETsensitized emission} = \frac{S - \beta D - (\gamma - \alpha\beta)A}{1 - \beta\delta}$$

To calculate the FRET efficiency, the sensitized emission from equation 5 is divided by the acceptor fluorescence intensity, A (Equation 6 [217]). The obtained FRET efficiency, E_a , is independent of fluorescence intensities, which can vary over time due to protein expression levels.

$$\text{Equation 6.} \quad \text{FRETefficiency, } E_a = \text{FRETsensitized emission} / A$$

Table 4. The eight images required for sensitized emission FRET. Table was redrawn based on a table from the W.M. Keck Center for Cellular Imaging [221]. The wavelengths for the filters are specified in the fluorescence microscopy section.

Symbol	Sample	Excitation filter	Emission filter
a	Donor only	Donor	Donor
b	Donor only	Donor	Acceptor
c	Acceptor only	Donor	Acceptor
d	Acceptor only	Acceptor	Acceptor
d2	Acceptor only	Donor	Donor
e (D)	Donor and Acceptor	Donor	Donor
f (S)	Donor and Acceptor	Donor	Acceptor
g (A)	Donor and Acceptor	Acceptor	Acceptor

Frequency Domain Fluorescence Lifetime Imaging Microscopy

The frequency domain MEM-FLIM system used (Lambert Instruments B.V.) [238], consists of a multi-LED light source containing 3W LEDs with peak intensities at 446 nm (for Cerulean) and 469 nm (for GFP), a signal generator and a prototype directly modulatable CCD camera. The MEM-FLIM system was mounted on a Nikon Eclipse Ti inverted microscope with a 100x oil phase contrast objective (1.40 NA). The filter combinations used for imaging Cerulean were ex. 436/20 nm; em. 480/40nm and for GFP em. 480/30 nm; ex. 535/40 (Nikon). Erythrosine B (Sigma-Aldrich 87613), a fluorescein derivative, with a lifetime of 0.086 ns was used as a reference. Erythrosine B was dissolved in H₂O and used with a concentration that matched the brightness of the samples. The MEM-FLIM system was operated using LI-FLIM software version 1.2.24 (Lambert Instruments B.V.).

Phase contrast images were taken using transmission light and 0.1s exposure time. FLIM data was collected using 0.7s exposure time and modulated LED light for excitation. Fluorescence lifetime data was collected using a modulation frequency of 40 MHz. For obtaining single cell fluorescence lifetime data the additional 1.5x magnification on the Nikon Microscope was used and the exposure time for collecting fluorescence images was extended to 1.5s. The LI-FLIM software was used for calculating the fluorescence lifetimes from phase shift data, see Zhao *et al.* [238] for details.

Acceptor photo bleaching

Acceptor photo bleaching was performed as described previously [95]. Briefly, for all strains the following pictures were made: three pictures before bleaching with the following filter settings: phase contrast, donor excitation and emission, and acceptor excitation and emission, now the acceptor was bleached for one minute at 100% light transmission using the mCherry filters, and then three pictures after bleaching were made with the following filter settings: phase contrast, donor excitation and emission, and acceptor excitation and emission. ImageJ was used to determine the fluorescence intensities of the donor before and after bleaching the acceptor. Pictures were taken from the donor-only strain (*DOW05*), and from the strain with donor and acceptor (*DOW23*) with and without induction of the *tev* protease encoding gene.

The FRET efficiency can be calculated with Equation 7 [95].

Equation 7.
$$\text{FRET efficiency, } E = (I_{DA^*} - I_{DA}) / I_{DA^*}$$

I_{DA} is the donor fluorescence intensity in presence of the acceptor and I_{DA^*} is the donor fluorescence intensity after photo bleaching the acceptor.

Results

Single cell observations of FRET detected via sensitized emission

The aim of this work was to identify the best FRET-pair and to perform FRET at the single cell level in *B. subtilis* using fluorescence microscopy. Therefore, the suitability of various fluorescent proteins (FPs) for FRET purposes in *B. subtilis* was tested by expressing them pairwise and covalently linked. The FPs tested here were Cerulean (a cyan FP [167]), Venus (a yellow FP [148]), and sfGFP(Sp) [155] as donor and tagRFP (a red-orange FP, Evrogen), mCherry (a red FP [183]), and mKate2 (a far-red FP, Evrogen) as acceptor. The respective genes were cloned in the *amyE* locus of *B. subtilis* under control of the IPTG-inducible $P_{hyperspank}$ promoter, by using the newly constructed *amyE* integration vector pDOW (Figure 1), which allows for efficient BglBrick [5] assembly (Figure 2A).

Measuring both high and low intracellular FRET efficiency is essential for benchmarking the methodology used in this study. Covalently linked pairs of fluorophores were constructed, using a linker that contains a TEV protease recognition site (Figure 2B). The functionality of the TEV-protease was tested before the search for the best FRET pair was started, to ensure that the protease is able to separate the two fluorophores from each other. Induction of TEV protease should induce uncoupling of the FRET pair, which results in loss of sensitized emission of the acceptor. Western blotting with GFP specific antibodies was performed to visualize the presence and size of the GFP containing proteins. As shown in Figure 2C, lane 3, the GFP-tagRFP synthetic dimer was readily produced. Upon induction of the *tev* gene, the heterodimer was efficiently cleaved into the monomers GFP and tagRFP (lane 4). Expression of the *tev* gene was a bit leaky, resulting in the presence of monomeric GFP without induction of *tev* expression (lane three). The band around 37 kDa in lane three is assumed to be a degradation product of the dimer. Overall, these results show that induction of the *tev*-protease gene results in an efficient separation of the FP pair (Figure 2C, lane 4).

The process of data acquisition and analysis to calculate the FRET efficiency is shown with single cell images of the FRET pair GFP-tagRFP (Figure 3 and Table 4). First, cells with only donor and only acceptor were imaged under the microscope in three channels (Figure 3 A -D2). Next, cells with donor and acceptor (the FRET pair) were imaged in the same three channels both with and without induction of TEV-protease (Figure 3E-G). Note the significant decrease in acceptor fluorescence (Figure 3F) in the presence of TEV-protease. The contributions of donor emission in the acceptor channel (Figure 3B) and the excitation of the acceptor by donor excitation (Figure 3C) were very small, but nevertheless these contributions need to be taken into account, because

this light in the FRET channel is not due to sensitized emission of the acceptor. After measuring the fluorescence intensities from all cells (Figure 3) the FRET efficiency measured via sensitized emission was calculated with Equation 6.

FRET efficiencies of the different fluorophore pairs detected with sensitized emission are shown in Table 5. The following criteria were used to select the most suitable FRET pair from the various combinations of FPs: first, the signal to noise levels of the separate fluorescent proteins should be high (Table 6), so localization and dynamics of individual proteins fused to a given fluorescent protein can be studied. Second, the difference in FRET efficiency between the covalently bound and cleaved fluorophores should be high. The highest signal to noise levels for the individual fluorophores were observed in the case of GFP, mKate2 and tagRFP (Table 6). Therefore, GFP was selected as FRET donor in subsequent protein-protein interaction experiments. The best acceptors were tagRFP and mKate2. The quantum yields were 0.48 versus 0.40 [39,137] and the relative brightness was 142 versus 74 for tagRFP and mKate2, respectively (as percentage of EGFP) [39]. Both fluorophores are monomeric [39], but the higher quantum yield of tagRFP will make protein interaction studies with the tagRFP easier for FRET analysis via sensitized emission since more of the donor resonance energy transfer to the acceptor will result in emission from the acceptor [185].

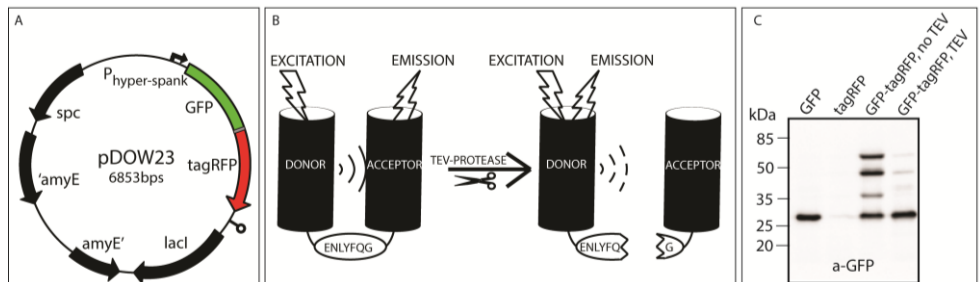


Figure 2. (A) The *amyE* integration vector pDOW23 with FRET-pair GFP-tagRFP. (B) Schematic representation of two fluorescent proteins and the linker containing the TEV-protease recognition site (ENLYFQG). (C) A Western Blot to show the cleaving of coupled fluorophores by the TEV-protease. GFP protein was visualized by chemiluminescence with GFP-antibodies. The lanes contain cell free extract from the following strains: lane 1, *DOW05* (*thrC::Pxyl-tev amyE::gfp*), lane 2, *DOW13* (*thrC::Pxyl-tev amyE::tagRFP*), lane 3, *DOW23* (*thrC::Pxyl-tev amyE::gfp-tagRFP*) from a culture without induction of the *tev* protease gene and lane 4, *DOW23* (*thrC::Pxyl-tev amyE::gfp-tagRFP*) in which the *tev* protease gene was induced with 1% (w/v) xylose. Predicted sizes for GFP and tagRFP monomer are 27 kDa, and the complex 55 kDa.

Based on the criteria of high signal to noise fluorescence and a large difference in FRET efficiency between the bound and cleaved fluorophores, GFP-tagRFP was chosen as the best FRET pair in *B. subtilis* (Table 5). Both the

fluorescence intensities and the FRET efficiency of the Cerulean-Venus, the GFP-mCherry, and the Venus-mCherry combinations were much lower than of the GFP-mKate2 or GFP-tagRFP combinations; therefore these pairs were excluded from further analysis.

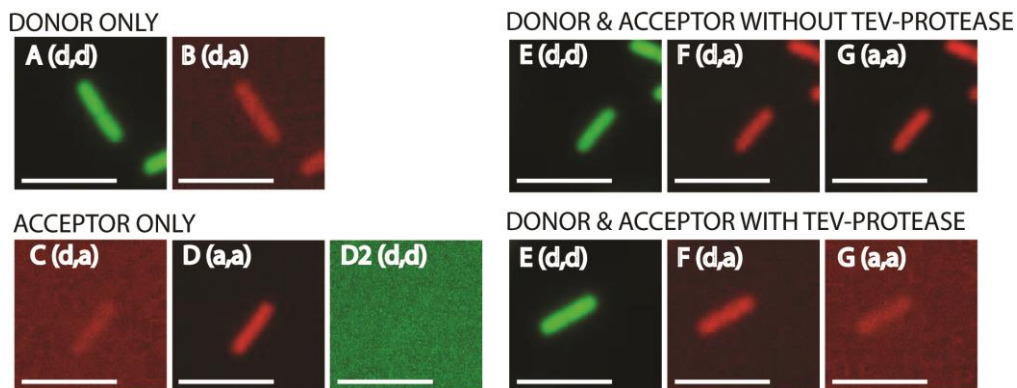


Figure 3. Fluorescence intensities of single cells for the FRET-pair GFP-tagRFP. Microscope excitation and emission filter settings are shown between brackets (d=donor, a=acceptor). For donor the filters (excitation, emission) were: GFP, GFP; for acceptor: mCherry, mCherry; and for FRET the filters were: GFP, mCherry. In all cases a GFP/mCherry polychroic mirror was used (400-470, 490-570, 580-630 and 640-730 nm range). **A** and **B** are cells where only donor fluorophore is present (GFP). **C**, **D** and **D2** are cells where only acceptor fluorophore is present (tagRFP). **E**, **F** and **G** (upper panel) are cells where donor-acceptor fluorophore (GFP-tagRFP) are coupled and TEV-protease is not induced. **E**, **F** and **G** (lower panel) are cells where donor-acceptor (GFP-tagRFP) are uncoupled by induction of TEV-protease. The same signal scaling is used for all images. Note that the signals are false colored (GFP: green, tagRFP: red). Scale bar is 5 μ m.

FRET detection via sensitized emission can be confirmed by acceptor photo bleaching

To support the above-presented FRET detection method via sensitized emission, an acceptor photo bleaching experiment on the GFP-tagRFP fluorophore pair was performed. FRET efficiency can be determined via acceptor photo bleaching [95]. When FRET occurs, the acceptor molecule quenches the donor fluorescence (resulting in decreased donor fluorescence), but when the acceptor is destroyed by photo bleaching it cannot quench the donor anymore, so increased donor fluorescence can be detected.

To specifically photo bleach tagRFP, we placed live cells under the microscope and excited with 572/35 nm with 100% of the output of solid state TruLight Illumination for one minute. This resulted in a decrease of 35% of the tagRFP fluorescence.

Indeed, using the GFP-tagRFP pair, the donor (GFP) emission was lower when FRET occurs than when GFP and tagRFP are uncoupled by TEV-cleavage. The pre-bleach fluorescence intensities of GFP were: 362 AU without TEV protease vs. 437 AU when TEV was produced. Moreover, after acceptor photo bleaching, an increase in donor fluorescence was observed when the GFP-tagRFP was coupled: the fluorescence intensities of GFP were 410 AU (13% increase) when GFP-tagRFP was coupled vs. 429 AU (1.8% decrease) when GFP-tagRFP was uncoupled. Acceptor photo bleaching increases the GFP fluorescence with 13% when the fluorophores were linked to each other. When the fluorophores were uncoupled by the TEV-protease, the donor fluorescence was approximately the same before and after photo bleaching (437 vs. 429), which is a good control for this method.

The FRET efficiency E (see Equation 7) is $(I_{DA^*} - I_{DA})/I_{DA^*} = (410 - 362)/410 = 0.12$ for GFP-tagRFP in this acceptor photobleaching experiment.

In total, we showed that the GFP-tagRFP pair can be efficiently used as a FRET pair for protein interactions in live *B. subtilis* cells.

Table 5. The FRET efficiency E_a of the different FRET pairs, measured via Sensitized Emission.

	FRET efficiency, E_a			
	R_0	Donor-Acceptor covalently bound	Donor-Acceptor Cleaved by protease	Difference
Cerulean-Venus	5.3 ^a	0.02 +/- 0.00	0.01 +/- 0.00	0.01
GFP-mCherry	5.28[185]	0.05 +/- 0.03	0.02 +/- 0.00	0.03
GFP-mKate2	~5.31 ^b	0.14 +/- 0.02	0.00 +/- 0.03	0.14
GFP-tagRFP	5.74[185]	0.22 +/- 0.09	0.01 +/- 0.06	0.21
Venus-mCherry	5.7 ^a	0.03 +/- 0.02	0.01 +/- 0.00	0.02

^a <http://www.microscopyu.com/tutorials/java/fluorescence/fpfret/index.html>

^b Calculated based on the GFP, mKate2, and tagRFP spectra from www.evrogen.com. For formulas see reference [66,114]. The spectral overlap of GFP-tagRFP and GFP-mKate2 are very similar (Evrogen spectra), but the extinction coefficient ϵ_A of mKate2 is smaller than the ϵ_A of tagRFP (62,500 vs. 100,000 M⁻¹ cm⁻¹). Multiplying the spectral overlap $J(\lambda)$ of GFP-tagRFP with 0.625 resulted in a calculated R_0 of 5.31 for GFP-mKate2.

Table 6. Fluorescence intensities of *B. subtilis* cells with the various fluorescent proteins. The column with the FRET channel, the most important part of the data, is highlighted. Fluorescence intensities were measured with three different microscope filter settings for excitation and emission filters: donor,donor; donor,acceptor; and acceptor,acceptor (as indicated by the letters between brackets^a. d=donor, a=acceptor). ^bSensitized emission is determined from this sample and these filter settings. The values here are a triplicate of the average intensity of 50 cells. The standard deviations are shown as well.

	Fluorescence intensity						
	Donor only		Acceptor only		Donor and acceptor (FRET)		
	(d,d) ^a	(d,a) ^a	(a,a) ^a	(d,a) ^a	(d,d) ^a	(d,a) ^{a,b}	(a,a) ^a
Cerulean	4.86 ±0.86	2.42 ±0.45					
Venus			373.16 ±40.85	3.81 ±0.47			
Cerulean-Venus					4.18 ±1.71	9.29 ±2.68	266.44 ±43.12
Cerulean, Venus cleaved					3.73 ±0.67	5.24 ±0.89	214.32 ±15.61
GFP	432.39 ±85.25	11.23 ±2.47					
mCherry			57.00 ±22.97	2.14 ±0.60			
GFP-mCherry					583.88 ±33.12	29.31 ±5.39	165.42 ±14.77
GFP, mCherry cleaved					555.99 ±18.56	21.61 ±1.61	127.14 ±23.68
GFP	471.13 ±20.20	13.98 ±1.62					
mKate2			77.40 ±16.53	4.94 ±1.06			
GFP-mKate2					483.29 ±55.88	33.74 ±5.99	98.90 ±21.60
GFP, mKate2 cleaved					536.91 ±114.16	20.70 ±4.79	86.11 ±31.93
GFP	421.92 ±84.29	11.53 ±1.73					
tagRFP			41.06 ±7.36	3.82 ±0.69			
GFP-tagRFP					572.89 ±12.98	38.21 ±9.20	72.16 ±13.73
GFP, tagRFP cleaved					563.96 ±57.18	19.44 ±1.31	36.28 ±25.79
Venus	163.11 ±16.79	15.82 ±7.10					
mCherry			81.55 ±6.49	4.62 ±1.39			
Venus-mCherry					190.35 ±56.06	33.11 ±11.96	190.63 ±1.20
Venus, mCherry cleaved					138.84 ±24.14	22.76 ±9.61	144.52 ±21.69

FRET efficiency dynamics in time-lapse experiments

This study focusses on finding appropriate FRET-pairs for studying temporal behavior of protein-protein interactions. The GFP-tagRFP FRET pair was used in a time-lapse experiment to determine if the FRET efficiency is stable over time. Both covalently bound and TEV-protease treated GFP-tagRFP produce a constant FRET efficiency (Figure 4). A FRET-efficiency altering process like unequal protein degradation was hereby excluded. Any FRET-efficiency dynamics found in future protein-protein interaction experiments can be attributed to the given protein-protein interactions.

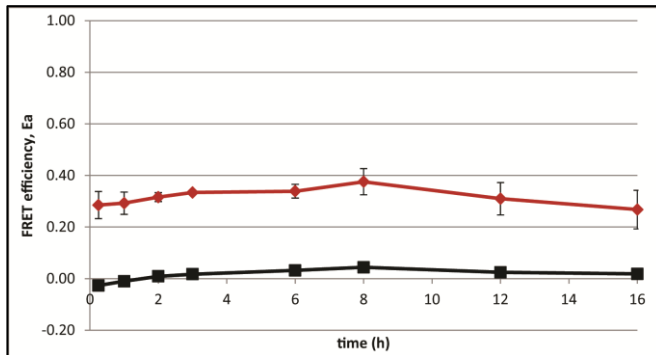


Figure 4. The FRET efficiency, E_a , was determined over time with a fluorescence microscopy time-lapse experiment. The covalently bound GFP-tagRFP, e.g. no TEV-protease, results in a high FRET efficiency (red line) and when the GFP-tagRFP is uncoupled by inducing the TEV-protease encoding gene, it results in a low FRET efficiency (black line). Error bars show the standard deviation of three replicate experiments. At least 50 single cells were analyzed at each time point.

FRET-FLIM

The fluorescence lifetime of GFP on its own was 2.56 ns (Table 7). When GFP was coupled to an acceptor, the fluorescence lifetime was reduced, i.e. 2.22 ns for GFP-tagRFP, and when the GFP and the acceptor were uncoupled by expression of TEV-protease the GFP fluorescence lifetime increased again (Table 7). However, the fluorescence lifetime of GFP in the uncoupled FRET pair did not increase back to the situation of GFP only, which might indicate that the cleavage of the fluorophores was not 100%.

The FRET efficiency can be calculated from the fluorescence lifetimes with equation 8 [114].

Equation 8.
$$\text{FRET Efficiency } E = 1 - \frac{\tau_{DA}}{\tau_D}$$

where τ_{DA} is the fluorescence lifetime of the donor in presence of an acceptor and τ_D is the fluorescence lifetime in the absence of an acceptor. The highest

FRET efficiencies were 11% and were obtained for GFP-mKate2 and GFP-tagRFP, the FRET efficiency for GFP-mCherry was only 4%. The Cerulean fluorescence lifetime could not be determined, because of technical limitations (non-appropriate filters on the MEM-FLIM mounted microscope).

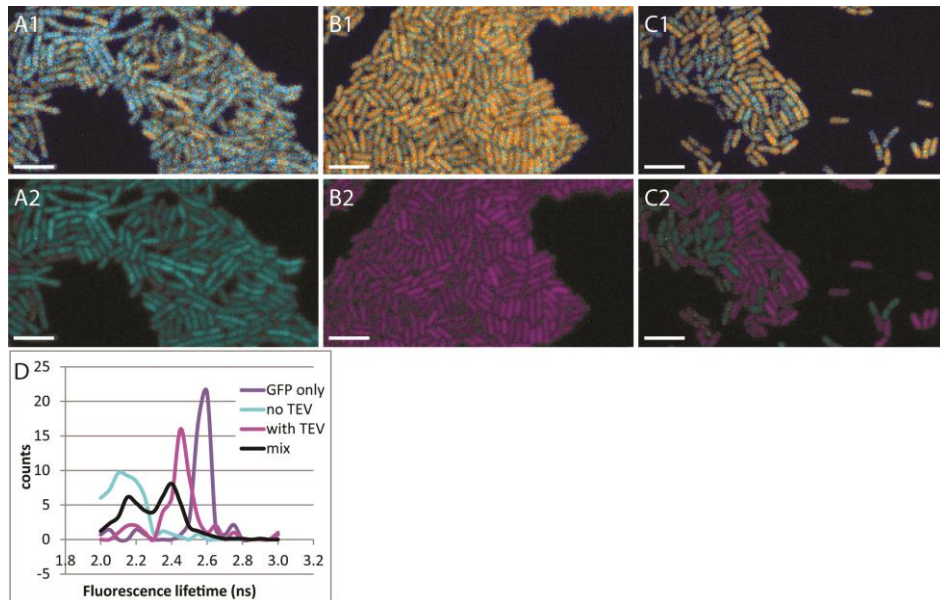


Figure 5. Single cells FLIM measurements. (A1) *B. subtilis* cells are shown where the GFP-tagRFP fluorophores are linked. **(B1)** *B. subtilis* cells are presented where the GFP and tagRFP fluorophores are cleaved apart. **(C1)** *B. subtilis* cells where GFP-tagRFP fluorophores are linked are mixed in a 1:1 ratio with *B. subtilis* cells where the GFP-tagRFP fluorophores are cleaved apart; resulting in a mix of cells with either short GFP fluorescence lifetime due to quenching by tagRFP or long GFP fluorescence lifetime. Visualization of cells in A1, B1, and C1 was done with a Look-Up-Table from LI-FLIM. **A2, B2** and **C2** present the same cells, but now a MatLab script was used to categorize the cells into two categories: cells with short GFP lifetimes are shown in cyan and cells with long GFP lifetimes are shown in magenta. **(D)** Fluorescence lifetime based histogram of the cells described in A2-C2, black, cyan, magenta and dotted lines present GFP_only, linked fluorophores, cleaved fluorophores and a mix of the two populations, respectively. Scale bar is 5 μm .

Cells containing GFP-tagRFP were used to study the usability of the prototype MEM-FLIM system for FRET-FLIM measurements at the single bacterial cell level (Figure 5). In the top part of Figure 5 cells with coupled fluorophores, cells with uncoupled fluorophores or a mix of cells with coupled and uncoupled fluorophores were false-colored with a look-up-table from the LI-FLIM software. Using a MatLab script for automated cell sorting, these cells were categorized into two groups based on fluorescence lifetime values; cells

with short lifetime were false-colored cyan and with long lifetime were false-colored magenta; threshold value was set to 2.3 ns (Figure 5A 2-C2). This script was also used to make a fluorescence lifetime based histogram (figure 5D). The histogram confirms that the cells from Figure 5C 2 contained cells with short and long fluorescence lifetime. This showed that the MEM-FLIM prototype allows single bacterial cell FLIM and can resolve inter-individual fluorescence lifetimes.

Table 7. The FRET efficiency E_a of the different FRET pairs, measured with FLIM. The fluorescence lifetime of GFP_only is 2.56 ns. The fluorescence lifetimes shown here are calculated with the LI-FLIM software from the average of all pixels in five regions of interest filled with a monolayer of cells.

	Fluorescence lifetime (ns)		
	Donor-Acceptor covalently bound	Donor-Acceptor Cleaved by protease	E_a
GFP-mCherry	2.37 +/- 0.03	2.47 +/- 0.01	0.04
GFP-mKate2	2.24 +/- 0.02	2.51 +/- 0.03	0.11
GFP-tagRFP	2.22 +/- 0.02	2.51 +/- 0.01	0.11

Discussion

Intermolecular FRET analysis allows *in vivo* examination of protein-protein interactions. It has been successfully applied for studying the sensor kinases CitA and DcuS in *E. coli* [172] and the Fts division proteins in *E. coli* [2]. The proteins from the competence machinery in *B. subtilis* have been studied via acceptor photo bleaching [106] and the chemotaxis pathway in *E. coli* has been studied extensively with acceptor photo bleaching as well [94], but acceptor photo bleaching does not allow examination of the dynamics.

Here we studied which FRET-pair would be a suitable candidate for *in vivo* FRET analysis in *B. subtilis*. FRET detected via sensitized emission showed that, out of the pairs tested, the GFP-tagRFP pair is the best candidate for FRET purposes in *B. subtilis*, based on the relative brightness and the quantum yield of tagRFP (see also results section). Earlier work showed the suitability of GFP-tagRFP and GFP-mCherry FRET-pairs in HeLa cells [158,185]. However, the observed FRET efficiency in *B. subtilis* is low for GFP-mCherry using both sensitized emission and FLIM (Table 5 and 7), despite the fact that the spectral overlap between GFP and mCherry is high as well as the fluorescence intensities. In case of sensitized emission the low FRET efficiency for the GFP-mCherry combination could also be the result of the calculation method used in our study (equation 6). Division by A – the acceptor fluorescence intensity – results in lower FRET efficiency for GFP-mCherry, because A is much higher for GFP-mCherry than for GFP-tagRFP or GFP-mKate2 (Table 6). However, FLIM

measurement data is independent of intensities and the FRET-FLIM data confirms the data from the sensitized emission experiments (Table 5 and 7). In both cases GFP-mKate2 and GFP-tagRFP are the best two FRET pairs.

GFP-mCherry is often used as a FRET pair in interaction studies with high FRET efficiencies. In this study it might be that the properties of the linker prevent proper orientations of both fluorophores resulting in poor FRET efficiencies for this FRET-couple. FRET efficiency is dependent on three criteria for obtaining FRET. Of those criteria only the spectral overlap is independent of the construct used. The fluorophore distance and relative orientation of the donor and acceptor molecules depend on the linker sequence. Therefore, the FRET efficiencies reported here reflect the situation with the TEV-protease cleavable linker. FRET-efficiencies in earlier work range from 4 to 46% [2,106,172,212].

Individually, the fluorescent proteins are efficiently produced (Table 6) and, when linked together, the GFP-tagRFP pair has the highest FRET efficiency. The benefit of red-shifted FRET-pairs is in accordance with earlier work [66,185], and one possible explanation is the larger Förster radius [66].

The FRET-FLIM set-up used here allows measurements of FRET-efficiency on a single bacterial cell level (Figure 5). This shows the potential of this system to study the dynamics in protein-protein interactions. At this point, the prototype CCD-sensor has limited sensitivity, only allowing single bacterial cell FLIM with highly expressed FRET pairs and is therefore not yet widely applicable for studies in bacteria. However, when fusion proteins are put under control of strong promoters, relevant data might be obtainable, even for normally low-expressed proteins. Alternatively, improved systems could be incorporated in existing microscopy set-ups allowing fast FRET readouts during e.g. time lapse microscopy or microfluidic experiments for the study of protein-protein interaction dynamics.

Chapter 4

Probing the dynamics of CcpA HPr interactions in *Bacillus subtilis* by FRET

Ruud G.J. Detert Oude Weme and Oscar P. Kuipers.

Abstract

Protein complexes have been suggested to be the prokaryotic equivalent of organelles. Studying protein-protein interactions at the single cell level will give more insight into the heterogeneity of those interactions.

In this study the dynamics of the interaction between CcpA and HPr was investigated. CcpA and HPr proteins were labeled with GFP and tagRFP, respectively, and Förster Resonance Energy Transfer (FRET) was used to study their interaction. FRET was detected both via sensitized emission and FRET-FLIM, however, detectable interaction between CcpA and HPr could not be observed with the applied methods. This could be due to the ratio of CcpA:HPr in the cells, which is probably outside the range of 1:10 or 10:1 so the FRET signal can get lost in the background. It could also be the result of the linker that was used to fuse the proteins with the fluorescent proteins; the linker might not bring the fluorophores in close proximity or in proper orientation. Future experiments with a more sensitive FLIM device will make it possible to study protein-protein interactions at the single cell level. Also, the heterogeneous character of the protein-protein interactions can be examined. Here, using a spectrum scan on the culture level, we could show that CcpA and HPr interact only during the exponential part of the growth phase. As suggested before, this observation confirms that CcpA and HPr ensure a rapid growth of the bacterium because it helps to make efficient use of nutrients.

Introduction

Bacteria have been seen as vesicles without internal structural organization for a long time, but due to the crowded macromolecular environment in cells, a high level of organization is expected and has indeed been observed [18,111,116,211].

Many proteins in the cytoplasm localize to specific areas within the cell [111], by a so-called diffusion-and-capture mechanism [116]. However this has mainly been shown for cell-pole located proteins. Besides protein localization, also protein-protein interactions are important, and in the crowded cell associations between molecules are ubiquitous [138,140]. A large number of protein-protein interactions in *Bacillus subtilis* were found by using the Yeast-two-hybrid (Y2H) technique, where on average five interactions per protein have been found [131]. Furthermore, the existence of a higher-scale physical protein-protein interaction in *B. subtilis*, termed the TCA-cycle metabolon, was shown by both crosslinking of proteins with formaldehyde for affinity pull-down followed by identification via mass spectrometry, and by applying a bacterial-two-hybrid system [138].

Gram positive bacteria like *B. subtilis* employ a mechanism called carbon catabolite control (CCC) to ensure the prioritized usage of preferred carbon sources, such as glucose, when different carbon sources are present [63,70]. CcpA and HPr are the main proteins in controlling CCC in Gram-positive bacteria (see also chapter 5). The metabolite fructose-1,6-bisphosphate is an intermediate of glucose metabolism that triggers HPrK/P to phosphorylate HPr on Ser46. HPr-Ser46-P then forms a complex with CcpA, which binds to specific DNA sites called catabolite responsive elements (*cre*) [180]. When the *cre* site is located upstream of the promoter, gene expression will be upregulated, whereas gene expression will be repressed when the *cre* site is located downstream of the promoter. The first evidence for the interaction between CcpA and HPr in *Bacillus megaterium* [46], underlined that HPr must be phosphorylated on the Serine46 in order to interact with CcpA. The same study revealed that fructose-1,6-bisphosphate (FBP), fructose-1-phosphate (F1P) and glucose-6-phosphate (G6P) enhance CcpA and HPr complex formation [46]. *In vitro* studies using Surface Plasmon Resonance (SPR) in *B. megaterium* and *B. subtilis* showed that CcpA binding to a *cre* site increases 50-fold when HPr-Ser46-P is added [9,180]. While the first structure of the CcpA-HPr-Ser46-P complex has been solved without the DNA binding domain of CcpA from *B. megaterium* [179], the structure of the full complex was resolved later for *B. subtilis* [176]. Interestingly, the interaction between CcpA and HPr was not detected in the previously mentioned Y2H study [131].

The aim of this study was to resolve the interaction of CcpA and HPr in live cells over time. Therefore, the genes coding for GFP and tagRFP were fused downstream to the genes coding for CcpA and HPr at their native locus with their native promoter (C-terminally, based on the crystal structure because both C-termini are freely available at the side of the complex (Figure 1A, [176])). The native promoter was used to ensure naturally occurring copy numbers of the proteins. The resulting proteins were fluorescently labeled: CcpA-GFP and HPr-tagRFP. Förster Resonance Energy Transfer (FRET, see also chapter 2 and [160]) was used to examine the protein-protein interactions. FRET was detected via sensitized emission and FLIM (chapter 2).

CcpA and HPr were expected to show an interaction when the cells were grown on a glucose supplemented medium and no interaction was expected when the cells were grown on a ribose supplemented medium as ribose is not a CCC activating sugar [188]. However, using both FRET detected via sensitized emission and FRET-FLIM, we could not detect this interaction on any of these media.

Materials and methods

Bacterial strains, plasmids, oligonucleotides, and growth conditions

All strains, plasmids, and oligonucleotides used here can be found in Table 1, Table 2, and Table 3. *Escherichia coli* MC1061 was used as an intermediate host for cloning. All strains were grown on Lysogeny Broth (LB) for cloning, and on Spizizen's Minimal Medium (SMM) with 0.5% glucose and trace elements for protein-protein interactions experiments, this medium will be called Chemically Defined Medium (CDM) from here on [77]. Spectinomycin (Sigma) was used at a final concentration of 100 µg/ml in LB, chloramphenicol (Sigma) at a final concentration of 5 µg/ml in LB, and kanamycin (Sigma) at a final concentration of 10 µg/ml in LB.

Recombinant DNA techniques

Standard lab routines like PCR, DNA purification, restriction and ligation were done as described previously [171]. Phusion DNA polymerase, Fast Digest Restriction enzymes, and T4 DNA ligase were obtained from ThermoScientific (St. Leon-Rot, Germany). PfuX7 DNA polymerase [154] was a gift from Bert Poolman's lab (University of Groningen). USER enzyme was obtained from New England Biolabs. The PCR purification kit and the plasmid isolation kit were from Roche.

Construction of strains with fluorescently labeled CcpA and HPr

USER cloning [154] was used to construct the CcpA-GFP and HPr-tagRFP translational fusions. Therefore, the genes *ccpA* and *ptsH* coding for CcpA or HPr, their respective flanking regions, the gene coding for the fluorophore and the gene coding for antibiotic resistance were cloned into the pUC18 plasmid. The GFP coding sequence was cloned in frame with *ccpA* in the native locus of the *B. subtilis* genome immediately downstream of the *ccpA* gene to ensure that the C-terminal *ccpA-gfp* fusion product was under control of the native *ccpA* promoter. The following amino acid linker was used to fuse CcpA and GFP: SAGSAAGSGA (DNA sequence: TCGGCTGGCTCCGCTGCTGGTTCTGGCGCA) [223]. For ligation, the following purified PCR products were mixed in equimolar concentrations: *ccpA*, *gfp(Sp)*[155], *spec^r* (from pDOW01, chapter 2), *ytxD*, and pUC18. 1 µl USER enzyme was added to this mixture and ligation was performed in two steps (20 minutes at 37°C and 20 minutes at room temperature). Subsequently, this mixture was transformed to competent *E. coli* MC1061 cells.

The tagRFP (Evrogen) coding sequence was cloned in frame with *ptsH* in the native locus immediately downstream of *ptsH* to ensure that the C-terminal *ptsH-tagRFP* fusion product was under control of the native promoter

of the *ptsGHI* operon. The same amino acid linker as mentioned above was used to fuse HPr and tagRFP. In the ligation reaction, the following purified PCR products were mixed in equimolar concentrations: *ptsGH*, *tagRFP* (from pDOW13, chapter2), *ptsI*, *cam^r* (from pSG1151 [120]), *spIAB'*, and pUC18. 1 μ l USER enzyme was added to this mixture and ligation was performed in two steps (20 minutes at 37°C and 20 minutes at room temperature). Subsequently, this mixture was transformed to competent *E. coli* MC1061 cells. The sequences of the pUC_ccpA and pUC_ptsH plasmids were confirmed by sequencing at MacroGen (Amsterdam, The Netherlands). Naturally competent *B. subtilis* cells were transformed with these pUC-derivatives as described before [77], which integrated in the *B. subtilis* genome at the native locus of *ccpA* or *ptsH* via double homologous recombination. In the resulting strains, the original *ccpA* or *ptsH* gene is replaced by the corresponding gene fusions with either *gfp* or *tagRFP*.

Western blotting

Western blotting was done as described in chapter 2. Anti-CcpA (rabbit serum, [109]) or anti-RFP (rabbit serum, Invitrogen Molecular Probes) antibodies were used for detection of the CcpA-GFP or HPr-tagRFP protein fusions, respectively.

Single cell protein-protein interaction experiments

B. subtilis CcpA-GFP, *B. subtilis* HPr-tagRFP, and *B. subtilis* CcpA-GFP HPr-tagRFP were each streaked on LB agar plates with appropriate antibiotics from -80°C stocks and grown overnight at 37°C. A single colony was taken from the plate to inoculate 3 ml LB with antibiotic and grown for eight hours at 37°C while shaking at 200 rpm. The LB grown culture was diluted 1:1000 into CDM with glucose or ribose as the carbon source and further grown overnight at 37°C while shaking at 200 rpm. After 16 hours, the cultures were diluted to an OD₆₀₀ of 0.08 in 6 ml fresh CDM and grown at 37°C while shaking at 200 rpm. A 100 μ l sample was taken every hour for spectrophotometric determination of the cell density at OD₆₀₀ and simultaneously another 100 μ l sample was 10x concentrated by centrifugation (10,000 rpm, 1min) for protein-protein interaction experiments. These were either performed with the wide-field microscope (Personal DeltaVision) or with the MEM-FLIM system on the Nikon microscope (see chapter 2 for microscope details). Cells were immobilized for microscopy on a 1% agarose slide.

Four pictures were taken for each strain for the FRET detected via sensitized emission: 1. Phase contrast (GFP transmission light), 2. FRET (GFP excitation, mCherry emission), 3. Donor (excitation and emission with GFP filters) and 4. Acceptor (excitation and emission with mCherry filters). The light

exposure time and the light transmission were always kept constant with 0.5s and 32% T, respectively.

Data analysis was done exactly as described in chapter 2. In brief, pixel intensities of the images were measured with ImageJ (<http://rsb.info.nih.gov/ij/index.html>) and background signals were subtracted. The FRET efficiency E_a was calculated as described in chapter 2.

Single cell protein-protein interactions studied with Fluorescence Lifetime Imaging Microscopy (FLIM)

B. subtilis CcpA-GFP and *B. subtilis* CcpA-GFP HPr-tagRFP strains were cultivated as described above. Samples for FLIM experiments were taken from liquid cultures at indicated time points. FLIM experiments with single cells were done as described in chapter 2. Cells from the liquid cultures were concentrated 10 times by centrifugation to do FLIM experiments with a multilayer of cells.

Single cells protein-protein interactions with cells fixed with formaldehyde

B. subtilis strains were cultivated as described above. At indicated time points in the growth curve 200 μ l culture was spun down (5 min, 10,000 rpm) and resuspended in 200 μ l 2% formaldehyde in PBS (fresh made, formaldehyde stock solution from J.T. Baker was stabilized in 10-15% methanol). Subsequently the culture was incubated for 20 minutes at room temperature, spun down again and resuspended in 10 μ l 50 mM PBS (pH 7.0). Subsequently, the strains were used for fluorescence microscopy.

Whole culture protein-protein interaction experiments

The protein-protein interaction experiment was also determined with the BioTek Synergy Mx plate reader. There, the cultivation of the strains was the same as described above, but with the following change: the overnight CDM cultures were grown six hours longer on 37°C while shaking at 200 rpm. Now the strains were diluted 1:50 in 200 μ l fresh CDM with glucose or ribose in a 96 well microplate (polystyrene, flat bottom, Greiner Bio-one, Germany). The plate was loaded in the plate reader, incubated at 37°C overnight and every 30 minutes the OD₆₀₀ was measured, and the GFP was excited at 485 nm followed by a spectrum scan (505-745 nm). This spectrum scan was done for each of the three strains. The fluorescence intensity from the donor only and from the acceptor only strains were subtracted from the donor + acceptor intensity.

Functionality of the CcpA-GFP and HPr-tagRFP protein fusions tested via lacZ activity

A 248 bp promoter region of *ackA* [198] and a 305 bp promoter region of *citZ* (predicted by SoftBerry [194]) were taken from the *B. subtilis* genome by PCR amplification with the primers indicated in Table 3. Purified *ackA* and *citZ* PCR products were restricted with *Sall* and *EcoRI* and ligated into equally restricted *placZ*. Subsequently, these ligation products were transformed to competent *E. coli* MC1061 cells and constructs were confirmed by sequencing at MacroGen (Amsterdam, The Netherlands). Naturally competent *B. subtilis* wild type cells and naturally competent *B. subtilis* CcpA-GFP HPr-tagRFP cells were transformed with either one of the two promoter *placZ* plasmids or with empty *placZ* plasmid as described before [77]. These *placZ* plasmids integrated into the *B. subtilis* genomes at the *amyE* locus via double homologous recombination.

B. subtilis wild type or *B. subtilis* CcpA-GFP HPr-tagRFP strains containing a *Pempty-lacZ*, *PackA-lacZ*, or *PcitZ-lacZ* were inoculated into 3 ml LB with kanamycin and grown overnight at 37°C while shaking at 200 rpm. After 16 hours, each of the six cultures was diluted to an OD₆₀₀ of 0.04 in 5 ml fresh LB medium and grown to early exponential phase (OD₆₀₀ of 0.4). 1 ml culture was harvested by centrifugation (1 min, 10,000 rpm) and immediately used to determine the β-galactosidase activity, measured in Miller units, as described before [88].

Table 1. *B. subtilis* strains used in this study.

Strain	Genotype	Source or reference
<i>E. coli</i> MC1061	F ⁻ <i>araD139 Δ(ara-leu)7696 galE15 galK16 Δ(lac)X74 hsdR2 (r_K⁻m_K⁺) mcrA mcrB1 rpsL (Str^r)</i>	Laboratory stock, [27]
<i>B. subtilis</i>		
168	<i>trpC2</i>	Bacillus Genetic Stock Center, [236]
DOW31	<i>trpC2 ccpA-GFP(Sp) Spec^r</i>	This study
DOW32	<i>trpC2 ptsH-tagRFP Cam^r</i>	This study
DOW33	<i>trpC2 ccpA-GFP(Sp) Spec^r and ptsH-tagRFP Cam^r</i>	This study
DOW34	<i>trpC2 amyE::Pempty-lacZ Kan^r</i>	This study
DOW35	<i>trpC2 amyE::PackA-lacZ Kan^r</i>	This study
DOW36	<i>trpC2 amyE::PcitZ-lacZ Kan^r</i>	This study
DOW37	DOW33 with <i>amyE::Pempty-lacZ Kan^r</i>	This study
DOW38	DOW33 with <i>amyE::PackA-lacZ Kan^r</i>	This study
DOW39	DOW33 with <i>amyE::PcitZ-lacZ Kan^r</i>	This study

Table 2. The plasmids used in this study.

Plasmid	Genotype	Source or reference
pUC18	<i>Amp^r lacZ'</i>	NCBI accession L09136
pUC_CcpA	<i>Amp^r lacZ' ccpA-GFP Spec^r ytxD</i>	This study
pUC_ptsH	<i>Amp^r lacZ' ptsG ptsH-tagRFP ptsI cam^r splAB'</i>	This study
placZ	<i>Amp^r amyE' Kan^r lacZ amyE</i>	Bacillus Genetic Stock Center and [237]
placZ-PackA	<i>Amp^r amyE' Kan^r PackA-lacZ amyE</i>	This study
placZ-PcitZ	<i>Amp^r amyE' Kan^r PcitZ-lacZ amyE</i>	This study

Table 3. Sequences of the oligonucleotides used in this study. Restriction sites are shown in italics.

Oligonucleotide	Sequence (5' -> 3')
pUC18_REV	ATCCCCGGGTUCCGAGCTCGAATTC
pUC18_FW	AGAGTCGACCUGCAGGCATGCAAGCTTGG
CcpA_FW	TACCCGGGAUUTTATGCTTTCTCGTTTATTAG
CcpA_REV	AGCCAGCCGAUGACTTGGTTGACTTTCTAAG
GFPopt_FW+linker	ATCGGCTGGCUCCGCTGCTGGTTCTGGCGCAATGGTTTCTAAAGGT GAAGAATTG
GFPopt_REV	AAGCTTGCUCTTTGTTTTTCTATTATATAACAATTCATCCATACCATGT GTAATAC
spec_FW	AGCAAGCTUCACCTTTATGGTGAACGTAACGTGACTGGCAAGAG
spec_REV	AAGAAGATUACCAATTAGAATGAATATTTT
ytxD_FW	AATCTTCTUGCTTTTTTTCATGGGGAGAAATG
ytxD_REV	AGGTCGACTCUCTAAGCTTCATGTACAGATCCCTTTTTT
ptsG_FW	TACCCGGGAUUTTGGATTCCGATTTGCCATCCGCAAATTTAATC
ptsH_REV	AGCCAGCCGACUCGCCGAGTCTTCGCTTTTC
tagRFP_FW	AGTCGGCTGGCUCCGCTGCTGGTTCTGGCGCAATGTCAGAACTTAT CAAGGAAAATATG
tagRFP_REV	ATTCTTGCATTAUTTATGTCCCAATTTACTAGG
ptsI_FW	ATAATGCAAGAAUTAAAAGGGATTGG
ptsI_REV	AGCGAAAAAUAAAAACCAGACAGGCCGGAGGC
camR_FW	ATTTTTCGCUACGCTCAAATC
camR_REV	ATGAAGCCUTTGAAGTGAAGCTGATAC
splA_FW	AGGCTTCAUAAGTAAGGGTATAGAAGG
splA_REV	AGGTCGACTCUTAGCCTGCTTTTGAACCTTTTAC
ackA_FW_Sall	ACGGGTGACCATGATTGACGCTCCTTTATAC
ackA_REV_EcoRI	ATCTGAATTCACACAAAATACAGAGGGAAAAAC
citZ_FW_Sall	ACGGGTGACCATATATAACATCTCCTTTTCAATAAATTC
citZ_REV_EcoRI	CTCCGAATTCATGCAAAAACCCGCAATAAAG

Results

Expression levels of the CcpA-GFP and HPr-tagRFP proteins

Based on the CcpA-HPr-Ser46-P crystal structure [176], we decided to fuse the fluorescent proteins to the C-termini of CcpA and HPr, because those termini are located freely at the surface of the complex (Figure 1A).

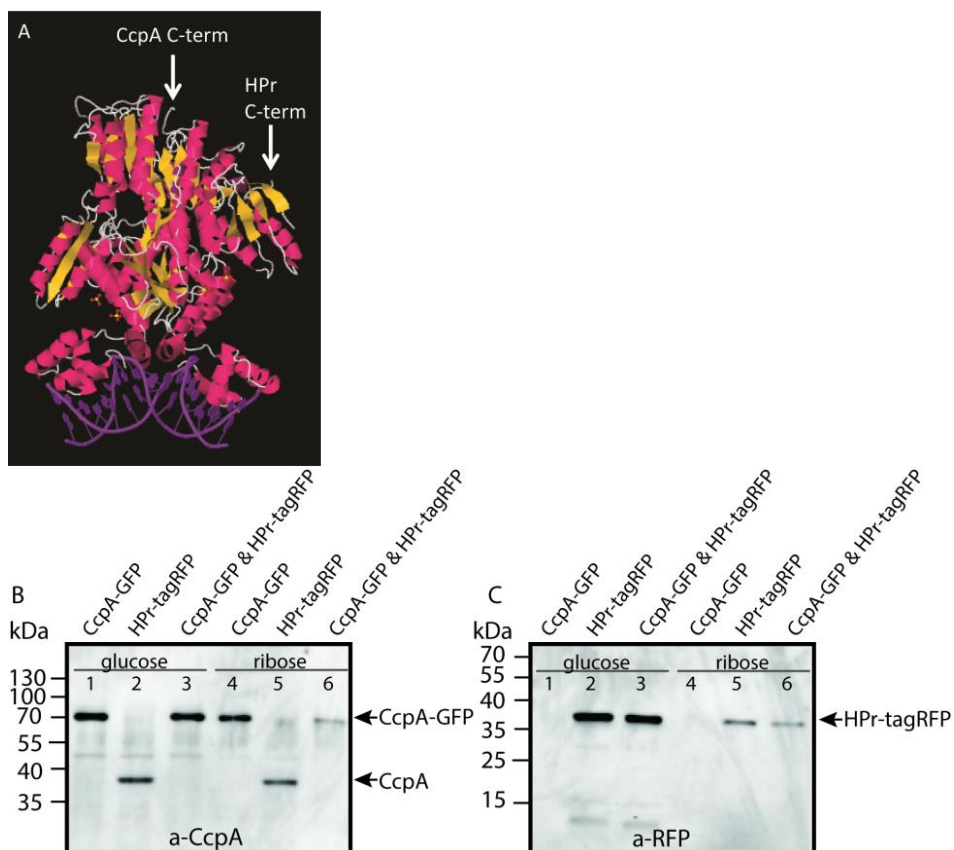


Figure 1. (A) Crystal structure showing the heterodimer of CcpA-HPr-Ser46-P in complex (figure adapted from PDB 3OQM [176]). The fluorescent proteins were fused to the indicated C-termini. **(B and C)** Western Blots showing the protein fusion products CcpA-GFP and HPr-tagRFP in cell free extract of three *B. subtilis* strains carrying the indicated protein fusions. The three strains were grown on CDM with glucose (lane 1-3) or with ribose (lane 4-6) as the carbon source. **(B)** The CcpA-GFP protein fusion was visualized by chemiluminescence with CcpA-antibody. The predicted size for CcpA is 37 kDa and for CcpA-GFP it is 65 kDa. **(C)** The HPr-tagRFP protein was visualized by chemiluminescence with RFP-antibody. Predicted size for HPr is 9 kDa and for HPr-tagRFP it is 36 kDa.

It was expected that fusion of fluorescent proteins at the C-termini would not interfere with complex formation and functionality of CcpA and HPr (see also LacZ activity test in this chapter). The expression levels of CcpA-GFP or HPr-tagRFP in the strains *B. subtilis* CcpA-GFP (strain DOW31), *B. subtilis* HPr-tagRFP (strain DOW32), and *B. subtilis* CcpA-GFP and HPr-tagRFP (strain DOW33) were verified by Western blotting with an anti-CcpA or an anti-RFP antibody. During growth in CDM with glucose or ribose as carbon source, both protein fusions were fully expressed, although the protein copy number on ribose was markedly lower (Figure 1B and C). The native, non-fused CcpA protein was detected in strain DOW32 (lane 2 and 5 in Figure 1B), but unlabeled HPr from strain DOW31 could not be visualized because an HPr antibody was not available (Figure 1C). Taken together, it could be judged that the expression of the desired fusion constructs was successful within the desired strain backgrounds.

CcpA and HPr interactions in live single cells

The protein fusions were found to be correct (Figure 1), so protein-protein interaction experiments were performed. FRET is a promising technique for live cell protein interaction studies because there is no need to fix cells and fluorophore intensities can be measured for continuous intervals of time (see chapter 2 for a FRET introduction and [160]). Thus, the FRET technique was used to study the dynamics of protein-protein interactions of CcpA and HPr.

Three *B. subtilis* strains carrying the CcpA-GFP fusion, the HPr-tagRFP fusion, or the CcpA-GFP plus the HPr-tagRFP protein fusions were grown in CDM with either glucose or ribose as a carbon source. The interaction was measured in the CcpA-GFP plus HPr-tagRFP strain and the other two strains (donor only and acceptor only) were necessary to do corrections to determine the FRET efficiency. Earlier work showed that glucose is the most important sugar for CCC [45,63,70] and that there is almost no CCC when *B. subtilis* is grown on ribose [188]. CcpA and HPr have to interact to perform CCC, thus it was expected to observe an interaction between CcpA and HPr when the strains were grown on CDM with glucose. The experiment with ribose as carbon source served as a negative control where no protein-protein interaction was expected.

An interaction between CcpA and HPr was observed at the beginning of the exponential growth phase when glucose was used as a carbon source (filled squares, Figure 2A). No protein-protein interaction between CcpA and HPr was observed when ribose was used as a carbon source (open squares, Figure 2A), as expected because earlier work already showed that CCC is most active when cells were grown on a preferred sugar [63,70].

However, this CcpA HPr interaction is probably weak under native circumstances in view of the low FRET efficiency. Only one of several attempts resulted in a quantifiable FRET signal (Figure 2A). The experiment was repeated many times; the interaction was examined at various phases during the growth curve (Figure 2C) and also in a CDM medium with glucose plus ribose (Figure 2D). Fluorescence intensities of the separate protein fusions were good (data not shown), but FRET efficiency calculations only yielded efficiencies very close to zero.

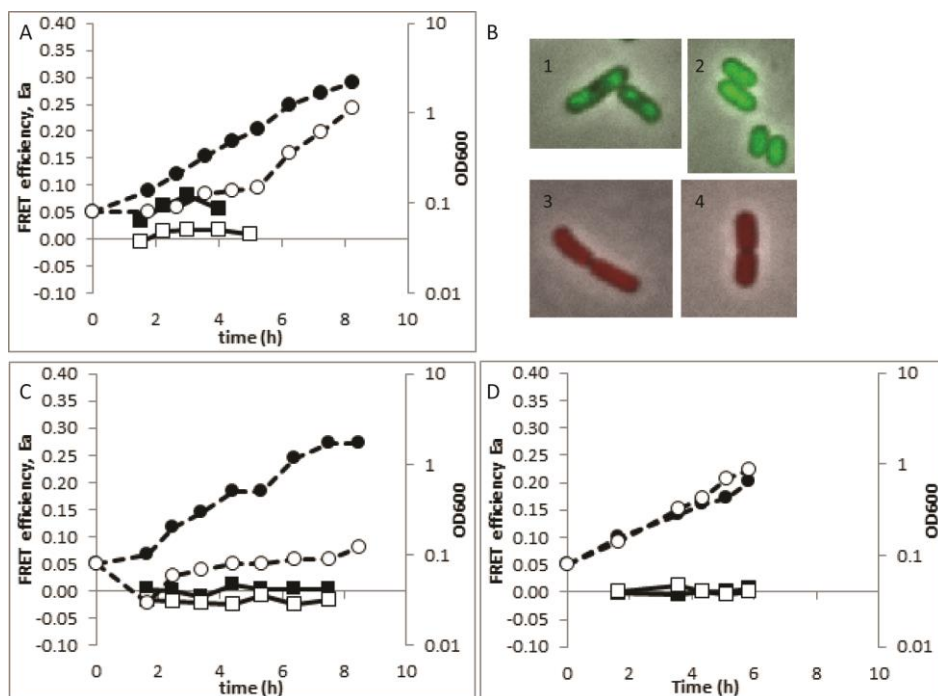


Figure 2. (A) The interaction between CcpA and HPr was represented over time by the FRET efficiency (squares). Protein-protein interaction between CcpA and HPr was observed with glucose as carbon source (filled squares), but not with ribose as carbon source (open squares). The OD₆₀₀ was represented by the circles. **(B)** 1 *B. subtilis* CcpA-GFP on CDM with glucose, 2 *B. subtilis* CcpA-GFP on CDM with ribose, 3 *B. subtilis* HPr-tagRFP on CDM with glucose, 4 *B. subtilis* HPr-tagRFP on CDM with ribose. Image 1 and 2 were false-colored green and image 3 and 4 were false-colored red. **(C)** The interaction experiment from Figure 2A was repeated but the interaction could not be shown again. **(D)** The interaction between CcpA and HPr was measured in CDM with glucose (filled squares) and in CDM with glucose and ribose (open squares) as combined carbon sources.

Fluorescence microscopy indicated that when the CcpA-GFP strain was grown on CDM with glucose the CcpA-GFP localized on the nucleoid (Figure 2B1), but when grown on CDM with ribose the CcpA-GFP was everywhere in the cytoplasm (Figure 2B2). This could be an indication that the CcpA protein is still functional when fused to GFP. HPr-tagRFP localizes in both CDM with glucose or with ribose everywhere in the cytoplasm (Figure 2B3 and 4), as expected because HPr has two functions: it is a phosphocarrier in the EII sugar uptake system and an interaction partner of CcpA.

CcpA and HPr interactions studied with FLIM

The above described FRET detected via sensitized emission is an indirect way to measure protein-protein interactions, because it depends on fluorescence intensities, donor and acceptor ratio, and on the corrections for spectral bleedthrough. Since the FRET results were puzzling, we decided to employ Fluorescence Lifetime Imaging Microscopy (FLIM, see chapter 2 for more details) to examine the interactions. As opposed to FRET detected via sensitized emission, FRET-FLIM is a direct method, in which the fluorescence lifetime of the donor is measured directly and quantitatively. The fluorescence lifetime of the donor (CcpA-GFP in this case) is defined as the time needed to decay to $1/e$ (=37%) of the initial fluorescence intensity directly after excitation. Interaction with an acceptor (in this case HPr-tagRFP) can quench the donor fluorescence: it offers an additional way for the CcpA-GFP to return to the ground state i.e. to decrease the fluorescence lifetime of CcpA-GFP. This difference in CcpA-GFP fluorescence lifetime can be measured with FLIM.

To this end, interaction between CcpA and HPr was studied here with a MEM-FLIM prototype (see chapter 2). Unfortunately, results from single cell measurements showed that the MEM-FLIM prototype was not sensitive enough for reliably determining fluorescence lifetimes for these low copy fluorescent proteins (data not shown). This could be improved by imaging a multilayer of *B. subtilis* cells with the MEM-FLIM device. We were able to measure fluorescence lifetime values, but the difference between samples and the negative controls was statistically not significant (Figure 3).

Though FRET-FLIM was not successfully applied for this study, we could show that this method, at its current developmental stage, only works for induced, high copy proteins (see chapter 2).

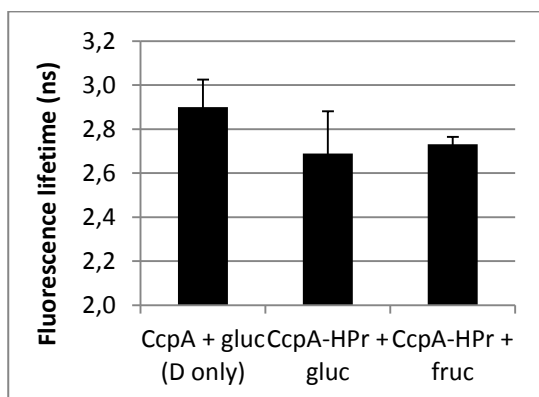


Figure 3. FRET-FLIM was used to examine the interaction between CcpA and HPr. The bars represent the average CcpA-GFP fluorescence lifetime which was measured from a multilayer of cells: in the donor only strain (CcpA-GFP, first bar), and in the strain where also the HPr-tagRFP fusion was present. The strain with the two protein fusions was grown on CDM with glucose (second bar) or on CDM with fructose (third bar).

CcpA and HPr interactions in live cell cultures

After the attempts to study the CcpA HPr interaction on the single cell level, we examined the CcpA HPr interaction on the culture level. Therefore, a spectrum scan from 500-750 nm was done for the three *B. subtilis* strains with a time-interval of 30 minutes while the cells were growing in CDM in a 96-well plate. The GFP emission (maximum at 507 nm) and the tagRFP emission (maximum at 584 nm) are within this wavelength area. The GFP was excited in this experiment and an interaction between CcpA and HPr should result in sensitized emission of the tagRFP. With the plate reader it was technically not possible to record all required images for proper FRET efficiency calculations (see Table 4 in chapter 2). However, a rough estimation of the FRET efficiency could be obtained by subtracting the fluorescence signal of the donor only strain and of the acceptor only strain from the fluorescence signal of the donor + acceptor strain (Figure 4). The observed increase in acceptor emission in Figure 4A is an indication that an interaction between CcpA and HPr occurs. This FRET efficiency estimation differed over time: CcpA and HPr interacted during the exponential phase; from 4 till 10 hours (Figure 4A). The interaction only occurred when the strains were grown on CDM with glucose and not when the strains were grown on CDM with glucose plus ribose or with ribose (Figure 4B and C).

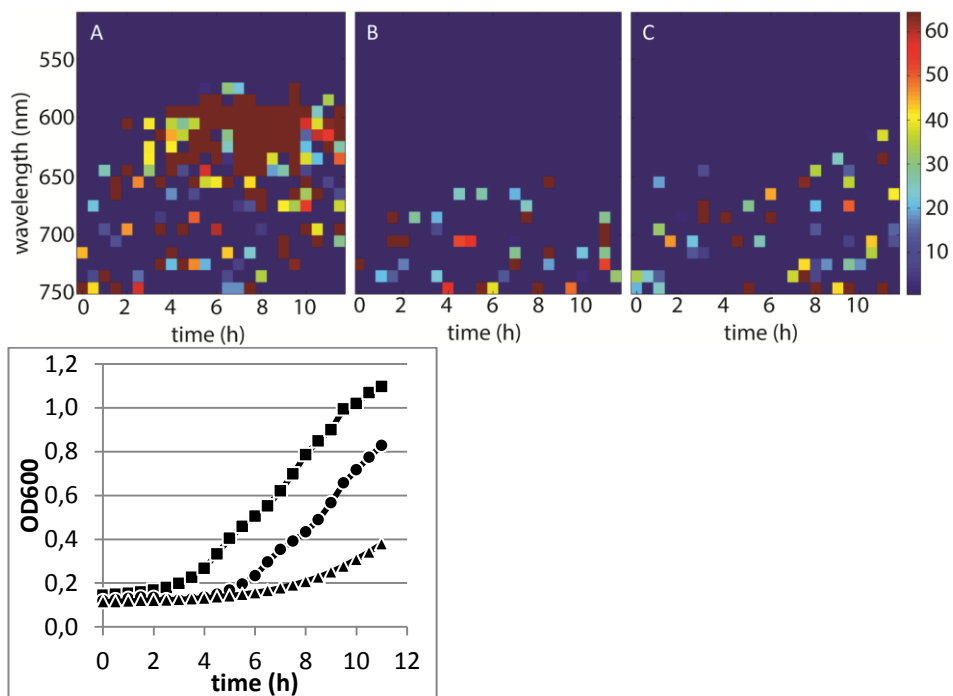


Figure 4. The interaction between CcpA and HPr was studied on the culture level. With a microtiter plate reader a spectrum scan was made from 500-750 nm from the three *B. subtilis* strains. Shown in figure A-C is the fluorescence intensity of *B. subtilis* CcpA-GFP HPr-tagRFP minus the signal from *B. subtilis* CcpA-GFP and minus the signal from *B. subtilis* HPr-tagRFP. All three strains were grown in CDM medium with either (A) glucose, (B) glucose + ribose, or (C) ribose as carbon source. Figure A-C were made in MatLab, the heat map for the fluorescence intensity is shown on the right. (D) The OD₆₀₀ of the *B. subtilis* CcpA-GFP HPr-tagRFP strain (DOW33) on CDM with three different carbon sources; glucose (squares), glucose + ribose (circles), or ribose (triangles).

CcpA and HPr interactions in cells fixed with formaldehyde

One possibility for the fact that interactions could not be observed, might be that the interactions are too short-lived and extremely transient (as suggested by Williamson *et al.* [227]). Incubation of cells in a formaldehyde solution is a common method for cell fixing used for PALM and TIRF microscopy and for pull-down studies to analyze protein interaction partners. Therefore, we fixed the cells with formaldehyde to study the interaction between CcpA and HPr. However, we were not able to obtain significant CcpA HPr FRET efficiencies after cell fixation (data not shown).

Functionality of the CcpA-GFP and HPr-tagRFP protein fusions tested via *lacZ* activity

Earlier work showed that CcpA and HPr need to form a complex for efficient CCC [46,70,180]. Two promoter-*lacZ* fusions were made to test whether CcpA and HPr were still functional when fused to a fluorescent protein. The promoters of these genes (*ackA* and *citZ*) are normally regulated by CcpA [202], so if CcpA-GFP and HPr-tagRFP are still functional then the β -galactosidase activity of these promoter-*lacZ* fusions should be the same as for the unlabeled CcpA and HPr in the wild type strain.

As a positive control, we choose the promoter of the gene coding for acetate kinase *AckA*, which has been reported to be upregulated by CcpA in presence of glucose [198]. However, within the growth conditions used here (LB + 1% glucose), *ackA* up regulation could not be observed for both strains (Figure 5). The β -galactosidase activity was the same for both strains. Additionally, the gene coding for citrate synthase *CitZ*, the entry point of the citric acid cycle, is normally repressed by CcpA in presence of glucose, but the results from our experiments clearly indicated an up regulation (Figure 5). The β -galactosidase activity is more or less the same for both strains. The β -galactosidase activities were not as expected which could be due to the growth condition used here (LB + 1% glucose). It could be that gene regulation by CcpA is more tightly controlled in a minimal medium because there it is more important to make efficient use of the available nutrients (as discussed in chapter 5).

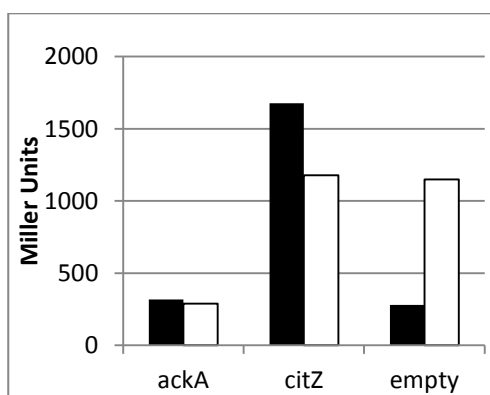


Figure 5. Promoter-*lacZ* fusions to show that CcpA-GFP and ptsH-tagRFP were still functional. *PackA-lacZ*, *PcitZ-lacZ*, and *Pempty-lacZ* fusions in a wild type *B. subtilis* strain (black bars) and in the *B. subtilis* CcpA-GFP HPr-tagRFP strain (white bars).

Discussion

The original goal of this PhD-project was to examine the TCA-cycle interactions, in live cells via FRET, which have been shown already by bacterial two hybrid experiments [138]. In that study it has been shown that malate dehydrogenase (Mdh), citrate synthase (CitZ), and isocitrate dehydrogenase (Icd) form a core metabolon which also interacts with aconitase (CitB) and fumarase (CitG). Based on that study, we made protein-FP fusions of Mdh, CitZ, and Icd with GFP and tagRFP in such a way that each possible interaction between these three enzymes could be studied. However, those interactions could not be shown *in vivo* (data not shown). Williamson *et al.* suggest that metabolons are difficult to study because they are probably very fragile [227]. Other studies also hypothesize on the transient and weak character of such metabolons [38,143]. After our attempts to study the TCA-cycle metabolon *in vivo* we decided to study the dynamics of the interaction between CcpA and HPr *in vivo*, because of the potential of FRET and the successful development of a method to screen whether FP-pairs are good FRET pairs (chapter 2).

This study aimed at resolving the dynamics of the interaction between CcpA and HPr. Therefore, different growth conditions were investigated and different techniques to measure FRET were used. It seems that CcpA and HPr interact most during the beginning of the exponential growth phase to ensure a fast initial growth of the culture (Figure 2A). However, we were not able to reproducibly show the interaction or the dynamics of the interaction between CcpA and HPr in live *B. subtilis* cells.

One possibility to enhance the FRET efficiency could be to determine the functionality and efficacy of the linker used to construct the fusion proteins. In a future experiment where FRET will be used to study protein-protein interactions one should have a close look into which linker will be used to fuse the proteins of interest to a fluorophore in a FRET experiment. Arai *et al.* have studied the FRET efficiency between EBFP and EGFP with 8 different linkers, varying in length from 4 to 30 amino acids (aa), and varying from flexible to α -helical [6]. This resulted in a threefold variation in FRET efficiency, where the 19 aa flexible linker had the highest efficiency and the 30 aa α -helical linker had the lowest efficiency. In that study two fluorescent proteins were fused together with the goal of bringing the fluorescent proteins in the most optimal position for FRET. In this study a 10 aa long flexible linker was used, consisting of SAGSAAGSGA [223], to label CcpA or HPr with a fluorescent protein. The goal here was the same: bring the fluorescent proteins in the optimal position for FRET; thereby enabling the examination of the dynamics of the interaction between CcpA and HPr.

Without doubt, FRET has been proven to be a valuable technique for studying conformational changes of a protein, when both the donor and

acceptor are fused to that protein (intramolecular FRET). But intermolecular protein-protein interactions are difficult to measure, because of intrinsic limitations of FRET. There could be many reasons to explain the lack of significant FRET efficiencies: the crosslinking method, the linker used to fuse CcpA with GFP and HPr with tagRFP; it might be too flexible causing the donor and acceptor fluorophore to be not in the correct orientation or too long so the distance between the donor and acceptor is too large. There is an inverse 6th power relation between the distance and the FRET efficiency [114], so the FRET efficiency decreases rapidly when the distance increases. The copy number ratio of donor (CcpA-GFP) and acceptor (HPr-tagRFP) could also be out of the range for determination of FRET; the ratio should be between 1:10 and 10:1 [160]. If there is an excess of donor or acceptor then it might be difficult to measure FRET because a large amount of the donor or acceptor population is not interacting. According to earlier work HPr is 22x more abundant than CcpA in a glucose and ammonium minimal medium at mid-log and 7x more abundant 1.5 hour after glucose exhaustion [126]. In this study the CcpA : HPr ratio can only be estimated from fluorescence intensities; GFP is 10x brighter than tagRFP (chapter 2, table 5) and CcpA-GFP is 4.5x less bright than HPr-tagRFP (this chapter, data not shown) so the CcpA-GFP : HPr-tagRFP ratio is approximately 1:45. If that ratio is valid under these conditions then the FRET signal cannot overcome the background fluorescence. The copy number of the proteins in a cell could be another reason; more fluorescent proteins means more photons and thus a higher signal to noise ratio. The FRET method is particularly more suitable for eukaryotic cells where protein copy numbers are much higher [98,212].

We advise other researchers who wish to study protein-protein interactions (intermolecular FRET) to do this only when FRET will be detected via FLIM because that is intensity independent and thus not dependent on signal to noise ratios of fluorescence intensities. Furthermore, FLIM is a direct method: the decrease in fluorescence lifetime of the donor caused by interaction with an acceptor, FRET, is directly measured. Researchers interested in studying protein-protein interactions should also check whether the copy numbers of the proteins of interest are similar; within the range 10:1 or 1:10 [160]. The pitfall during this work was that the copy numbers of CcpA and HPr are probably out of this range and that the sensitivity of the MEM-FLIM system was not yet sensitive enough for bacterial cells. However, we foresee enormous potential for an improved, more sensitive MEM-FLIM system to study protein-protein interactions.

Acknowledgements

We would like to thank Dr. Elrike Frenzel (Molecular Genetics, University of Groningen) and Dr. Ákos T. Kovács (Terrestrial Biofilms Group, University of Jena) for critically reading of the manuscript.

Chapter 5

Probing the regulatory effects of specific mutations in three major binding domains of the pleiotropic regulator CcpA of *Bacillus subtilis*

Ruud G.J. Detert Oude Weme¹, Gerald Seidel², Oscar P. Kuipers¹.

¹Molecular Genetics Group, Groningen Biomolecular Sciences and Biotechnology Institute, University of Groningen, Nijenborgh 7, 9747 AG Groningen, The Netherlands.

²Lehrstuhl für Mikrobiologie, Institut für Mikrobiologie, Biochemie und Genetik der Friedrich-Alexander Universität Erlangen-Nürnberg, Staudtstrasse 5, 91058 Erlangen, Germany.

This chapter was published in: Probing the regulatory effects of specific mutations in three major binding domains of the pleiotropic regulator CcpA of *Bacillus subtilis*. 2015. *Front. Microbiol.* 6:1051.

doi: 10.3389/fmicb.2015.01051.

Abstract

Carbon catabolite control is required for efficient use of available carbon sources to ensure rapid growth of bacteria. CcpA is a global regulator of carbon metabolism in Gram-positive bacteria like *Bacillus subtilis*. In this study the genome-wide gene regulation of a CcpA knockout and three specific CcpA mutants were studied by transcriptome analysis, to further elucidate the function of specific binding sites in CcpA. The following three amino acids were mutated to characterize their function: M17(R) which is involved in DNA binding, T62(H) which is important for the allosteric switch in CcpA upon HPr-Ser46-P binding, and R304(W) which is important for binding of the coeffectors HPr-Ser46-P and fructose-1,6-bisphosphate. The results confirm that CcpA was also involved in gene regulation in the absence of glucose. CcpA-M17R showed a small relief of Carbon Catabolite Control; the CcpA-M17R mutant regulates fewer genes than the CcpA-wt and the palindromicity of the cre site is less important for CcpA-M17R. CcpA-T62H was a stronger repressor than CcpA-wt and also acted as a strong repressor in the absence of glucose. CcpA-R304W was shown here to be less dependent on HPr-Ser46-P for its carbon catabolite control activities. The results presented here provide detailed information on alterations in gene regulation for each CcpA-mutant.

Introduction

Gram-negative and Gram-positive bacteria employ a mechanism called carbon catabolite control (CCC) to use carbon sources in a preferential manner [63,70,201]. This mechanism ensures optimal use of the available nutrients and results in a fitness advantage in a natural environment. The Gram-positive bacterium *Bacillus subtilis* uses a global transcriptional regulator, carbon catabolite protein A (CcpA), to employ CCC. Together with the seryl phosphorylated form of the histidine-containing protein, HPr, are the main coeffector for transcriptional regulation of various operons, it is involved in regulation of carbon utilization, overflow metabolism, amino acid anabolism and nitrogen assimilation [45,63,70,196]. HPr is a phosphocarrier protein from the phosphotransferase system (PTS) transferring phosphoryl groups from its histidine 15 residue to EIIA enabling specific sugar transport by EII complexes. The regulatory function of HPr is initiated when a preferred carbon source like glucose is metabolized and the intracellular concentration of fructose-1,6-bisphosphate (FBP) increases. FBP stimulates the HPr kinase/phosphatase (HPrK/P), which phosphorylates HPr at serine 46 and thereby converting HPr into the CcpA-binding form [63,70,177]. Additionally, HPrSer46-P-CcpA complex formation can be stimulated by glucose-6-phosphate (G6P) and (FBP) [63,70]. Moreover, there is a second protein effector: the catabolite

responsive HPr (Crh) that binds CcpA at the same site as HPr-Ser46-P when Crh is phosphorylated at serine 46 by HPrK/P [178]. The binding of HPr-Ser46-P to CcpA triggers an allosteric switch in CcpA allowing CcpA to bind its cognate DNA sequences, the *catabolite responsive elements (cre)* [45,70,201]. These *cre* sites are semi-palindromic sequences with the following consensus: WTGNNARCGNWWCAW (R is G or A, W is A or T, and N is any base)[142,176]. After DNA binding CcpA can either act as a repressor, i.e. when the *cre* site is downstream of the promoter, (Carbon Catabolite Repression, CCR) or, in much fewer cases, as an activator, i.e. when the *cre* site is upstream of the promoter, (Carbon Catabolite Activation, CCA). However, there are also exceptions to this rule: the *cre* site of the levanase operon is upstream of the promoter but it is repressed by CcpA [136]. The expression of 10% of the genes in *B. subtilis* are affected by CcpA when glucose is present in the medium [63], and the expression of 8% of the genes are affected in the absence of glucose [144].

CcpA belongs to the LacI family [82] and consists of an N-terminal DNA binding domain, and a C-terminal core protein containing the HPr-Ser46-P binding site, an effector binding cleft for G6P and FBP and a dimerization domain [176,177]. The crystal structures of *B. subtilis* and *B. megaterium* CcpA-HPr-Ser46-P bound to different *cre* sites and structures of CcpA with FBP and G6P show which amino acids are important for DNA binding, for complex formation, and for coeffector binding [176,177]. Studies of point mutations in CcpA, HPr and Crh have contributed to elucidate the molecular function of several amino acids in the complex [47,86,110,198]. However, differential effects of distinct CcpA point mutations on CCR *in vivo* have also been found. This cannot be explained solely by a comparison of the available structures or interaction analyses because other regulators are also involved in gene regulation of carbon metabolism (e.g. regulon specific regulators such as RbsR).

In this study, we examined the regulons of specific CcpA mutants. Therefore, three specific amino acids in CcpA were mutated (Figure 1A) and examined by transcriptome analyses to study the effects on CCC. Two of these mutants, CcpA-M17R and CcpA-R304W, have been shown in a previous study to differentially regulate *gntR*, *xynP*, *alsS* and *ackA* [198]. Interestingly, these mutants are located in different regions: M17 is in the DNA binding domain and contacts the *cre* site specifically, while R304 makes an important contact to the Ser46-P of HPr. The third mutant, CcpA-T62H was found to repress *xynP* very strongly in the absence of glucose (unpublished data). Threonine 62 is the last residue of the allosteric switch domain, mediating the signal of HPr-Ser46-P binding to the DNA binding domain [176]. The aim of the transcriptome analysis presented here was to study the effect of the point mutations on a

genome-wide level and elucidate the mutant specific regulons. Furthermore we examined the presence of specific correlations between the deregulated or regulated genes and altered *cre* site binding. Will all genes and operons be affected equally by a specific mutation in CcpA or are some genes of the regulon more affected than others? This will provide novel insights on the importance of the residues M17, T62, and R304.

Materials and methods

Bacterial strains, plasmids and oligonucleotides

B. subtilis 168 *trpC2* strains (Table 1) were grown on Lysogeny Broth (LB). *E. coli* MC1061 was used as a cloning host. All plasmids are listed in Table 2 and the oligonucleotides in Table 3. The C-medium contains 70 mM K_2HPO_4 , 30 mM KH_2PO_4 , 25 mM $(NH_4)_2SO_4$, 0.5 mM Mg_2SO_4 , 10 μ M $MnSO_4$, 22 mg/l Ferric Ammonium Citrate, 250 μ M L-Tryptophan, and 0.4% (w/v) glucose. C-medium supplemented with glutamate contains 0.03% (w/v) L-Glutamate and when it was also supplemented with branched chain amino acids it contained 0.25% (w/v) L-Isoleucine, 0.25% (w/v) L-Leucine, 2.5% (w/v) L-Valine, and 2.5% (w/v) L-Methionine. Uridine 5'-monophosphate (Sigma) was added to C-medium in a final concentration of 20 mg/l.

Recombinant DNA techniques

PCR and DNA purification were done as previously described [171]. Pfu7 DNA polymerase [154] was a kind gift from Bert Poolman (University of Groningen), USER enzyme was obtained from New England Biolabs. Sequencing was done at MacroGen (Amsterdam, Netherlands).

Construction of *B. subtilis ccpA::spec*

The *B. subtilis ccpA* knockout strain was made by allelic replacement with a spectinomycin resistance gene. Therefore, 1000 bp flanking regions of *ccpA* were amplified from the *B. subtilis* genome by PCR. The first flanking region was upstream of *ccpA* (primers *aroA_FW* and *aroA_REV*) and the second flanking region was downstream of *ccpA* (primers *ytxD_FW* and *ytxD_REV*). PCR with Pfu7 as polymerase was also used to amplify pUC18 and the spectinomycin gene from pDOW01 [43] (see the primers in Table 3). Cloning of the DNA fragments (pUC18, *aroA*, *spec^r*, *ytxD*) was done using the uracil-excision DNA engineering method [154]. The ligation product, hereafter called pUC18- Δ *ccpA*, was transformed to *E. coli*. Plasmid sequence was confirmed by sequencing.

Natural competent *B. subtilis* [77] was transformed with pUC18- Δ *ccpA*, which integrated into the native locus of *ccpA*, thereby replacing the *ccpA* gene by a spectinomycin^r gene (strain DOW41 in Table 1). In the resulting *ccpA*

knockout strain the region from 223 bp upstream till 1037 bp downstream of the *ccpA* translational start site was knocked out; the promoter and the *ccpA* gene were deleted.

Colony PCR and PCR on isolated chromosomal DNA (with primers: *spec_FW*, *spec_REV*, *ccpA_FW_check*, *ccpA_REV_check*) were used to check whether the plasmid was inserted via double recombination and whether the *ccpA* gene was removed.

Construction of the *ccpA* mutant strains

All previous analyses of the CcpA mutants were done with C-terminally His-tagged CcpA, but the His-tag free plasmid pWH2422 was used here to rule out side-effects resulting from a His-Tag fused to CcpA. This plasmid carries wildtype *ccpA* without a His-tag encoding region under control of its own promoter and a lambda terminator downstream of the gene. For this purpose wildtype *ccpA* was amplified from plasmid pWH144 [86] using the primer *ccpAmut1* and *Blplin*, restricted with *XbaI* and *BlpI* and cloned into pWH144 yielding pWH2422. The plasmid pWH2422-*ccpA*-R304W was cloned analogously with a PCR fragment using the primer *ccpAmut1* and *Blplin* with the template pWH920 [198] carrying the mutant allele *ccpA*-R304W. Plasmids pWH2422-*ccpA*-M17R and pWH2422-*ccpA*-T62H were subcloned in pWH2422 from pWH1541-*ccpA*-M17R [198] and pWH144-*ccpA*-T62H via the restriction sites *XbaI* and *Clal*. Plasmid pWH144-*ccpA*-T62H was isolated from a plasmid pool of a randomization of T62. The randomization was done by a two-step PCR mutagenesis using the primers *ccpAmut1*, *BsuT62rand* and *hisbam*.

Natural competent *B. subtilis ccpA::spec* (strain DOW41 in Table 1) cells were transformed with the resulting pWH2422-*ccpA* mutant plasmids as described before [77], and plated on LB-agar plates supplemented with 2 µg/ml erythromycin. Colonies were checked for plasmid integrity with primers pUP19 and pRev19.

DNA Microarray analyses

Lysogeny Broth (LB), supplemented with 2 µg/ml erythromycin when necessary, was inoculated with *B. subtilis 168 trpC2* strains from -80°C and grown overnight at 200 rpm at 37°C. Next morning, the cells were diluted to an OD₆₀₀ of 0.04 in fresh LB with 2 µg/ml erythromycin and 1% (w/v) glucose and grown at 200 rpm and 37°C until the OD₆₀₀ was 0.3. Now 100 ml of cell culture was harvested by centrifugation (6000 rpm, 5min) and used for RNA isolation. Cell pellets were resuspended in 400 µl TE (DEPC) buffer, and transferred to screw-cap tubes with 0.5 g glass beads (<106 microns, Sigma), 50 µl 10% SDS and 500 µl phenol/chloroform:IAA (a 1:1 pre-made mixture of phenol acid and chloroform:IAA (24:1); from this mixture the organic phase

was used). The screw-capped tubes were placed in a bead beater for two times one minute to lyse the cells. Total RNA was isolated with the High Pure RNA Isolation Kit (Roche). The RNA concentration was measured with the NanoDrop (ND-1000 spectrophotometer, NanoDrop Technologies) and the quality was checked on a 1% agarose gel supplemented with 1% bleach.

Superscript III Reverse Transcriptase (Invitrogen) and 20 μg of total RNA were used for cDNA synthesis as described before [125]. Aminoallyl labeled cDNA was labeled with DyLight550 or DyLight650 (ThermoScientific). Now cDNA from *B. subtilis ccpA*-wt cells and cDNA from *B. subtilis ccpA*-mutant cells were mixed in a 1:1 ratio and hybridized overnight on home-made DNA microarray aminosilane glass slides [125]. Hybridization of cDNA on home-made slides was done three times with cDNA from three independent experiments, and the third time the dyes were swapped (see the NCBI GEO submission GSE69575 for details).

Slides were washed, dried and scanned with a GenePix 4200AL scanner (Axon Instruments, CA, USA). The images of the scans were analyzed with ArrayPro4.5 (Media Cybernetics Inc., Md, USA)

Further analysis was done with PrePrep [215], Prep, PostPrep and Cyber-T [214] as described before [125,132].

Bayes p-values were used to calculate the significance and average spot intensity values were used to calculate the fold change of gene expression as described before [123,132]. Results shown here are the average of two biological replicates and a technical replicate (dye-swap). Only genes with a Bayes p-value smaller than 0.001 and a fold change larger than 1.7 or smaller than -1.7 were used for further analysis.

The microarray data is available at the NCBI GEO database (<http://www.ncbi.nlm.nih.gov/geo/>) under accession number GSE69575.

Western Blotting

B. subtilis cells harboring the plasmids with a *ccpA* mutant were grown as described above. Two milliliters of cells were harvested by centrifugation (5min, 10,000 rpm) at an OD_{600} of 0.3. The pellets were resuspended in 200 μl 50 mM Tris-Cl pH 7.4, a spatula tip of glassbeads (<106 microns, Sigma) was added and subsequently cells were lysed by mini-bead beating (two times one minute, Mini-Beadbeater-16, Biospec products). After centrifugation (5min, 10,000 rpm) the supernatant was transferred to a clean tube. Total protein was measured with the DC Protein Assay (Bio-Rad) to ensure that equal amounts of protein were used. 30 μl of 2x SDS loading buffer was added to 20 mg of total protein in a volume of 30 μl and heated for five minutes at 90°C before loading on a 12% SDS-PAGE gel. After electrophoresis, the proteins were transferred to a PVDF membrane (60 minutes, 80 mA). The PVDF

membrane was incubated in PBST + 5% (w/v) skim milk at 4°C overnight. Next morning, the PVDF membrane was washed three times ten minutes with PBST and subsequently incubated at room temperature for two hours in PBST + 5% skim milk + 1:10,000 dilution of anti-CcpA antibody [109]. The membrane was again washed three times ten minutes with PBST and then incubated 1.5 hour in PBST + goat-anti-rabbit Ig-horseradish peroxidase (Amersham Biosciences) at room temperature. Now the membrane was washed two times ten minutes with PBST. 2 ml of ECL detection reagent (GE Healthcare) and the Molecular Imager ChemiDoc XRS+ (Bio-Rad) were used for signal visualization.

Table 1. *B. subtilis* strains used in this study.

Strain	Genotype	Source or reference
<i>E. coli</i> MC1061	F ⁻ <i>araD139</i> Δ (<i>ara-leu</i>)7696 <i>galE15 galK16</i> Δ (<i>lac</i>)X74 <i>hsdR2</i> (<i>r_K⁻m_K⁺</i>) <i>mcrA mcrB1 rpsL</i> (Str ^r)	Laboratory stock, [27]
<i>B. subtilis</i>		
168	<i>trpC2</i>	Bacillus Genetic Stock Center, [236]
DOW41	<i>trpC2 ccpA::spec^r</i>	This study
DOW42	DOW41 with <i>pHT304</i>	This study
DOW43	DOW41 with <i>pWH2422-ccpA-wt</i>	This study
DOW44	DOW41 with <i>pWH2422-ccpA-M17R</i>	This study
DOW45	DOW41 with <i>pWH2422-ccpA-T62H</i>	This study
DOW46	DOW41 with <i>pWH2422-ccpA-R304W</i>	This study

Table 2. The plasmids used in this study.

Plasmid	Genotype	Source or reference
pUC18		NCBI accession number L09136
pUC18- Δ <i>ccpA</i>	Amp ^r <i>aroA Spec^r ytxD</i>	This study
pHT304		[7]
pWH144- <i>ccpA</i> -T62H	pHT304 <i>ccpAhis</i> T62H	This study
pWH2422- <i>ccpA</i> -wt	pHT304 <i>ccpA</i>	This study [7]
pWH2422- <i>ccpA</i> -M17R	pHT304 <i>ccpA-M17R</i>	This study
pWH2422- <i>ccpA</i> -T62H	pHT304 <i>ccpA-T62H</i>	This study
pWH2422- <i>ccpA</i> -R304W	pHT304 <i>ccpA-R304W</i>	This study

Table 3. The oligonucleotides used in this study.

Oligonucleotide	Sequence (5' -> 3')
pUC18_FW	AGAGTCGACCUCCAGGCATGCAAGCTTGG
pUC18_REV	ATCCCCGGGTUCCGAGCTCGAATTC
spec_FW	AGCAAGCTUCACCTTTATGGTGAACGTAACGTGACTGGCAAGAG
spec_REV	AAGAAGATUACCAATTAGAATGAATATTTTC
ytxD_FW	AATCTTCTUGCTTTTTTTCATGGGGAGAAATG

<i>ytxD</i> _REV	AGGTCGACTCUCTAAGCTTCATGTACAGATCCCTTTTTTG
<i>aroA</i> _FW	TACCCGGGGAUAAAAAACCCCTTGAACATTG
<i>aroA</i> _REV	AAGCTTGCUAACGAGAAAGCATAAAAAAAG
<i>ccpA</i> _FW_check	GACGGCATCGTGTTTATGGG
<i>ccpA</i> _REV_check	TCTATACGGTGCGGCAGTTC
pUP19	ATTAAGTTGGGTAACGCCAG
pRev19	TCGTATGTTGTGTGGAATTG
<i>ccpA</i> mut1	ATAATATCTAGAACCAAGTATACGTTTTTCATC
Blplin	ATAATAATAGCTCAGCTTATGACTTGGTTGACTTTCTAAG
BsuT62rand	ACCTACAGTSNNTGTTTTTTT
hisbam	TATTATTATGGATCCTTAGCTTCCTTAGCTCCTGA

Results

Expression levels of the CcpA mutant proteins

The expression levels of the different CcpA proteins were verified by Western blotting with anti-CcpA antibody before starting with the transcriptome analysis. Therefore, cell free extracts from *B. subtilis* harboring the plasmids with the *ccpA* mutants were loaded on a SDS-PAGE gel, transferred to a membrane and incubated with anti-CcpA antibody (Figure 1B). The DC Protein Assay (Bio-Rad) was used to measure the total protein concentration in the cell free extract; this was used to ensure loading equal amounts of total protein on the gel. The *ccpA* on the pWH plasmid was expressed under the control of its native promoter, but despite the low copy number of the plasmid the amount of CcpA was higher than in wildtype *B. subtilis* (Figure 1B). The increase in CcpA expression from this plasmid has been observed before [198]. The expression of the CcpA mutants from plasmid were all very similar, so the observed changes in gene expression in the microarray are most likely due to the mutation in CcpA and not due to changes in the expression level. No CcpA was detected in the *ccpA* knockout strain, indicating the successful removal of the gene (Figure 1B). An unspecific band around 45 kDa was observed for all variants, which was not related to CcpA because it was also visible in the knockout strain and not related to the inserted plasmid because it was also visible in the wildtype strain.

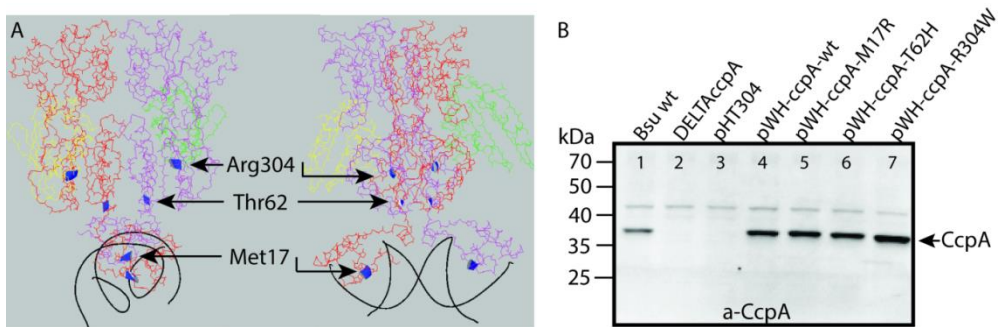


Figure 1. (A) The crystal structure of CcpA-HPr-Ser46-P in complex with *the AckA2-cre* site, viewed along the DNA (left) and perpendicular to the DNA (right). The two CcpA monomers were shown in red and purple, the two HPr-Ser46-P monomers were shown in yellow and green, and the DNA was shown in black. The amino acids that were mutated in this study were highlighted in ribbon style in blue (adapted from PDB 3OQM [176]). **(B)** The expression levels of the different CcpA mutants were shown on a Western Blot. Crude extracts of the *B. subtilis* strains with the different *ccpA* mutants were loaded on gel, transferred to a membrane and the CcpA proteins were visualized via chemiluminescence with a CcpA specific antibody. The size of the CcpA protein was 37 kDa. CcpA in lane 4-7 was expressed from plasmid. The *B. subtilis ccpA::spec* strain was utilized in lane 2-7, and complemented with *ccpA* on the indicated pHT304 derived plasmid. The empty pHT304 vector served as negative control.

The effects of the CcpA knockout and of the point mutations in the CcpA protein (M17R, T62H, or R304W) were studied on the transcriptome level at the early exponential growth phase (OD₆₀₀ of 0.3) and always compared to the transcriptome of *B. subtilis pWH-ccpA-wildtype*. All strains were grown in LB, either in the presence or absence of 1% glucose. Our goal was to study whether all genes of the regulon will be up- or down regulated equally or in a differential way. The results will be presented for each mutant separately in the sections below.

The gene regulation of CcpA knockout compared to wildtype CcpA

The *ccpA* knockout strain had an altered gene regulation for 216 genes when the strain was grown in LB + 1% glucose (Table 5, supplementary file, sheet1&2). There is a large variety in the fold changes between the differentially regulated genes, confirming that the strength of transcriptional activation or repression by CcpA differs for each regulon. The expression of 189 of these genes was upregulated, confirming that CcpA mainly functions as a repressor. 61 of these 216 genes were members of the originally annotated CcpA regulon which consists of 213 genes [128,202]. The CcpA regulon as listed in SubtiWiki has been compiled from different papers (personal communication with Jörg Stülke, Göttingen, Germany) and might also contain

indirectly regulated genes. Categorizing these 216 genes into COGs showed that most genes were from the groups Energy production and conversion and Carbohydrate transport and metabolism (Figure 3). When the *ccpA* knockout strain was grown in LB then the expression of 89 genes was changed (Table 5, supplementary file, sheet4&5), of which 31 genes belong to the CcpA regulon as listed in SubtiWiki. 55 genes were more abundant now compared to CcpA-wt, showing that CcpA was still active in the absence of glucose because those 55 genes were repressed by CcpA-wt. Most genes can be categorized again in Energy production and conversion and Carbohydrate transport and metabolism (Figure 3). The findings from the *ccpA* knockout strain served as a reference to interpret the results from the CcpA-mutants. Our main questions were: are the CcpA-mutants more or less active in repression or activation than the wildtype? Are all genes affected to similar extents or in a differential way?

The gene regulation of CcpA-M17R compared to wildtype CcpA

Most likely CcpA-M17R lost part of its capacity to repress genes, as can be concluded from the large number of derepressed genes. The gene regulation of the CcpA-M17R mutant differed significantly from the Δ CcpA mutant. Of the genes that were affected by CcpA-M17R 53% differed from the genes that were affected in the Δ CcpA strain (Figure 2A and supplementary file, sheet2). The number of affected genes was smaller (Table 5) indicating that the function of the CcpA-M17R mutant was similar to the CcpA-wt, but with lowered affinity for most binding sites. When the CcpA-M17R mutant strain was grown in LB + 1% glucose the gene regulation for 129 genes (115 up and 14 down) differed from CcpA-wt (Table 5, supplementary file, sheet1&2). Only 27 of these genes belonged to the CcpA regulon from SubtiWiki. Especially genes from COG categories: [C] Energy production and conversion, [R] General function prediction, and [T] Signal transduction mechanisms showed a weaker regulation by CcpA-M17R (Figure 3).

When the CcpA-M17R mutant strain was grown on LB then 67 genes (38 up and 29 down) had a changed gene regulation compared to CcpA-wt (Table 5, supplementary file, sheet4&5). 19 of these genes belonged to the CcpA regulon from SubtiWiki. Mainly genes from COG categories: [C] Energy production and conversion, [G] Carbohydrate transport and metabolism, and [J] Translation, ribosomal structure and biogenesis showed a weaker regulation by CcpA-M17R (Figure 3). The uniquely affected genes for CcpA-M17R in LB with and without glucose are shown in Table 4.

The gene regulation of CcpA-T62H compared to wildtype CcpA

The CcpA-T62 is important for signal transduction from the HPr-Ser46-P interaction interface to the DNA binding domain [176]. CcpA-T62H was found to be a stronger repressor. When the CcpA-T62H mutant strain was grown in LB + 1% glucose then only 9 genes were upregulated, but 50 genes were repressed (Table 5, supplementary file, sheet1&2). Only 5 of these 59 genes were also found in the Δ CcpA strain, the other 54 genes did not have an altered regulation in the Δ CcpA strain (Figure 2A). The uniquely affected genes for CcpA-T62H are shown in Table 4. Genes from COG categories [C] Energy production and conversion, [G] Carbohydrate transport and metabolism, [J] Translation, ribosomal structure and biogenesis, and [P] Inorganic ion transport and metabolism showed a stronger regulation by CcpA-T62H (Figure 3). Only 3 of the 59 genes belonged to the CcpA regulon from SubtiWiki. When the CcpA-T62H strain was grown in LB without glucose then the regulatory effect of CcpA-T62H was even stronger than in LB + 1% glucose (Table 5, supplementary file, sheet4&5). In LB without glucose there were 12 genes up- and 115 genes down regulated (Figure 2B, Table 5, supplementary file, sheet4&5) and 55 of them belonged to the CcpA regulon from SubtiWiki. Genes from COG categories [C] Energy production and conversion, [G] Carbohydrate transport and metabolism, [K] Transcription, [M] Cell wall/membrane/envelope biogenesis, [R] General function prediction only, and [T] Signal transduction mechanisms showed a stronger regulation by CcpA-T62H (Figure 3).

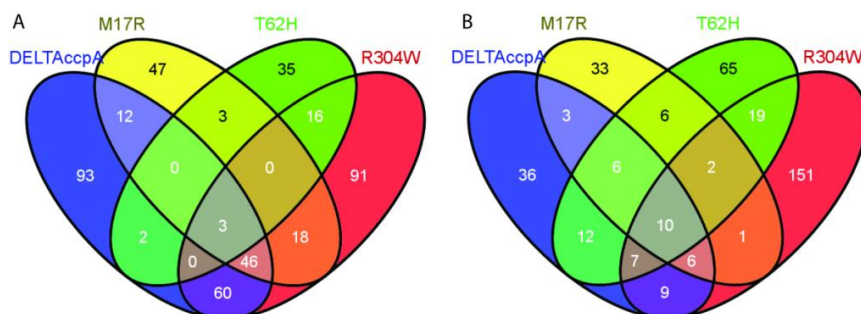


Figure 2. Venn diagram showing the genes that were differentially regulated in each one of the CcpA mutant strains. Numbers represent the genes that were differentially regulated in each CcpA mutant strain. Only genes with a fold change larger than 1.7 or smaller than -1.7 were used in the analysis. **(A)** Overview of the differentially regulated genes when the strains with the CcpA mutant were grown on LB + 1% glucose (see also supplementary file, sheet2). **(B)** Overview of the differentially regulated genes when the strains with the CcpA mutant were grown on LB (see also supplementary file, sheet5). Venn diagrams were made via <http://bioinfo.gp.cnb.csic.es/tools/venny/>. More detailed information on up- or downregulated genes is shown in Table 4.

The gene regulation of CcpA-R304W compared to wildtype CcpA

The arginine on position 304 is important to contact the Ser46-P of HPr. We hypothesized that the CcpA-R304W had a reduced affinity for the glucose sensor protein HPr-Ser46-P but there is still a large number of affected genes (165 up and 69 down) when the strain was grown in LB + 1% glucose. When the CcpA-R304W strain was grown in the absence of glucose the number of affected genes was almost as high; there were 206 genes affected (155 up and 51 down) of which 151 genes were unique for CcpA-R304W (Figure 2A,B, Table 5 and supplementary file, sheet4&5). 59 of the affected genes in LB only belonged to the CcpA regulon from SubtiWiki. The overlap of CcpA-R304W with Δ CcpA is much larger in the presence of glucose (109 genes), than in the absence of glucose (32 genes, compare Figure 2A and B) showing that the HPr dependent gene regulation of CcpA is disturbed, but not the HPr independent gene regulation of CcpA. Therefore, we can conclude that the role of HPr-Ser46-P is less pronounced for this mutant.

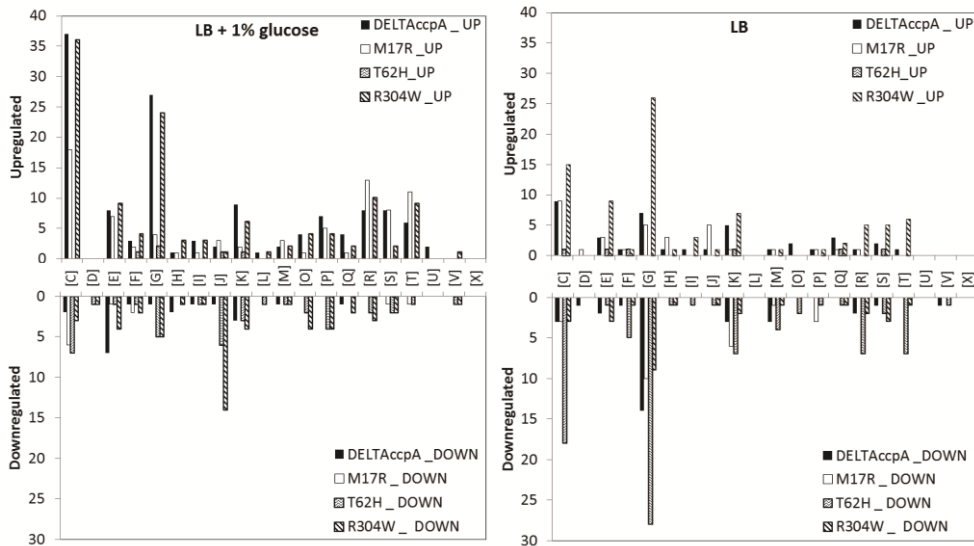


Figure 3. All differently regulated genes were categorized in Clusters of Orthologous Groups (COGs); [C] Energy production and conversion; [D] Cell cycle control, cell division, chromosome partitioning; [E] Amino acid transport and metabolism; [F] Nucleotide transport and metabolism; [G] Carbohydrate transport and metabolism; [H] Coenzyme transport and metabolism; [I] Lipid transport and metabolism; [J] Translation, ribosomal structure and biogenesis; [K] Transcription; [L] Replication, recombination and repair; [M] Cell wall/membrane/envelope biogenesis; [O] Posttranslational modification, protein turnover, chaperones; [P] Inorganic ion transport and metabolism; [Q] Secondary metabolites biosynthesis, transport and catabolism; [R] General function prediction only; [S] Function unknown; [T] Signal transduction mechanisms; [U] Intracellular trafficking, secretion, and vesicular transport; [V] Defense mechanisms; [X] No prediction. Categorization of genes was

done on the MolGen server (<http://server.molgenrug.nl/index.php/functional-analysis>) (see also supplementary file, sheet 9&10).

Table 4. Genes shown here were uniquely up- or downregulated in only one of the CcpA mutants in comparison to CcpA-wt; either in LB + 1% glucose (left side) or in LB without glucose (right side). Up means: these genes are more abundant (i.e. less repressed) in the CcpA-mutant than in CcpA-wt. Down means: these genes are less abundant (i.e. more repressed) in the CcpA-mutant than in CcpA-wt. The numbers refer to Figure 2A and B and represent the number of uniquely up- or downregulated genes per CcpA-mutant.

LB + 1% glucose						LB without glucose						
CcpA-M17R		CcpA-T62H		CcpA-R304W		CcpA-M17R		CcpA-T62H		CcpA-R304W		
47		35		91		33		65		151		
43	4	8	27	42	49	22	11	9	56	112	39	
Up:	Down:	Up:	Down:	Up:	Down:	Up:	Down:	Up:	Down:	Up:	Down:	
citT	glpD	manA	bdbB	acuA	abrB	fliM	cspB	gltC	acoA	abfA	ydzA	alsS
ctc	pyrE	manP	csfB	ald	ahpF	glyQ	dacA	hag	bdbA	acsA	yesL	cgeA
cydA	yckB	manR	dppC	amyE	aroE	hemC	feuA	ilvH	bdbB	amyE	yesM	cotV
cydB	yqjE	pyrC	fhuD	ansB	cspB	icd	flgE	purQ	csbA	araB	yesN	coxA
cydC		yjdF	gudB	bdbA	cspC	lytB	glpP	ydcS	csbC	araD	yfiD	cwdD
gtaB		yjdG	hbs	bofC	ctsR	mdh	pstC	yhfC	csbD	citM	yfiE	leuB
gutR		ynaF	lrpB	dctP	efp	oppD	yaaN	ykoL	dra	csbX	yfiH	leuS
icd		yydJ	nagP	dhaS	fabF	pdhC	yddT	yomL	etfA	cstA	yfmN	nin
ldh			spo0M	drm	frr	pgi	ydff	ywnJ	etfB	ctaD	ygaO	opuE
mcsA			sunA	etfB	ftsH	pgk	ydjM		galT	dctB	yhaS	pta
mcsB			ugtP	hemC	gltP	pgm	yybN		glpF	dctR	yhaX	sigE
mrgA			ycnI	katE	leuD	rplE			gntP	fabHB	yhfW	spolIAC
mrpB			ycnK	kdgK	maeN	rplF			gspA	fbaB	yisK	spoVAA
oppA			yeeG	kdgT	mntH	rpsK			kipR	glpT	yjdB	ssb
phrK			yezE	mmsA	rplQ	rpsS			melA	hutH	ykuN	ybcD
smf			yfhC	narG	rpmB	tpiA			mleA	hxlA	ykzA	ybcH
spo0E			yfmQ	nupC	rpmF	yaaD			mleN	iolC	ykzE	ybcM
treP			yhdN	punA	rpmGB	ykrS			nagP	iolH	yocF	yckE
xpaC			yisQ	qcrA	rpsO	ykrT			ndk	ioll	yocG	ycxC
ydaD			yjbD	qoxB	rpsT	yIbQ			nhaX	kbl	yomT	ydfR
ydaS			yjeA	recO	smpB	yvfV			nupC	kdgA	yomZ	ydjE
ydaT			yjmF	resA	sspE	yvzB			odhA	kdgK	yonE	yesS
ydbD			ylqC	resB	yabR				odhB	kdgT	yonH	yezD

Table 4. continued

LB + 1% glucose				LB without glucose			
CcpA-M17R	CcpA-T62H	CcpA-R304W		CcpA-M17R	CcpA-T62H	CcpA-R304W	
ydhK	yodC	resC	ybaR		pdp	lacA	yonK yfhC
yebE	yoeB	resD	yccG		rpsC	lcfA	yopY yhcA
yfhD	yozB	resE	yceJ		rsbV	malL	yoqF yhcB
yfkJ	yxkO	rocC	yczH		rsbW	mtlR	yoqS yhcC
yhzC		rplF	ydaH		rsbX	pel	yosB yhjB
yjcG		sunT	ydgB		sdhA	phrC	yosD yitJ
ykrS		ydhP	ydgF		sdhB	qcrB	yosJ yjbD
yoqZ		yfiD	ydhB		sunT	qcrC	ypiF yjeA
yoxC		yhfD	yebC		treR	rocB	ypzC yocN
ytiA		yolJ	yfjT		ybyB	rocC	yqaD yodC
ytzE		yoqX	yhbJ		ydaG	sacB	yqcK yqaS
yuaF		ypwA	yhcB		ydhM	senS	yqkK yqbM
yual		yraO	yjhB		ydhT	spolIIAH	yqzG yurO
yuiD		yrkA	ykoA		yfhD	sspO	yraO yurP
yvaA		ysiA	ylaG		yfiT	tyrZ	yrhP yutK
ywfC		ytxE	yodJ		yhaP	xepA	ytcP yvgW
ywmE		yuxI	yqeY		yolJ	xhIB	yteQ
ywzA		ywiE	yqjL		yoxC	xkdH	ytlI
yxiS		ywmA	yrvM		yqhA	xkdK	yugM
yxzF			yuiF		yqhB	xkdN	yugN
			yusG		ysbA	xkdO	yukJ
			yutF		ysbB	xkdT	yulD
			yuzG		ytiA	xkdV	yuxI
			yvsH		ytxJ	xkdW	yvcA
			yvzC		yvdI	xkdX	yvdJ
			ywrK		yvdR	xsa	yveN
					ywiE	xtmB	yvfL
					ywjB	ycbO	yvfM
					ywjC	ycbR	ywdC
					ywql	ycgB	ywmA
					yxal	ycaA	ywsA
					yxiE	ydhN	yxel
					yxnA	ydhS	yxC

Table 5. The number of genes with altered regulation for each mutant compared to CcpA-wt as found in this transcriptomics study. In total, 426 different genes had an altered regulation on LB + 1% glucose and 366 different genes had an altered regulation on LB without glucose (see also Figure 2).

	LB + 1% glucose		LB	
	Up	Down	Up	Down
Δ CcpA	189	27	55	34
CcpA-M17R	115	14	38	29
CcpA-T62H	9	50	12	115
CcpA-R304W	165	69	155	51

Functional analysis of the affected genes

For a more detailed look on the differences between the CcpA mutants all genes with a different regulation were functionally analyzed by categorizing those genes into Clusters of Orthologous Groups (COGs) (Figure 3). When the cells were grown on LB + 1% glucose then genes for energy production and conversion [C] were upregulated in all mutants, except for CcpA-T62H. Expression of genes for carbohydrate transport and metabolism [G] in Δ CcpA and CcpA-R304W showed the most difference. CcpA-T62H and CcpA-R304W showed a down regulation of translation, ribosomal structure and biogenesis genes [J] (Figure 3, LB + 1% glucose). When the cells were grown on LB without glucose then the CcpA-T62H and CcpA-R304W strains had most differences in gene regulation for genes in energy production and conversion [C] and carbohydrate transport and metabolism [G] compared to CcpA-wt (Figure 3).

Growth of the strains with the CcpA mutants on C-medium

A *ccpA* knockout strain shows a growth defect in glucose minimal medium [59,63]. Here we tested how the CcpA mutant strains performed in glucose minimal medium. In the strains with the CcpA mutants, some genes coding for proteins responsible for amino acid catabolism were deregulated. One of them was the gene *rocG* coding for glutamate dehydrogenase. Normally, the *rocG* gene is repressed by CcpA, but in both growth conditions used in this study and in strains with all CcpA variants except CcpA-T62H, the repression of *rocG* was released. Higher levels of RocG decrease the level of glutamate, which impairs the growth of these strains on a glucose minimal medium [63]. The altered gene regulation of *rocG* caused a growth deficiency of the CcpA mutant strains on minimal medium, which was shown on C-medium agar plates for the strains with the Δ CcpA, CcpA-M17R, and CcpA-R304W mutations (Figure 4A). The CcpA-T62H strain still repressed the *rocG* expression and did not have a growth defect (Figure 4A,B). The growth

deficiency of the mutants was almost fully restored to the same extent as CcpA-wt when the C-medium agar plates were supplemented with glutamate, except for CcpA-M17R (Figure 4B) and fully restored when the C-medium agar plates were supplemented with glutamate and branched chain amino acids (BCAA), except for CcpA-M17R (Figure 4C). The growth defect of the CcpA-M17R mutant strain was partially restored by the addition of glutamate (Figure 4B); however the addition of only glutamate was not enough. The remaining growth defect of the CcpA-M17R strain might be explained by the *pyrE* gene. *PyrE* is responsible for pyrimidine biosynthesis [202] and its gene expression was only down regulated in the CcpA-M17R strain. This strain did not show a growth defect in LB because LB is rich in nucleotides from the yeast extract. Therefore the C-medium was also supplemented with uridine 5'-monophosphate in addition to glutamate and BCAA, but the growth defect of the CcpA-M17R mutant strain was not restored (Figure 4D). The residual growth deficiency remains elusive and is probably dependent on more additives.

Examination of *cre* sites for analysis of CcpA-M17R

The methionine on position 17 in CcpA is involved in DNA binding, therefore the sequence of the *cre* site could play a role in the gene regulation by CcpA-M17R. Unfortunately, not all genes affected by CcpA-M17R could be taken into account, because many genes have no *cre* site; they are subjected to indirect control by CcpA [70,124,132]. All known *cre* sites for genes that had an altered regulation in the CcpA-M17R mutant were compared. Genes were grouped into three classes for the analysis; only affected in the Δ CcpA strain, affected in both Δ CcpA and CcpA-M17R, and only affected in the CcpA-M17R strain. The *cre* sequences were analyzed for their palindromic nature, but the differences between the groups of *cre* sites were not clear enough to draw conclusions (see supplementary file, sheet8, Table 1 and 4). Furthermore, the similarity of each group of *cre* sites to the consensus *cre* site was compared but there was no significant difference between all three regulatory groups (see supplementary file, sheet8, Table 1 and 4).

Weblogos for the groups of *cre* sites affected only in CcpA-M17R showed that these *cre* sites had a higher occurrence of G on position 4 and a less defined nucleotide on position 10 (supplementary file, sheet8, table1). The methionine on position 17 was shown to bind to thymine₁₂ in the *ackA* *cre* site [176], and the less defined nucleotide on position 10 found here could mean that the arginine reached further into its surroundings than the methionine.

The consensus *cre* site is W₁T₂G₃N₄N₅A₆R₇C₈G₉N₁₀W₁₁W₁₂W₁₃C₁₄A₁₅W₁₆ and the G₃, C₈, G₉, C₁₄ are most conserved [176]. Seven of the thirteen genes

or operons with a known *cre* site that were affected by CcpA-M17R also had a T on position 12 in the *cre* site, the other six had a C (3x), a G (2x), or an A (1x) on position 12, but those six had a T on position 11 (5x) or position 13 (1x). This finding could mean that the arginine on position 17 in CcpA also contacted a thymine in the *cre* site and that the longer sidechain of arginine could reach further into the surrounding (supplementary file, sheet8, Table 1 and 4).

Sensitivity for extracellular glucose

Earlier work shows that the transport of glucose decreases in a CcpA knockout strain [124]. We hypothesize that a decreased glucose uptake would result in a decreased growth rate. The growth rates of the different CcpA strains were examined on LB + 1% glucose and the Δ CcpA, CcpA-M17R, and CcpA-R304W strains grew a little bit slower than the CcpA-wt strain (supplementary file, sheet12), which could be due to a decreased glucose uptake. The growth of the CcpA-T62H strain was the same as the CcpA-wt strain, which could be explained by the strong repressive mode of CcpA-T62H.

None of the *pts* genes, the glucose permease, or glucose symporter were differently expressed in LB + 1% glucose or in LB in any of the mutant strains, which means that the uptake of glucose was not regulated at the level of gene expression, as shown before [188].

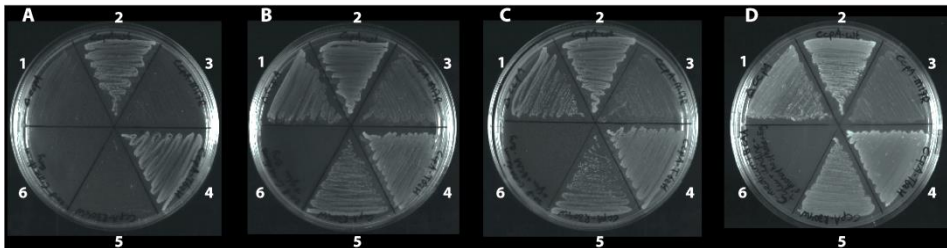


Figure 4. Growth of the strains with the CcpA mutants (A) on C-medium, (B) on C-medium supplemented with glutamate, (C) on C-medium supplemented with glutamate and branched chain amino acids, and (D) on C-medium supplemented with glutamate, branched chain amino acids and uridine 5'-monophosphate. All strains are *B. subtilis* *ccpA::spec* and strain 2-5 have *ccpA* on a plasmid. 1 is Δ *ccpA*, 2 is *ccpA*wt, 3 is *ccpA*-M17R, 4 is *ccpA*-T62H, 5 is *ccpA*-R304W, 6 is empty.

Discussion

CcpA is a global regulator of carbon catabolite control in *B. subtilis* and needs HPr or Crh as a coeffector [63,144,196]. It has been previously estimated that there are 150 *cre* sites in *B. subtilis*, which are involved in the regulation of around 300 genes [63]. Moreno *et al.* reported in a genome-wide

transcriptome study that about 85 genes are activated by CcpA and 250 genes are repressed by CcpA in LB + glucose medium [144]. However, according to the CcpA regulon from SubtiWiki [128,202] there are only 11 genes activated by CcpA and 202 repressed. The genes mentioned in the SubtiWiki CcpA regulon are probably directly regulated by CcpA; the class 1 genes [124] and the other genes found by Moreno *et al.* are probably indirectly regulated; the class 2 genes [124]. Class 1 genes have a *cre* site and class 2 genes are affected when CcpA alters the glucose uptake (through altered phosphorylation of HPr) and thereby changes the concentration of intracellular inducers [15,124]. There are also class 0 genes, which are independent of CcpA [124]. In a transcriptome study Yoshida *et al.* have found 66 genes of which the repression was glucose dependent [232]. Here we found 244 genes which had a glucose dependent regulation in one of the CcpA mutant strains (supplementary file, sheet2).

Marciniak *et al.* [132] have categorized all known (and predicted) *B. subtilis* *cre* sites from high to low affinity. To do so, they have replaced the native *ccpA* promoter by an inducible promoter, then the fold change in gene expression was examined for a low, medium and high level of *ccpA* expression. The correlation between the fold change in gene expression and the position of the *cre* site compared to the transcriptional start site (TSS) was mapped [132]. The information found was used in this transcriptomics study to sort the affected genes on the basis of *cre* to TSS distance, and check whether it correlated to the fold change in gene expression but there was no clear correlation between fold change and *cre* to TSS distance. The fold change was very similar over a range of *cre* to TSS distances (supplementary file, sheet7).

The genes that are controlled by CcpA are in most cases also controlled by a second regulator, which is substrate specific (personal communication with Jörg Stülke). Thus, it is impossible to find the whole CcpA regulon in the Δ CcpA experiment. The other genes found in this study that do not belong to SubtiWiki's CcpA regulon could be unidentified members of the CcpA regulon, or a member of the class 2 genes [124]. On the other hand, the CcpA regulon from SubtiWiki contains 213 genes, but 152 of them were not altered in the Δ CcpA strain. One explanation for the missing genes from the CcpA regulon from SubtiWiki could be that the list of genes in the CcpA regulon from SubtiWiki is composed from various experiments with various growth conditions, e.g. also from late exponential, or stationary growth phase or in minimal media containing glucose.

18 genes from the CcpA regulon from SubtiWiki were affected both in the presence and absence of glucose; the *rbsRKDACB* operon for ribose was strongly deregulated in LB + 1% glucose and the *licHA*, *bgHP*, and *gntK* are

slightly deregulated in the presence of glucose and the other seven genes were the same in both conditions (supplementary file, sheet11).

The changes in gene regulation in absence of glucose in the Δ CcpA strain also showed that CcpA was involved in glucose independent gene regulation, as has been shown before [144]. Moreno *et al.* show that those genes are not involved in carbon metabolism [144], but that was not the case in this study. 46 of these 89 genes could be grouped into only four COG-categories: Energy production and conversion [C], Amino acid transport and metabolism [E], Carbohydrate transport and metabolism [G], and Transcription [K] (Figure 3 and supplementary file, sheet10).

The neutral methionine on position 17 in CcpA was changed to a positively charged arginine. The M17R mutation was expected to alter the DNA-binding affinity of CcpA; the positively charged arginine could cause stronger binding to the negatively charged DNA. CcpA-M17R is probably a weaker repressor, because the number of differentially regulated genes was lower than in the Δ CcpA strain. All upregulated genes are most likely the result of a weaker repression by CcpA-M17R because CcpA is mainly involved in gene repression. However, it was hard to explain the altered gene regulation by effects on DNA binding, as shown by *cre* site comparison; there were no clear differences in the *cre* sites from genes that were only affected in the Δ CcpA strain or in the CcpA-M17R strain (supplementary file, sheet8, table 1 and 4). The palindromicity of the *cre* sites in the group of genes that was affected by CcpA-M17R was lower than in the group of genes that was only affected by Δ CcpA; this could indicate that the palindromicity of the *cre* site is less important for CcpA-M17R.

The CcpA protein consists of a N-terminal DNA binding domain and a core domain for coeffector and HPr binding, linked together with a hinge helix region. The threonine on position 62 is located in the core protein, just above the hinge-helix, and is important for the conformational change in the CcpA protein upon HPr binding [176]. This conformational change is believed to improve DNA binding. The threonine to histidine mutation on position 62 has been found during a random mutagenesis study of CcpA-T62, where CcpA-T62H was found to repress *xynP* strongly in the absence of glucose (Thesis G. Seidel, Erlangen, Germany, 2005).

We found a large number of down regulated genes in the CcpA-T62H strain, especially in the absence of glucose. Therefore, we suggest that the CcpA-T62H variant was a stronger repressor than CcpA-wt. The downregulated genes might not be regulated by wildtype CcpA under the chosen conditions. The high number of affected genes in LB without glucose could indicate that the role of HPr-Ser46-P for complex formation was less important for this mutant, since catabolite repression was observed in the absence of glucose.

There were only a few genes upregulated in case of CcpA-T62H compared to CcpA-wt and the other mutants. We can conclude that the T62H substitution forces CcpA into a conformational change that happens normally in CcpA upon HPr-Ser46-P binding; this change is probably beneficial for DNA binding. The binding of a CcpA mutant protein to *cre* sites without the prior binding of CcpA to the corepressor HPr-Ser46-P was observed before for five CcpA mutants in *B. megaterium* [110].

The most important residue for the interaction of CcpA with HPr-Ser46-P is the arginine at position 304 in CcpA [176,198]. HPr will be phosphorylated on serine 46 by HPrK/P when glucose is used as a carbon source [64,70] and subsequently HPr-Ser46-P will form a complex with CcpA. The formation of this complex stimulates the CcpA-HPr-Ser46-P heterodimer formation needed to bind to DNA [46,64,176]. The positively charged arginine at position 304 was mutated to the neutral, but bulkier tryptophan which probably made binding of this CcpA mutant to the negatively charged HPr-Ser46-P more difficult.

The large number of genes affected by CcpA-R304W in the presence of glucose suggest HPr independent gene regulation. There were 234 genes affected by CcpA-R304W in the presence of glucose, 205 genes were affected in the absence of glucose, and 69 genes were affected in both conditions. The *rbsRKDACB* operon for ribose was strongly deregulated in the Δ CcpA strain, but much less deregulated in CcpA-R304W (supplementary file, sheet11) indicating that the repressor function of CcpA-R304W decreased which is probably due to the decreased binding of HPr-Ser46-P. The large number of genes affected by CcpA-R304W in the absence of glucose also suggest HPr independent gene regulation, because HPr is not phosphorylated in the absence of glucose so the CcpA-HPr complex formation is reduced but CcpA-R304W is still affecting the regulation of many genes (Table 5, supplementary file, sheet4&5).

Another explanation could be that the signal transduction in the protein has changed due to the mutation. Maybe the R304W mutation fixes CcpA into the HPr-Ser46-P bound conformation. Or possibly binding of the coeffectors fructose-1,6-bisphosphate (FBP) and glucose-6-phosphate (G6P) is more difficult. Earlier work shows that the affinity of HPr-Ser46-P to CcpA increased more than twofold by the presence of 40 mM FBP or G6P [180], but if coeffector binding is reduced then the affinity of CcpA-R304W to HPr-Ser46-P is also reduced. It will be interesting to measure the binding affinity of CcpA-R304W to HPr-Ser46-P with SPR in a future study.

It is known that a ptsH-S46A strain lost part of its repressing power [47,136] and here we showed that CcpA-R304W also lost part of its ability to repress gene expression. These results show that CcpA and HPr depend on

each other and either one of the mutations makes complex formation more difficult.

The regulation of genes in some COGs really differed from CcpA-wt, i.e. they were not regulated by the CcpA-wt but only by the CcpA-mutant. Genes in COGs for Energy production [C], carbohydrate metabolism [G], translation [J], posttranslational modification [O], and inorganic ion transport [P] are more strongly repressed in the CcpA-T62H and CcpA-R304W mutants than in the CcpA-wt strain in LB + 1% glucose (Figure 3) which shows the differential regulatory character of the CcpA mutants.

In general, we should take into account that the CcpA mutants studied here could have effects on gene regulation which cannot be seen in LB medium with a CcpA mutant because there might be unknown triggers for CcpA which are absent in LB +/- glucose. Furthermore, LB medium without added glucose still contains low amounts of glucose and other repressing sugars which might still control the most sensitive target genes. The mutations might uncouple regulation from these triggers. Future experiments in chemically defined medium or in a HPr knockout in the CcpA mutant strains could be done to reveal triggers involved in CcpA dependent gene regulation which were not present when the strains were grown in LB.

In conclusion, the point mutations in CcpA in this study were made to get more insight into the gene regulation mechanisms of CcpA. The main finding here was that the M17R mutation resulted in a small relief of CCR. CcpA-T62H was a stronger repressor than CcpA-wt and can do CCR also in the absence of glucose. CcpA-R304W had a strong regulatory affect in presence and absence of glucose and we suggest that CcpA-R304W is less dependent on HPr-Ser46-P, FBP, and G6P. However, SPR measurements should show the binding affinity of the CcpA mutants to the *cre* sites in presence or absence of HPr-Ser46-P.

Acknowledgements

We would like to thank Dr. Maïke Bartholomae and Dr. Lance Keller (Molecular Genetics, University of Groningen) for critically reading of the manuscript.

Funding: RD and OK were financially supported by a specific SYSMO2 grant from ALW-NWO. GS was financially supported by a specific SYSMO2 grant from the BMBF.

Supplementary file

Supplementary file can be found at the Frontiers in Microbiology website: <http://journal.frontiersin.org/article/10.3389/fmicb.2015.01051>. See also [44].

File 1: Data Sheet 1.xlsx. The titles of the twelve different sheets in the file are listed below. Row 1 in every sheet gives an explanation of the data shown in that sheet.

- 1_LBgluc_All signif_fold>1.7
- 2_LBgluc_Venn_diagram_fold>1.7
- 3_LBgluc_Regulatory_groups
- 4_LB_ALLsignif_fold>1.7
- 5_LB_Venn_diagram_fold>1.7
- 6_LB_Regulatory_groups
- 7_LBgluc_CRE-TSSdistance
- 8_cre_palindromicity
- 9_LBgluc_COGcat
- 10_LB_COGcat
- 11_CcpA_regulon
- 12_growth curves

Chapter 6

An osmotic upshift to 0.6 M NaCl causes population heterogeneity and partial antibiotic resistance in *Bacillus subtilis*

Ruud G.J. Detert Oude Weme¹, Luiza Morawska¹, Tamara Hoffmann², Erhard Bremer², Ákos T. Kovács^{1,#}, Oscar P. Kuipers¹.

¹Molecular Genetics Group, Groningen Biomolecular Sciences and Biotechnology Institute, University of Groningen, Nijenborgh 7, 9747 AG Groningen, The Netherlands.

²Philipps-University Marburg, Department of Biology, Laboratory for Microbiology, Karl-von-Frisch-Str. 8, D-35032 Marburg, Germany.

Current address: Terrestrial Biofilms Group, Institute of Microbiology, Friedrich Schiller University Jena, Neugasse 23, 07743 Jena, Germany.

Abstract

The soil is the natural habitat of many microorganisms where they face different levels of osmotic pressure. Cells can cope with osmotic upshift via the uptake of osmoprotectants such as glycine betaine from their environment or by synthesizing osmoprotectants such as proline. In our experiments the synthesis of proline was the only opportunity for the cells to cope with osmotic upshift due to the absence of osmoprotectants in the medium. We investigated whether cells in an isogenic culture respond homo- or heterogeneously to an osmotic upshift. A promoter *proHJ-gfp* fusion was used to study the expression of the osmotically induced proline biosynthesis pathway (*proHJ*) at the single cell level.

Here, we show that *B. subtilis* responds heterogeneously to an osmotic upshift. We show a switching point in the response at 0.6M NaCl. At this stress level, some cells have a high *proHJ* expression and can possibly produce enough of the osmoprotectant proline to cope with the osmotic stress, and these cells can continue cell elongation and division. Other cells that lacked a high *proHJ* expression, did not produce enough proline and could not continue cell elongation and division. At 0.5M NaCl the *proHJ* expression is low, but all cells can elongate and divide. At 0.7M NaCl, the *proHJ* expression was high, but cells did not manage to restore elongation and division. Furthermore, we showed that some cells possibly enter a dormant state after being exposed to an osmotic upshift. Those dormant cells did not grow nor lyse in the experiments and were found to be insensitive to the bactericidal antibiotic kanamycin. This work provides more insight into the response of *B. subtilis* at the single cell level to osmotic upshift.

Introduction

Microorganisms face different levels of osmotic pressure in their natural habitat, e.g. the soil [229], because the soil is subjected to periods of rain or drought. Therefore, microbes acquired various mechanisms to cope with the effect of osmotic pressure to retain viability and cell division [228]. Both Gram positive and Gram negative bacteria use various compatible solutes to counteract the effects of osmotic upshifts (for reviews see [80,189,228,229]). Moreover, turgor pressure is essential for cell elongation and division [102,225,226]. The turgor pressure decreases upon osmotic upshift due to the water outflow, which impairs cell elongation and thereby cell division [168,225].

The Gram positive soil bacterium, *Bacillus subtilis* applies a step-wise strategy to cope with osmotic stress. The first and rapid step in the cellular response to counteract the outflow of water and restore the turgor pressure is

the uptake of potassium ions by KtrAB and KtrCD [84]. Subsequently, potassium ions are replaced by compatible solutes such as proline or glycine betaine [22,23,229]. Compatible solutes can be taken up into the cytoplasm at high concentrations and are a sustainable solution for the cell, whereas potassium ions are not a long term solution because they interfere with cellular functions [229].

Glycine betaine is one example of a compatible solute in *B. subtilis*, which is sequestered from the environment via the Opu membrane transporters [21,229], which have a high affinity for compatible solutes. An overview of all known compatible solutes in *B. subtilis* has been published previously [229]. Glycine betaine can also be synthesized from the precursor choline [16]. However, when there are no compatible solutes (or precursors) present in the surroundings, *B. subtilis* can counteract the osmotic upshift in another way; it can replace the potassium ions with proline, which is a self-synthesized compatible solute of *B. subtilis* [22].

The osmotic stress-induced proline synthesis pathway has been studied in detail [12,22] and revealed proline synthesis from glutamate in three steps (Figure 1A). ProJ phosphorylates glutamate to produce γ -glutamyl phosphate in an ATP-dependent manner, ProA converts this compound to glutamate-5-semialdehyde, which will spontaneously cyclize into Δ -pyrroline-5-carboxylate, and ProH subsequently converts it to proline. *B. subtilis* cells always have a large pool of intracellular glutamate [225] that facilitates proline production in sufficient amounts.

The general stress response protein SigB is the regulator for salt-stress related gene regulation [79,85], but a SigA specific promoter region has also been reported for the *proHJ* operon [22].

Most studies on salt stress have been performed on the whole cell culture level. In this study we will analyze the response of single cells upon salt stress. Furthermore, we will analyze if osmotic upshift induces the presence of persister cells in a culture. Persistent cells are metabolically inactive and insensitive to antibiotics [129]. It is already known that environmental stress induces the occurrence of persister cells [105,129] and here we study it specifically for osmotic upshift.

In the last decade, phenotypic variation in an isogenic culture, also called heterogeneity, has been investigated in great detail [1,54,90,156,191,218]. This phenotypic variation mostly originates from noise in gene expression [1,54,156] and is believed to be beneficial for the fitness of the population.

In this study we investigated the response of an isogenic *B. subtilis* culture to osmotic upshift on the single cell level. For this purpose, the gene expression of the *proHJ* operon involved in the proline biosynthesis pathway

was studied at the single cell level over time. Therefore the *proHJ* promoter was fused to the gene coding for GFP.

To examine how *B. subtilis* copes with osmotic upshift solely through proline synthesis, a growth medium lacking any osmoprotectants was used. We hypothesize that *B. subtilis* needs to overcome a threshold level of *proHJ* expression in order to synthesize enough proline that can restore cell elongation and division during an osmotic upshift. We examined whether all cells in a *B. subtilis* culture respond in the same way to an osmotic upshift or if only part of the population adapts to the higher salinity. Also, the minimum level of *proH* expression is examined that is required for the cells to proceed with cell division. The data presented here suggest that only cells with high expression of *proH* can continue growth and cell division upon a certain osmotic upshift. The data presented here also suggest that part of the *B. subtilis* culture enters the persister state upon osmotic upshift.

Materials and methods

Bacterial strains, plasmids and oligonucleotides

B. subtilis 168 *trpC2* was used here (Table 1). *Escherichia coli* MC1061 was used as a host for cloning. Plasmids are listed in Table 2 and oligonucleotides are listed in Table 3.

Recombinant DNA techniques

PCR and DNA purification and restriction were done as described before [171]. Phusion DNA polymerase, FastDigest restriction enzymes, and T4 DNA ligase were obtained from Fermentas (St. Leon-Rot, Germany). Sequencing to verify the construct was done at MacroGen (Amsterdam, The Netherlands).

Strain construction

A promoter *proHJ-gfp* fusion was made to follow the expression of the *proH* gene at the single cell level. A 934 bp region with the *proH* promoter and the first 29 codons of *proH* was amplified from the *B. subtilis* genome by PCR with primers *proH_FW_Sall* and *proH_REV_EcoRI* (Table 3), restricted with *Sall* and *EcoRI* and ligated into *Sall* and *EcoRI* restricted pSG1151. The resulting pSG1151-*P_{proHJ}* plasmid contains a promoter *proH-gfpmut1* fusion with a 934 bp fragment from the *B. subtilis* genome.

Natural competent *B. subtilis* [77] was transformed with pSG1151-*P_{proHJ-gfp}*, which integrated in the *B. subtilis* genome in the *proH* promoter region via Campbell type integration (single crossover).

Flow cytometry

B. subtilis 168 P_{proHJ} -*gfp* was streaked on Lysogeny Broth (LB) agar plates supplemented with 5 µg/ml chloramphenicol (Sigma-Aldrich) from -80°C glycerol stock and incubated overnight at 37°C. Next morning, 3 ml of LB supplemented with chloramphenicol was inoculated with a single colony and grown for eight hours at 37°C and 200 rpm. Now the culture was diluted 1:1000 in 3 ml Spizizen's Minimal Medium (SMM) with 0.5% glucose and trace elements [77], from here on referred to as CDM and grown overnight at 37°C and 200 rpm. The overnight culture was diluted to an OD₆₀₀ of 0.08 in 6ml fresh CDM and grown for 5 hours at 37°C and 200 rpm. Now the cells were at an OD₆₀₀ of 0.3 and the cells were osmotically stressed by the addition of 840 µl 4.27M NaCl (in SMM); final concentration 0.6M NaCl. The cells were further incubated at 37°C and 200 rpm and samples for flow cytometry were taken at indicated time points. Therefore, cells were diluted to an OD₆₀₀ of 0.03 in filtered 50 mM potassium phosphate buffer (pH 7.0). Flow cytometry was done with the Becton Dickinson FACSCanto (BD, Breda, The Netherlands) with a flow rate of 10,000 events per second and the following photomultiplier tube settings: FSC: , SSC: , and FL-1 . Data analysis was done with the FACSDiva software from BD. Histograms were made with the Data Analysis Tools from Microsoft Excel.

Time-lapse fluorescence microscopy

The *B. subtilis* 168 P_{proHJ} -*gfp* was cultivated as described in the flow cytometry section above. The overnight culture was diluted to an OD₆₀₀ of 0.08 in 6 ml fresh CDM or in 6 ml fresh CDM with 0.2 M NaCl and grown again at 37°C and 200 rpm. After five hours of growth, the cells were diluted in 500 µl fresh CDM according to this correction for the optical density $(0.35/OD_{600}) * 250 = x$ µl in 500 µl CDM. From there 1.5 µl of culture was transferred to a 1.5% low melting agarose (Sigma) slide with CDM + a final concentration of 0.6 M NaCl (unless stated otherwise) for time-lapse fluorescence microscopy.

Time-lapse fluorescence microscopy was done as described before [40] with a Personal DeltaVision microscope system (Applied Precision), with Softworx 3.6.0 software. The microscope setup consisted of an Olympus IX71 inverted microscope body, a 60x phase contrast objective (Olympus PlanApo 1.42 NA), a CoolSNAP HQ2 camera (Princeton Instruments), and a solid state TruLight Illumination (Applied Precision). For each pre-cultured strain on the slide two points were followed with the software controlled stage. A phase contrast picture and a GFP fluorescence picture were made at intervals of twelve minutes to follow cell growth and dynamics of the *proH* promoter activity.

GFP fluorescence intensities of single cells were analyzed over time with ImageJ (<http://rsb.info.nih.gov/ij/index.html>) by manually drawing lines in single cells. After subtraction of background fluorescence the GFP intensities of single cells were plotted in graphs.

Differences in fluorescence intensities of growing and not growing cells in a time-lapse movie were further analyzed with a one-tailed Student's t-Test.

Table 1. *B. subtilis* strains used in this study.

Strain	Genotype	Source or reference
<i>E. coli</i>		
MC1061	F ⁻ <i>araD139</i> Δ (<i>ara-leu</i>)7696 <i>galE15 galK16</i> Δ (<i>lac</i>)X74 <i>hsdR2</i> ($r_K^- m_K^+$) <i>mcrA mcrB1 rpsL</i> (Str ^r)	Laboratory stock
<i>B. subtilis</i>		
168	<i>trpC2</i>	Bacillus Genetic Stock Center
DOW61	<i>P_{proHJ}-gfpmut1 cat</i>	This work

Table 2. The plasmids used in this study.

Plasmid	Genotype	Source or reference
pSG1151	<i>bla cat gfpmut1</i>	[120]
pSG1151- <i>P_{proHJ}-gfp</i>	<i>Bla cat P_{proHJ}-gfpmut1</i>	This work

Table 3. The oligonucleotides used in this study. Restriction sites are shown in italics.

Oligonucleotide	Sequence (5' -> 3')
<i>proH</i> _FW Sall	CGATGGTCGACAAACAGCGGGATTATGGTCAAC
<i>proH</i> _EcoRI_REV	TCGGCGAATTCTCCGCCATAGATCCTGCTC

Results

The time needed for *B. subtilis* to adapt to osmotic upshift

Proline can serve as a compatible solute, when there are no compatible solutes available in the medium, and the *B. subtilis proHJ* proline biosynthesis genes are osmotically induced [22,75].

To follow the expression of the *proHJ* genes upon osmotic upshift, the *proHJ* promoter with its own RBS and the first twenty-nine codons of *proH* were transcriptionally fused to the gene coding for GFP (Figure 1A). Flow cytometry was used to determine the time interval *B. subtilis* needed to adapt to an osmotic upshift. Exponentially growing *B. subtilis* cells were exposed to an osmotic upshift of 0.6M NaCl, and the expression of the promoter *proHJ-gfp* fusion was followed over time. The salt stress resulted in an initial

decrease in fluorescence. After 60 to 90 minutes *B. subtilis* showed higher GFP expression driven by the *proHJ* promoter (Figure 2A). The increased level of P_{proHJ} expression means that *B. subtilis* responds to osmotic upshift of 0.6M NaCl, which is in agreement with earlier work [22]. The error bars in the graph (Figure 2A) showed the standard deviation from the mean fluorescence. The difference between the stressed (black bars) and unstressed (white bars) cultures was much smaller than expected. The last four time points were shown in more detail in Figure 2B, where the fluorescence signal of unstressed cells was subtracted from the fluorescence signal of cells exposed to osmotic upshift. The low number of cells in Figure 2B could indicate that only a small fraction of the culture had adapted to the osmotic upshift, when one keeps in mind that the bars in Figure 2A represented 50,000 cells. In chronological order the subsequent peaks in Figure 2B represented 102, 234, 889, 1122 cells. The small number of responding cells was explained by the small difference between the stressed and unstressed cultures (Figure 2A). Weak expression from P_{proHJ} could also explain the small difference observed between stressed and non-stressed cells.

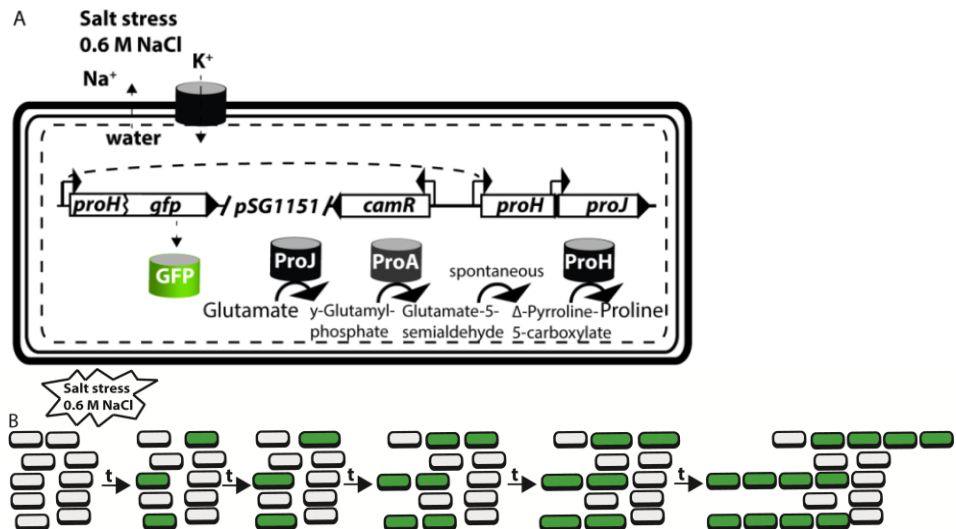


Figure 1. (A) Schematic overview of the *proHJ* genes of *B. subtilis* involved in osmotically induced proline biosynthesis proceeded by the *proH* promoter-*gfp* fusion in the same genomic locus. The enzymatic reaction by *proJ*, *proA*, and *proH* that results in proline synthesis from glutamate is highlighted. The dotted rectangular line represents the shrinking cell upon the water outflow due to the osmotic upshift. Figure adapted from [22]. **(B)** Proposed heterogenous response of *B. subtilis* upon osmotic upshift; cells with osmotically induced *proH* become green, synthesize the compatible solute proline and restore cell elongation as shown in the third and fifth step.

Only cells with high level of proHJ after osmotic upshift can divide

The flow cytometry data in Figure 2 gave a first indication that the cells in an isogenic culture respond heterogeneously to osmotic upshift.

It is already known from earlier work that the intracellular concentration of proline increases upon increasing osmotic upshifts [22] and interestingly, a large variation in the intracellular proline concentration has been found in that study when the cells have been stressed with 0.6M NaCl.

More insight into the expression of *proHJ* at the single cell level upon osmotic upshift was acquired using time-lapse fluorescence microscopy. For that purpose, *B. subtilis* with P_{proHJ} -*gfp* was grown to exponential phase in liquid CDM medium and subsequently cells were transferred to an agarose slide with the same CDM medium including 0.6M NaCl, resulting in exposure to an osmotic upshift. The fluorescence intensities of five cells from a time-lapse movie were measured over time to examine the behavior of the isogenic culture at the single cell level (Figure 3B). Cell divisions during the time-lapse were indicated on the fluorescence intensity lines. Only the cells with higher fluorescence intensity, i.e. with higher expression levels of *proHJ*, can divide whereas cells with low fluorescence intensities and thus low levels of *proHJ* cannot divide (Figure 3B,C). Differences in fluorescence intensities between cell lineages in Figure 3BC and Figure 4AB were significant (Students t-Test, $p < 0.001$). This finding supported our hypothesis that cells need to overcome a threshold level of *proHJ* expression to grow during osmotic upshift; more *proHJ* expression leads to more ProH and Proj proteins and thus to the synthesis of more proline.

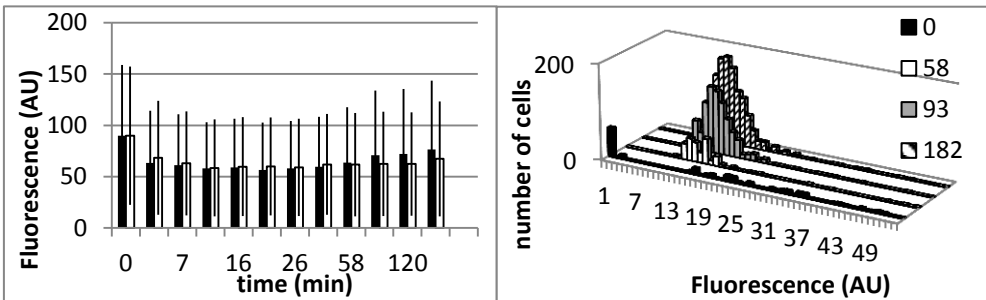


Figure 2. (A) The response of the strain with P_{proHJ} -*gfp* to an osmotic upshift of 0.6M NaCl (black bars) and the activity of the same strain in absence of an osmotic upshift (white bars) was measured via flow cytometry, each bar represents the mean fluorescence signal from 50,000 cells. **(B)** The graph shows the fluorescence intensity of the culture at indicated selected time points where the fluorescence signal from non-stressed cells was subtracted from the fluorescence signal of cells exposed to osmotic upshift. The black-filled column is time point zero, the white-filled column is at 58 min, grey-filled column is at 93 min and the dashed-filled column is at 182 min.

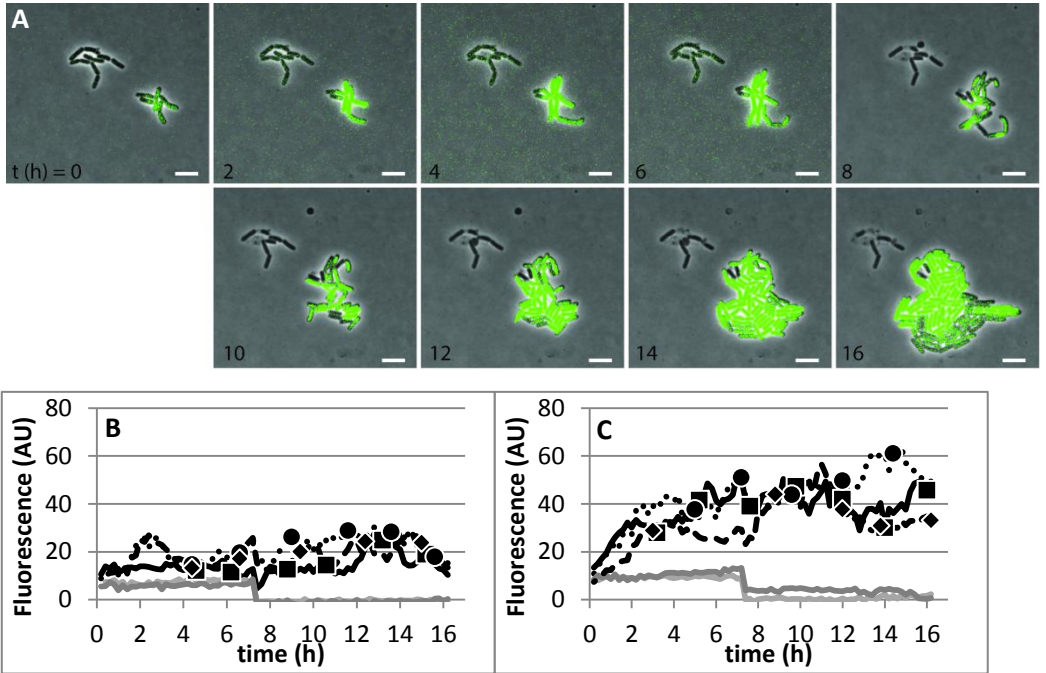


Figure 3. The fluorescence intensity of single *B. subtilis* *proH-gfp* cells in response to osmotic upshift followed over time. **(A)** Screenshots from the time-lapse movie taken at indicated time points. **(B)** Fluorescence intensities of five *B. subtilis* P_{proHJ} -*gfp* cells were measured over time after preculturing in CDM media and transferring to a time-lapse microscope slide consisting of 1.5% agarose in CDM + 0.6M NaCl to start the osmotic upshift. **(C)** Fluorescence intensities of five *B. subtilis* P_{proHJ} -*gfp* cells were measured over time after preculturing in CDM + 0.2M NaCl. Each line represented one cell over time, dots on the lines represented cell divisions.

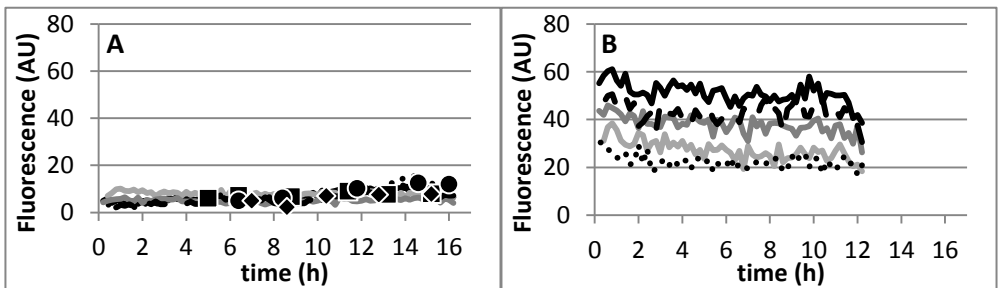


Figure 4. The fluorescence intensity of single *B. subtilis* P_{proHJ} -*gfp* cells in response to different osmotic upshifts. **(A)** Single *B. subtilis* P_{proHJ} -*gfp* cells in response to osmotic upshift of 0.5M NaCl and **(B)** single *B. subtilis* P_{proHJ} -*gfp* cells in response to osmotic upshift of 0.7M NaCl.

When the osmotic upshift experiments in Figure 3 were repeated with a salt concentration of 0.5M NaCl a rather different behavior of the cells was observed (Figure 4A). The fluorescence intensity in the P_{proHJ} -*gfp* cells remained lower at this lower NaCl concentration and no correlation between cell division and high or low fluorescence intensity level was observed.

Interestingly, osmotic upshift experiments using 0.7M NaCl showed a contradictory behavior. While the fluorescence intensity was much higher, no cell division was occurring; the cells were unable to cope with the too severe stress conditions. This could probably be explained by the high rate of water outflow out of the cells, the subsequent uptake of potassium ions, after which the cells were trying to replace the potassium ions by proline, so the expression level of *proHJ* was high, but cells did not manage to restore cell elongation and division. Earlier work has shown that *B. subtilis* has a longer lag phase when it is exposed to higher salt concentrations (about 10 hours in 1.2M NaCl) [17,22], but that was in liquid cultures. Here, on an agarose time-lapse slide with CDM plus 0.7M NaCl cell division did not occur even hours after exposure to the NaCl (Figure 4B).

We showed here that the cellular response of *B. subtilis* is at a switching point during an osmotic upshift of 0.6M NaCl; some cells adapted and some cells did not adapt to the osmotic upshift. Both data from this study (Figure 3 and Figure 4) and the large deviation in the intracellular proline concentration found at 0.6M NaCl in earlier work [22] show the heterogeneous response. Only in CDM with 0.6M NaCl the cells respond heterogeneously, whereas in CDM with 0.5M or 0.7M NaCl the cells respond homogeneously.

Osmotic upshift induces the presence of persister cells

We noticed that many cells in the time-lapse fluorescence microscopy movies did not grow nor lyse so these cells might be in a dormant state. The dormant state is a metabolically inactive state where cells are insensitive to antibiotics and this state is also called persistence [62,129,162], not to be confused with spores which are also called dormant. In a bacterial culture there is always a small fraction of dormant cells (10^{-4} – 10^{-6} [129]) due to bet-hedging [50,129,218]. The question here was whether osmotic upshift induced the presence of dormant cells in a culture. A culture exposed to an osmotic upshift of 0.6M NaCl was compared to an unstressed culture. The presence of dormant cells was examined by testing the sensitivity of the cultures to the bactericidal antibiotic kanamycin by incubating the cultures for 4 hours in CDM with kanamycin and then colony forming units (CFU) were counted on LB agar plates.

The growth rate of *B. subtilis* decreased upon osmotic upshift, as expected (Figure 5A), but the osmotic upshift resulted in the presence of kanamycin insensitive cells, i.e. in dormant cells (Figure 5B). There were $4 \cdot 10^7$ living cells/ml left in the osmotic upshift stressed culture whereas no living cells were left in the unstressed culture.

The sensitivity of *B. subtilis* cultures to kanamycin after exposure to osmotic upshift was studied in more detail. Cells were precultured in CDM, exposed to salt and then to kanamycin (Figure 6A) and subsequently followed by time-lapse fluorescence microscopy at the single cell level on CDM with 1.5% agarose (Figure 6B). The culture that was not exposed to osmotic upshift but only to kanamycin for 4 hours grew poorly due to its sensitivity to kanamycin. The culture that had been exposed to osmotic upshift for 90 minutes and subsequently to kanamycin for 4 hours grew good during the time-lapse experiment, showing that osmotic upshift induced the presence of dormant, kanamycin insensitive cells. The culture that was only exposed to osmotic upshift also grew good (Figure 6). Remarkably, the culture that was exposed to osmotic upshift and kanamycin grew to higher cell density than the culture that was only exposed to osmotic upshift.

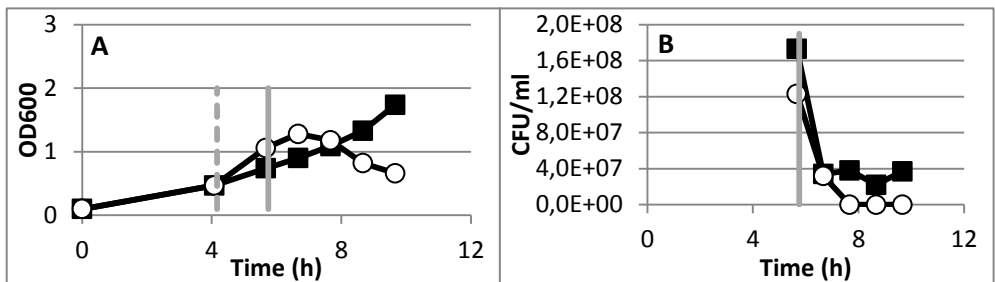


Figure 5. The growth and sensitivity of *B. subtilis* $P_{proHI-gfp}$ to kanamycin after exposure to osmotic upshift. **(A)** OD₆₀₀ of *B. subtilis* $P_{proHI-gfp}$ which was split into two equal volumes after 4 hours; one of the cultures (black squares) was exposed to an osmotic upshift of 0.6M NaCl (indicated by the dashed grey line) and the other culture was not stressed (open circles). 75 minutes later 10 μ g/ml kanamycin was added to both cultures (indicated by the grey line). **(B)** Colony Forming Units (CFU) in both cultures (squares: osmotically stressed, and circles: not stressed) were counted via dilutional plating on LB agar plates after the addition of kanamycin (grey line).

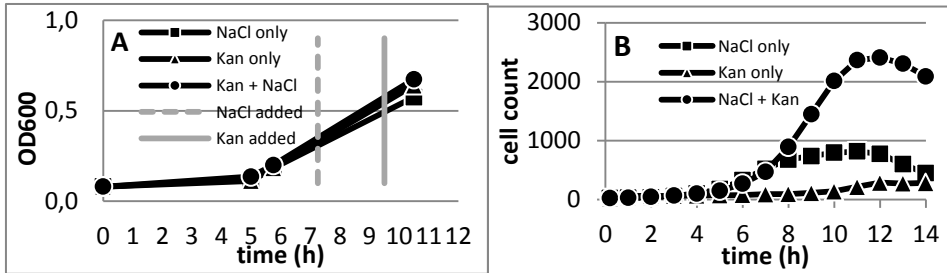


Figure 6. Three identical *B. subtilis* P_{proHJ} -*gfp* cultures were grown in liquid CDM. **(A)** At an OD_{600} of 0.3 0.6M NaCl (dotted grey line) was added to culture one and three (squares and circles), two hours later 10 μ g/ml kanamycin (grey line) was added to culture two and three (triangles and circles) and after an additional 3 hours incubation all three cultures were transferred to CDM + 1.5% agarose (without NaCl) for time-lapse fluorescence microscopy. **(B)** Cell count during the time-lapse microscopy (symbols are the same as in figure A).

Discussion

In this study, we examined the heterogeneous response of *B. subtilis* cells to an osmotic upshift. Two phenotypes could be observed in a *B. subtilis* culture upon a 0.6M NaCl osmotic upshift in CDM medium in the absence of added osmoprotectants. Part of the culture adapted to the osmotic upshift by responding to the stress, e.g. by increasing the *proHJ* expression and continued cell growth and division and the other part of the culture did not adapt and was unable to restore cell growth.

Here, we showed that such a heterogeneous response only occurred in CDM with 0.6M NaCl (Figure 3 and Figure 4) in contrast to CDM with 0.5 or 0.7M NaCl. All cells had a low fluorescence intensity in CDM with 0.6M NaCl at the beginning of the time-lapse experiment and only the cells with increasing fluorescence intensity from P_{proHJ} -*gfp* were able to grow and they outnumbered the low fluorescent cells at the end of the experiment. *B. subtilis* showed a homogeneous response in CDM with salt concentrations of 0.5 or 0.7M NaCl (Figure 4). The fluorescence intensity in the P_{proHJ} -*gfp* harboring cells was low when *B. subtilis* was stressed with 0.5M NaCl, so most likely the levels of ProH and ProJ were low but cell division was not affected and most cells were able to respond to this milder stress condition (Figure 4A). The fluorescence intensity in the P_{proHJ} -*gfp* harboring cells was highly increased when *B. subtilis* was stressed with 0.7M NaCl. Most likely the levels of ProH and ProJ were also high, but cell division was not restored and cells were not able to cope with this stress condition (Figure 4B). The level of osmotic upshift

in *B. subtilis*' natural environment (the soil) varies greatly [21], but here we showed that 0.6M NaCl presents a switching point in the cellular response.

Such a heterogeneous response phenomenon has been described before as responsive diversification [105]; the two phenotypes – adapting and non-adapting cells – were generated from a homogeneous, isogenic *B. subtilis* population in response to an environmental change. Heterogeneity is a form of bet-hedging (risk spreading) and has been shown during diauxic shift recently [105,193]. *B. subtilis* responds to salt stress in a deterministic way when the *proHJ* operon is osmotically induced [22]. However, in response to the stress conditions, the *proHJ* expression seems to be stochastic, as only certain cells had a high expression of *proHJ*. These cells can synthesize enough proline to serve as osmoprotectant and support growth. It would be interesting to determine whether the history of the cells also influences such a heterogeneous response or whether the heterogeneous response depends solely on stochastic regulatory processes in the cells independently of its previous culturing conditions. Previous work has shown that *B. subtilis* cells respond homogeneously to certain environmental stress conditions like 0.4M NaCl or 1% ethanol [233]. Our study adds an interesting example to the heterogeneous responses of *B. subtilis*; in response to 0.6M NaCl salt stress.

Bacterial cells can enter a dormant state stochastically or upon exposure to environmental stress, nutrient limitation, in a biofilm, or in interaction with a host (reviewed by [129]). The occurrence of persister cells has been shown in detail for carbon limitation [105]. Here we showed that upon osmotic upshift part of a *B. subtilis* culture entered into a dormant state; they did not grow or lyse and cells were insensitive to the bactericidal antibiotic kanamycin (Figure 5). In literature dormant bacterial cells mostly refer to spores [89,118,218], but in this study dormant cells do not refer to spores but to metabolically inactive cells. These cells are also called persisters because they are insensitive to antibiotics.

What can be the mechanism for cells to go into the dormant state? In *E. coli* it has been shown that an increased HipA activity in a *hipA* mutant formed much more persistent cells than wild type *E. coli* [10]. However, *B. subtilis* does not have *hipA* or an homolog. Another explanation could be the concentration of (p)ppGpp (guanosine pentaphosphate) in cells. (p)ppGpp is also called the alarmone [91,129,130]. In *E. coli* it has been shown that cells with a stochastically high level of (p)ppGpp slowed down their growth rate due to the activation of toxin-antitoxin loci and those cells are multidrug tolerant [130]. In *B. subtilis* RelA is responsible for the synthesis and degradation of (p)ppGpp [224] and the expression of *relA* is a bit upregulated after salt stress according to earlier work [152]. It would be interesting to test the sensitivity of a *B. subtilis* *DELTArelA* strain to kanamycin. However a recent study showed

that a *relA* knockout strain had an undetectable level of (p)ppGpp but was insensitive to antibiotics [205]. These *E. coli* and *B. subtilis* studies show contradictory results about the relation between the (p)ppGpp concentration and the sensitivity to antibiotics. Maybe another factor than (p)ppGpp plays a role in the persister phenotype in *B. subtilis*.

Chapter 7

Summary and general discussion

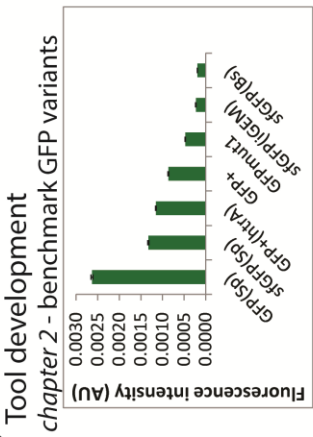
Studying the dynamics of protein-protein interactions was the main goal of this PhD-project. It has been suggested that protein complexes might be the prokaryotic equivalent of organelles [96,231]. An example of protein-protein interactions are metabolons, with the suggested function of substrate channeling.

Protein-protein interaction studies are mainly done by yeast/bacterial-two-hybrid studies and *in vitro* via crosslinking combined with pull-down and identification via mass spectrometry. However, for yeast-two-hybrid, knowledge about potential interaction partners is required and yeast-two-hybrid can give false positive results [67]. *In vitro* it is not possible to study the dynamics of these interactions or whether these interactions occur heterogeneously in an isogenic culture. Protein-protein interactions have not been studied intensively *in vivo* because the available tools have limitations. The focus of this thesis was to study these interactions *in vivo* (**chapter 3 and 4**). Fluorescence Resonance Energy Transfer (FRET) is an important tool to study protein-protein interactions *in vivo*, but also has its limitations. The donor and acceptor have to be in close proximity, in a good dipole-dipole orientation, and should have spectral overlap.

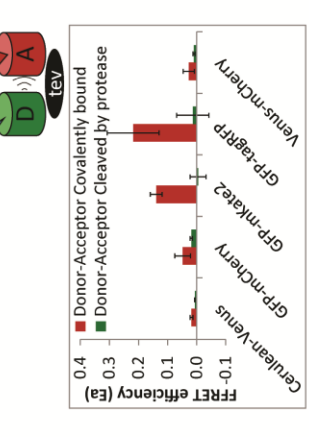
Studying the function of specific amino acids in different functional domains of CcpA was the second field of interest during this PhD-project (**chapter 5**). CcpA is a pleiotropic regulator for the expression of genes involved in carbon metabolism.

Heterogeneity in an isogenic culture upon osmotic upshift was the last field of interest (**chapter 6**). Earlier work by Brill *et al.* where the intracellular proline concentration was measured at different levels of osmotic upshift by sodium chloride, showed a large variation in the proline concentration at 0.6M NaCl [22]. The response of *B. subtilis* to osmotic upshift was measured here at the single cell level with a promoter-*gfp* fusion. We examined whether the large variation in the proline concentration at an osmotic upshift of 0.6M NaCl was due to heterogeneity.

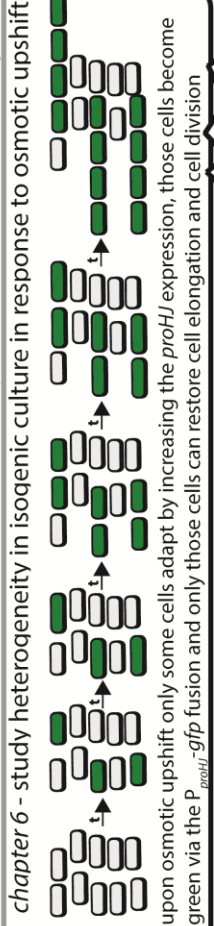
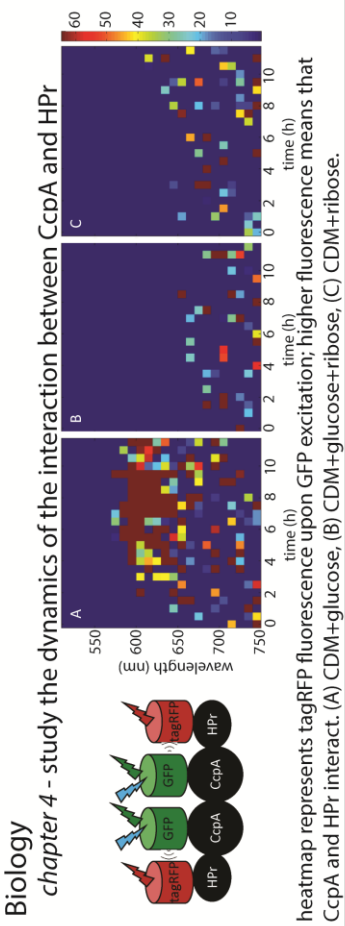
The work from all projects is summarized per chapter in figure 1.



GFP(Sp) is the brightest GFP
chapter 3 - test the suitability of FPs as FRET pair



GFP-tagRFP & GFP-mKate2 are good FRET pairs



Salt stress
 0.6 M NaCl

Figure 1 (on page 112). The major finding of each chapter of this PhD-project is shown here in part of the cell. **Chapter 2 and 3** on the left side are tool development activities: benchmarking GFP variants and comparing FP pairs for their suitability as FRET pairs, respectively. FRET was detected here via sensitized emission and FLIM. In **chapter 4** the acquired knowledge of FRET was applied to study the dynamics of the interaction between CcpA and HPr. FRET turned out to be not so suitable to study protein-protein interactions. In **chapter 5** the function of specific amino acids in different functional domains of CcpA were studied at the transcriptome level. Shown here is the number of affected genes per CcpA-mutant strain in both LB with glucose and LB without glucose. In **chapter 6** the heterogeneity in an isogenic *B. subtilis* culture upon osmotic upshift was studied and we showed a switching point in the cellular response at an osmotic upshift of 0.6M NaCl.

Benchmarking GFP variants

Since the first heterologous expression of Green Fluorescent Protein in *E. coli* in 1994 [29] it was clear that GFP would be very valuable for molecular biology. Engineering of brighter and faster maturing variants is still ongoing. We have benchmarked seven GFP variants; five variants that already existed plus two of them which were codon optimized (**chapter 2**). These brighter GFP variants can be used for promoter-*gfp* fusions of weak promoters or can be fused to low copy proteins to study their localization or use them in single cell FRET applications.

Testing the suitability of FPs as FRET pair

The potential of FRET has been the motivation to develop variants of GFP with different colors, and which are brighter and mature faster [208]. Fluorescent proteins (FPs) from other organisms than *Aequorea victoria* made the fluorescent toolbox even larger [183]. In **chapter 3** the suitability of FPs as FRET pair was tested. FRET is the non-radiative energy transfer from an excited donor fluorophore to an acceptor fluorophore. For a successful FRET the donor and acceptor have to be in close proximity, which was achieved here by crosslinking them with a short linker. The linker contained the sequence of the TEV-protease recognition site so the FPs could be cleaved *in vivo* upon induction of the TEV-protease, thereby we could detect both high and low FRET efficiencies. The donor and acceptor must have a good dipole-dipole orientation, so the linker between the FPs is important, but it is difficult to predict which linker will have the best characteristics. The linker used in **chapter 3** worked well.

The emission spectrum of the donor should overlap with the absorbance spectrum of the acceptor, which is easy to achieve with the large number of available FPs. However, the spectral overlap is also the reason that

corrections have to be made, because donor emission can go into the acceptor channel and donor excitation light can directly excite the acceptor. In **chapter 3** FRET detected via sensitized emission and a correction method are presented. GFP-tagRFP and GFP-mKate2 were detected to be the best FRET-pairs. We did not obtain proper results with Cerulean-Venus (CFP-YFP derivatives, **chapter 3**). CFP-YFP is the most common FRET-pair, but their spectral overlap is larger compared to other pairs and thus their FRET signal might be lost easier due to the corrections. Here GFP was chosen as a donor because it is much brighter than CFP. The advantage of (most) red-shifted FRET pairs is that their spectral overlap is smaller so undesired donor emission in the acceptor channel and undesired excitation of acceptor by donor excitation light are reduced. Furthermore the cellular auto fluorescence is lower with red-shifted FPs and there is less photo toxicity.

GFP-tagRFP was therefore used in **chapter 4** to construct protein-FP fusions for studying protein-protein interactions in living *B. subtilis* at the single cell level.

Single cell FRET to study protein-protein interactions

The initial plan of this PhD-project was to study the tricarboxylic acid (TCA) cycle metabolon data from Meyer *et al.* [138] in *B. subtilis in vivo* by using FRET. By studying these interactions *in vivo* we wanted to elucidate the dynamics of these interactions in space and time. However, as discussed in **Chapter 4**, we were not able to show interactions between CitZ, Icd, and Mdh by using FRET (data not shown). An explanation could be the suggested transient nature of protein-protein interactions [38,143]. The FRET signal could get lost in the background when the donor and acceptor interact only part of the time. The suggested low affinity of an enzyme complex for substrate channeling might be another reason [34,87]. It is also possible that the distance between the donor and acceptor fluorophore was too large or that their dipole-dipole orientation was not aligned properly. Another explanation could be that the sensitivity of our FRET method was too low.

After those unsuccessful experiments with TCA-cycle protein-protein interactions we focused on the interaction of CcpA and HPr. It is known that CcpA and HPr form a complex before binding to DNA to affect gene expression regulation and the CcpA HPr complex is stable for a longer time [176,180]. With FRET detected via sensitized emission and with FRET-FLIM we were not able to show an interaction between CcpA and HPr (**chapter 4**). Piston *et al.* state that in an intermolecular FRET experiment the donor and acceptor ratio should be between 1:10 and 10:1, otherwise the FRET signal will get lost in the background because a too large part of the donor or acceptor fluorophores cannot interact [160]. The CcpA:HPr ratio was estimated to be 1:45 (based on

fluorescence intensities, **chapter 4**) and this could be a reason that an interaction was not observed. With a spectrum scan we were able to show that CcpA and HPr interact, but only in a glucose minimal medium during the exponential phase (**chapter 4**, figure 4). This interaction suggests that CcpA and HPr only interact during the exponential growth phase to ensure rapid growth of *B. subtilis*.

The linker that was used to fuse CcpA-GFP and HPr-tagRFP was a 10 amino acid long flexible linker, but it might be too long or too flexible to bring the fluorophores in close proximity and in a good orientation. Therefore, we think that in future protein-FP fusions a few different linkers should be tested in parallel for their performance in a FRET experiment.

The resonance energy transfer efficiency could be improved in future protein-protein interaction experiments. Grunberg *et al.* have used affinity tags on the FPs to stabilize the interaction between FKBP12-mCitrine and FRB-mCherry and thereby they were able to visualize the interaction via FRET-FLIM in live cells [72]. The affinity tag was based on domain-peptide interaction modules with proline rich motifs from the yeast protein Sho1 and might help in future attempts to study the CcpA and HPr interaction.

Alternatively, FRET experiments could be tried with CcpA fused to Cy3 and HPr fused to BHQ-2 which is a non-fluorescent quencher of Cy3. This combination of fluorescent Cy3 and BHQ-2 as a quencher were used before [32]. A reduction of Cy3 fluorescence due to the quenching would prove that CcpA and HPr interact. There is no need for image correction due to spectral overlap. This could be very beneficial for the signal-to-noise ratio.

In conclusion, it turned out to be very difficult to obtain a good signal-to-noise ratio with intermolecular FRET detected via sensitized emission. Future *in vivo* studies on protein-protein interactions should only be done when the MEM-FLIM device (**chapter 3**) is sensitive enough for single bacterial cells. With MEM-FLIM it will become possible to study the dynamics of protein-protein interactions *in vivo* and at the single cell level. MEM-FLIM can be used for time-lapse microscopy and the fluorescence lifetime can be easily visualized in single cells with a heat map. A change in the fluorescence lifetime will represent (a change in) the interaction between CcpA and HPr.

With MEM-FLIM, the percentage of donor population that is in interaction with an acceptor could be calculated from fluorescence lifetime decay patterns. Normally, the GFP fluorescence lifetime decay is mono-exponential, but if only part of the CcpA-GFP population is in interaction, then the lifetime decay is not mono-exponential anymore because there are two different CcpA-GFP populations.

Function of specific amino acids in CcpA studied at the transcriptome level

CcpA is the pleiotropic regulator for the expression of genes involved in carbon metabolism. When glucose is present in the medium, then most genes which are involved in the metabolism of other carbon sources are repressed by CcpA, to ensure optimal use of energy. In **chapter 5** we studied the function of three specific amino acids located in different functional parts of CcpA. The mutated amino acids were: the methionine at position 17 which is involved in DNA binding, the threonine at position 62 which is located in the core protein next to the hinge helix which is involved in the conformational change of CcpA upon HPr-Ser46-P binding, and the arginine at position 304 which is involved in HPr-Ser46-P binding. Those amino acids were selected to be mutated based on the crystal structure of CcpA in complex with HPr-Ser46-P [176]. The transcriptome profiles of the *ccpA* mutant strains were studied at the beginning of the exponential growth phase using LB medium with and without glucose. The transcriptome from the *ccpA*-wt strain was always used as a control.

The CcpA-M17R mutant was expected to have an altered DNA-binding property; therefore slight changes in the list of regulated genes were expected, but we did not find a clear difference in the target genes that could be explained by a change in *cre* (catabolite responsive element) binding of the CcpA-M17R mutant. CcpA-T62H was found to be a stronger repressor than CcpA-wt, both in presence and absence of glucose. We suggest that the T62H mutation forces CcpA in a conformational change which normally occurs upon HPr-Ser46-P binding. CcpA-R304W had a reduced affinity to bind HPr-Ser46-P, but this dimer formation is necessary to bind to DNA. HPr is only phosphorylated at Serine46 in presence of glucose and only phosphorylated HPr can form a dimer with CcpA [180] and chapter 1 figure 5. However, both in presence and absence of glucose the number of affected genes was higher than in wild type CcpA.

Not all genes from the CcpA regulon [202] were found to be affected in one of the *ccpA* mutant strains. Maybe the gene regulation by CcpA is stricter in a glucose minimal medium. In this study we examined the effects of various CcpA mutants only in LB with or without glucose. It should also be noted that the CcpA regulon described on SubtiWiki is based on different articles. The missing of certain differentially regulated genes could also be a false-negative result of the microarray technique due to possible low spot intensity or high background signal.

Results from this study might be useful for the optimization of so-called cell factories. The uptake of nutrients and the secretion of proteins

could be improved by the altered gene regulation in one of the *ccpA* mutant strains. This could be interesting when CcpA relieves the repression of industrially interesting genes, which is the case for *amyE* (amylase) and *mall* (amylase) in the CcpA-R304W mutant strain. The gene regulation of the *ccpA* mutant strains is shown in **chapter 5** and in an attachment, where all affected genes are listed.

In this study we used DNA microarrays by which gene expression levels from various growth conditions or mutant strains can be screened easily. A disadvantage of this technique is that two conditions or strains can only be compared via binding competition of fluorescently labeled cDNA to the microarray probe, so the fold changes are relative.

Next generation RNA sequencing is the successor of DNA microarrays. RNA sequence data is quantitative instead of ratio based. Thus, a more precise comparison of the *ccpA* mutant strains can be obtained with RNA sequencing data. Also, small and long non-coding anti-sense RNA molecules can be also detected easily with RNA sequencing methods. RNA sequencing is becoming cheaper and the software tools for data analysis are getting more and more user-friendly.

Heterogeneity and presence of persister cells upon osmotic upshift

Earlier work from project partners showed that there is a large deviation in the intracellular proline concentration when *B. subtilis* was osmotically stressed with 0.6M NaCl [22]. Proline is an osmoprotectant that can be synthesized by *B. subtilis*. Synthesis of proline was the only way for the cells to cope with osmotic upshift in the growth media used here due to the lack of other components that can serve as osmoprotectant, like glycine betaine or ectoine. We examined whether this variation in proline concentration is reflected in *proHJ* expression, e.g. whether *proHJ* expression is heterogeneous. Therefore the *proHJ* promoter was fused to *gfp* to study the *proHJ* expression at the single cell level. ProH, ProJ, and ProA are responsible for proline biosynthesis from glutamate and *proHJ* transcription is osmotically induced ([22] and **chapter 6**). We showed a heterogeneous response in *B. subtilis* upon osmotic upshift, with a switching point at 0.6M NaCl. At an osmotic upshift of 0.6M NaCl part of the culture had a high *proHJ* expression and was able to restore cell elongation and cell division while the other part of the culture did not have an increased *proHJ* expression and could not continue growth. At 0.5M NaCl the *proHJ* expression was low, but cells continued dividing. At 0.7M NaCl the *proHJ* expression was high, but cells did not manage to restore cell division. These observations indicated that the cellular response to an osmotic upshift is heterogeneous (**chapter 6**).

Upon osmotic upshift there were cells that were neither growing nor lysing in the time-lapse microscopy experiments. These cells could be dormant cells. Dormant cells are metabolically inactive and insensitive to antibiotics, and are also called persister cells [129]. We showed that part of the *B. subtilis* culture was insensitive to the bactericidal antibiotic kanamycin upon osmotic upshift in liquid cultures (**chapter 6**).

Knowledge about persister cells is important during clinical use of antibiotics. Maybe the use of antibiotics can be adapted to increase the effectivity and thereby reduce the chance that resistant strains can be formed. Our preliminary results showed that upon addition of glucose after osmotic upshift cells became metabolically active and become sensitive to antibiotics again. Maybe the clinical use of antibiotics could also be combined with glucose to keep the bacteria sensitive to antibiotics.

Time-lapse fluorescence microscopy was used here to study the heterogeneous response of *B. subtilis* upon osmotic upshift. Time-lapse microscopy is a nice tool, but image analysis is a time consuming part of the data analysis. Various image analysis software programs, like MicrobeTracker [190], Schnitzcells [234], and TLMtracker [99], were used to analyze the fluorescence microscopy data. The authors of these programs are very enthusiastic about the programs, but they also acknowledge that the success of these programs varies a lot per application. Every program was written for a specific goal or bacterium and that makes cell recognition more difficult for other goals or bacteria. The programs were quite successful in cell recognition in independent frames, especially MicrobeTracker. However, when subsequent time-frames have to be analyzed from a time-lapse movie it turned out to be difficult to keep track of individual cells in subsequent frames and to link mother and daughter cells after cell division. This is necessary to precisely follow a cell lineage and to visualize whether *proHJ* expressing cells could grow better upon osmotic upshift. We did not manage to do the time-lapse image analysis with any of these programs and eventually did the time-lapse image analysis manually with ImageJ, similarly as done before by de Jong *et al.* [41].

In future osmotic stress experiments, it would be nice to use microfluidics to study fluctuations in the osmotic stress level and determine whether *proHJ* expression is fluctuating in response to the stress level. The effect of various osmoprotectants could be studied in more detail. The effect of antibiotic insensitivity upon osmotic upshift could also be studied in great detail when the antibiotic is added to the flow medium subsequently after osmotic stress. Then it could be visualized whether the *proHJ* expressing cells are still sensitive to the antibiotic, while indeed the non-responding cells are truly in a dormant state.

The time required for the cells to respond to osmotic upshift can also be examined more precisely with microfluidics. In the time-lapse method in **chapter 6** there were approximately two hours between transferring the cells to the slide, i.e. to the medium where the cells faced the osmotic upshift, and the first fluorescence image. This cannot be done faster because the temperature of the slide needs to become stable (for autofocusing) and the slide needs to be scanned to select points of interest to follow over time. Microfluidics would solve this technical problem and would provide a proper approach to detect fast and also slow response to energy or osmotic stress as has been observed for sigB regulated pathways in *B. subtilis* [122,233].

Concluding remarks

The work that was done during this PhD-project will be helpful for future FRET experiments to study protein-protein interactions in live bacterial cells at the single cell level (**chapter 2 and 3**). Future studies on protein-protein interactions with FRET-FLIM will give more insights in their dynamics and whether these interactions occur homo- or heterogeneously within cells of an isogenic culture. This will ultimately lead to a better understanding of the spatiotemporal organization of cellular components inside the cell (**chapter 4**). We got more insight into the function of individual amino acids in the regulator CcpA by mutating them and studying their effect on gene regulation at the transcriptome level. Point mutations in CcpA could be interesting when industrially interesting genes are no longer repressed by CcpA (**chapter 5**). The response of *B. subtilis* upon osmotic upshift has been studied in detail and a switching point in the growth restoration was revealed at an osmotic upshift of 0.6M NaCl (**chapter 6**).

References

1. Acar M, Mettetal JT, van Oudenaarden A. **2008**. Stochastic switching as a survival strategy in fluctuating environments. *Nat Genet*; 40: 471-475.
2. Alexeeva S, Gadella TW, Jr, Verheul J, Verhoeven GS, den Blaauwen T. **2010**. Direct interactions of early and late assembling division proteins in *Escherichia coli* cells resolved by FRET. *Mol Microbiol*; 77: 384-398.
3. Anagnostopoulos C, Spizizen J. **1961**. Requirements for Transformation in *Bacillus Subtilis*. *J Bacteriol*; 81: 741-746.
4. Andersen JB, Sternberg C, Poulsen LK, Bjorn SP, Givskov M, Molin S. **1998**. New unstable variants of green fluorescent protein for studies of transient gene expression in bacteria. *Appl Environ Microbiol*; 64: 2240-2246.
5. Anderson JC, Dueber JE, Leguia M, Wu GC, Goler JA, Arkin AP, et al. **2010**. BglBricks: A flexible standard for biological part assembly. *J Biol Eng*; 4: 1.
6. Arai R, Ueda H, Kitayama A, Kamiya N, Nagamune T. **2001**. Design of the linkers which effectively separate domains of a bifunctional fusion protein. *Protein Eng*; 14: 529-532.
7. Arantes O, Lereclus D. **1991**. Construction of cloning vectors for *Bacillus thuringiensis*. *Gene*; 108: 115-119.
8. Aslan K, Lakowicz JR, Geddes CD. **2005**. Plasmon light scattering in biology and medicine: new sensing approaches, visions and perspectives. *Curr Opin Chem Biol*; 9: 538-544.
9. Aung-Hilbrich LM, Seidel G, Wagner A, Hillen W. **2002**. Quantification of the influence of HPrSer46P on CcpA-cre interaction. *J Mol Biol*; 319: 77-85.
10. Balaban NQ, Merrin J, Chait R, Kowalik L, Leibler S. **2004**. Bacterial persistence as a phenotypic switch. *Science*; 305: 1622-1625.
11. Barbe V, Cruveiller S, Kunst F, Lenoble P, Meurice G, Sekowska A, et al. **2009**. From a consortium sequence to a unified sequence: the *Bacillus subtilis* 168 reference genome a decade later. *Microbiology*; 155: 1758-1775.
12. Belitsky BR, Brill J, Bremer E, Sonenshein AL. **2001**. Multiple genes for the last step of proline biosynthesis in *Bacillus subtilis*. *J Bacteriol*; 183: 4389-4392.
13. Berggard T, Linse S, James P. **2007**. Methods for the detection and analysis of protein-protein interactions. *Proteomics*; 7: 2833-2842.
14. Blaser MJ. **2006**. Who are we? Indigenous microbes and the ecology of human diseases. *EMBO Rep*; 7: 956-960.
15. Blencke HM, Homuth G, Ludwig H, Mäder U, Hecker M, Stülke J. **2003**. Transcriptional profiling of gene expression in response to glucose in *Bacillus subtilis*: regulation of the central metabolic pathways. *Metab Eng*; 5: 133-149.
16. Boch J, Kempf B, Schmid R, Bremer E. **1996**. Synthesis of the osmoprotectant glycine betaine in *Bacillus subtilis*: characterization of the gbsAB genes. *J Bacteriol*; 178: 5121-5129.
17. Boch J, Kempf B, Bremer E. **1994**. Osmoregulation in *Bacillus subtilis*: synthesis of the osmoprotectant glycine betaine from exogenously provided choline. *J Bacteriol*; 176: 5364-5371.

18. Boersma AJ, Zuhorn IS, Poolman B. **2015**. A sensor for quantification of macromolecular crowding in living cells. *Nat Methods*; 12: 227-229.
19. Bramkamp M, Lopez D. **2015**. Exploring the existence of lipid rafts in bacteria. *Microbiol Mol Biol Rev*; 79: 81-100.
20. Branda SS, Gonzalez-Pastor JE, Ben-Yehuda S, Losick R, Kolter R. **2001**. Fruiting body formation by *Bacillus subtilis*. *Proc Natl Acad Sci U S A*; 98: 11621-11626.
21. Bremer E. **2002**. *Adaptation to changing osmolarity*. *Bacillus subtilis* and its closest relatives. editors, Sonenshein AL, Hoch JA, Losick R. Washington, DC: ASM Press. p. 385-391.
22. Brill J, Hoffmann T, Bleisteiner M, Bremer E. **2011**. Osmotically controlled synthesis of the compatible solute proline is critical for cellular defense of *Bacillus subtilis* against high osmolarity. *J Bacteriol*; 193: 5335-5346.
23. Brill J, Hoffmann T, Putzer H, Bremer E. **2011**. T-box-mediated control of the anabolic proline biosynthetic genes of *Bacillus subtilis*. *Microbiology*; 157: 977-987.
24. Britton RA, Eichenberger P, Gonzalez-Pastor JE, Fawcett P, Monson R, Losick R, *et al.* **2002**. Genome-wide analysis of the stationary-phase sigma factor (sigma-H) regulon of *Bacillus subtilis*. *J Bacteriol*; 184: 4881-4890.
25. Buescher JM, Liebermeister W, Jules M, Uhr M, Muntel J, Botella E, *et al.* **2012**. Global network reorganization during dynamic adaptations of *Bacillus subtilis* metabolism. *Science*; 335: 1099-1103.
26. Campanella ME, Chu H, Low PS. **2005**. Assembly and regulation of a glycolytic enzyme complex on the human erythrocyte membrane. *Proc Natl Acad Sci U S A*; 102: 2402-2407.
27. Casadaban MJ, Cohen SN. **1980**. Analysis of gene control signals by DNA fusion and cloning in *Escherichia coli*. *J Mol Biol*; 138: 179-207.
28. Celler K, Koning RI, Koster AJ, van Wezel GP. **2013**. Multidimensional view of the bacterial cytoskeleton. *J Bacteriol*; 195: 1627-1636.
29. Chalfie M, Tu Y, Euskirchen G, Ward WW, Prasher DC. **1994**. Green fluorescent protein as a marker for gene expression. *Science*; 263: 802-805.
30. Chan CS, Winstone TM, Turner RJ. **2008**. Investigating protein-protein interactions by far-Westerns. *Adv Biochem Eng Biotechnol*; 110: 195-214.
31. Chen HL, Bernard CS, Hubert P, My L, Zhang CC. **2014**. Fluorescence resonance energy transfer based on interaction of PII and PipX proteins provides a robust and specific biosensor for 2-oxoglutarate, a central metabolite and a signalling molecule. *FEBS J*; 281: 1241-1255.
32. Chen J, Petrov A, Johansson M, Tsai A, O'Leary SE, Puglisi JD. **2014**. Dynamic pathways of -1 translational frameshifting. *Nature*; 512: 328-332.
33. Commichau FM, Rothe FM, Herzberg C, Wagner E, Hellwig D, Lehnik-Habrink M, *et al.* **2009**. Novel activities of glycolytic enzymes in *Bacillus subtilis*: interactions with essential proteins involved in mRNA processing. *Mol Cell Proteomics*; 8: 1350-1360.
34. Conrado RJ, Varner JD, DeLisa MP. **2008**. Engineering the spatial organization of metabolic enzymes: mimicking nature's synergy. *Curr Opin Biotechnol*; 19: 492-499.
35. Cormack BP, Valdivia RH, Falkow S. **1996**. FACS-optimized mutants of the green fluorescent protein (GFP). *Gene*; 173: 33-38.

References

36. Cremazy FG, Manders EM, Bastiaens PI, Kramer G, Hager GL, van Munster EB, *et al.* **2005.** Imaging in situ protein-DNA interactions in the cell nucleus using FRET-FLIM. *Exp Cell Res*; 309: 390-396.
37. Crivat G, Taraska JW. **2012.** Imaging proteins inside cells with fluorescent tags. *Trends Biotechnol*; 30: 8-16.
38. Crosby KC, Pietraszewska-Bogiel A, Gadella TW,Jr, Winkel BS. **2011.** Forster resonance energy transfer demonstrates a flavonoid metabolon in living plant cells that displays competitive interactions between enzymes. *FEBS Lett*; 585: 2193-2198.
39. Day RN, Davidson MW. **2009.** The fluorescent protein palette: tools for cellular imaging. *Chem Soc Rev*; 38: 2887-2921.
40. de Jong IG, Beilharz K, Kuipers OP, Veening JW. **2011.** Live Cell Imaging of *Bacillus subtilis* and *Streptococcus pneumoniae* using Automated Time-lapse Microscopy. *J Vis Exp*; 53: 3145.
41. de Jong IG, Veening JW, Kuipers OP. **2010.** Heterochronic phosphorelay gene expression as a source of heterogeneity in *Bacillus subtilis* spore formation. *J Bacteriol*; 192: 2053-2067.
42. de Smit MH, van Duin J. **1990.** Secondary structure of the ribosome binding site determines translational efficiency: a quantitative analysis. *Proc Natl Acad Sci U S A*; 87: 7668-7672.
43. Detert Oude Weme RG, Kovacs AT, de Jong SJ, Veening JW, Siebring J, Kuipers OP. **2015.** Single Cell FRET Analysis for the Identification of Optimal FRET-Pairs in *Bacillus subtilis* Using a Prototype MEM-FLIM System. *PLoS One*; 10: e0123239.
44. Detert Oude Weme RG, Seidel G, Kuipers OP. **2015.** Probing the regulatory effects of specific mutations in three major binding domains of the pleiotropic regulator CcpA of *Bacillus subtilis*. *Front. Microbiol.*; 6: 1051. doi: 10.3389/fmicb.2015.01051.
45. Deutscher J. **2008.** The mechanisms of carbon catabolite repression in bacteria. *Curr Opin Microbiol*; 11: 87-93.
46. Deutscher J, Kuster E, Bergstedt U, Charrier V, Hillen W. **1995.** Protein kinase-dependent HPr/CcpA interaction links glycolytic activity to carbon catabolite repression in gram-positive bacteria. *Mol Microbiol*; 15: 1049-1053.
47. Deutscher J, Reizer J, Fischer C, Galinier A, Saier MH,Jr, Steinmetz M. **1994.** Loss of protein kinase-catalyzed phosphorylation of HPr, a phosphocarrier protein of the phosphotransferase system, by mutation of the ptsH gene confers catabolite repression resistance to several catabolic genes of *Bacillus subtilis*. *J Bacteriol*; 176: 3336-3344.
48. Dougherty WG, Parks TD, Cary SM, Bazan JF, Fletterick RJ. **1989.** Characterization of the catalytic residues of the tobacco etch virus 49-kDa proteinase. *Virology*; 172: 302-310.
49. Drews G. **2000.** The roots of microbiology and the influence of Ferdinand Cohn on microbiology of the 19th century. *FEMS Microbiol Rev*; 24: 225-249.
50. Dubnau D, Losick R. **2006.** Bistability in bacteria. *Mol Microbiol*; 61: 564-572.
51. Dubnau D. **1991.** Genetic competence in *Bacillus subtilis*. *Microbiol Rev*; 55: 395-424.
52. Eberhardt A, Wu LJ, Errington J, Vollmer W, Veening JW. **2009.** Cellular localization of choline-utilization proteins in *Streptococcus pneumoniae* using novel fluorescent reporter systems. *Mol Microbiol*; 74: 395-408.

53. Ellis RJ. **2001**. Macromolecular crowding: obvious but underappreciated. *Trends Biochem Sci*; 26: 597-604.
54. Elowitz MB, Levine AJ, Siggia ED, Swain PS. **2002**. Stochastic gene expression in a single cell. *Science*; 297: 1183-1186.
55. Erickson HP. **2009**. Size and shape of protein molecules at the nanometer level determined by sedimentation, gel filtration, and electron microscopy. *Biol Proced Online*; 11: 32-51.
56. Erkens GB, Hanelt I, Goudsmits JM, Slotboom DJ, van Oijen AM. **2013**. Unsynchronised subunit motion in single trimeric sodium-coupled aspartate transporters. *Nature*; 502: 119-123.
57. Errington J. **2003**. Regulation of endospore formation in *Bacillus subtilis*. *Nat Rev Microbiol*; 1: 117-126.
58. Errington J. **2003**. Dynamic proteins and a cytoskeleton in bacteria. *Nat Cell Biol*; 5: 175-178.
59. Faires N, Tobisch S, Bachem S, Martin-Verstraete I, Hecker M, Stülke J. **1999**. The catabolite control protein CcpA controls ammonium assimilation in *Bacillus subtilis*. *J Mol Microbiol Biotechnol*; 1: 141-148.
60. Förster T. **1948**. Intermolecular energy migration and fluorescence. *Annalen der Physik*; 2: 55-75.
61. Frick JS, Autenrieth IB. **2013**. The gut microflora and its variety of roles in health and disease. *Curr Top Microbiol Immunol*; 358: 273-289.
62. Fridman O, Goldberg A, Ronin I, Shoshitaishvili N, Balaban NQ. **2014**. Optimization of lag time underlies antibiotic tolerance in evolved bacterial populations. *Nature*; 513: 418-421.
63. Fujita Y. **2009**. Carbon catabolite control of the metabolic network in *Bacillus subtilis*. *Biosci Biotechnol Biochem*; 73: 245-259.
64. Fujita Y, Miwa Y, Galinier A, Deutscher J. **1995**. Specific recognition of the *Bacillus subtilis* gnt cis-acting catabolite-responsive element by a protein complex formed between CcpA and seryl-phosphorylated HPr. *Mol Microbiol*; 17: 953-960.
65. Giepmans BN, Adams SR, Ellisman MH, Tsien RY. **2006**. The fluorescent toolbox for assessing protein location and function. *Science*; 312: 217-224.
66. Goedhart J, Vermeer JE, Adjobo-Hermans MJ, van Weeren L, Gadella TW, Jr. **2007**. Sensitive detection of p65 homodimers using red-shifted and fluorescent protein-based FRET couples. *PLoS One*; 2: e1011.
67. Goll J, Uetz P. **2006**. The elusive yeast interactome. *Genome Biol*; 7: 223.
68. Goodsell DS. **1993**. *Escherichia coli : One of the Simplest Cells*. The Machinery of Life. : Springer. p. 55-63.
69. Gordon GW, Berry G, Liang XH, Levine B, Herman B. **1998**. Quantitative fluorescence resonance energy transfer measurements using fluorescence microscopy. *Biophys J*; 74: 2702-2713.
70. Görke B, Stülke J. **2008**. Carbon catabolite repression in bacteria: many ways to make the most out of nutrients. *Nat Rev Microbiol*; 6: 613-624.
71. Gruber S, Veening JW, Bach J, Blettinger M, Bramkamp M, Errington J. **2014**. Interlinked Sister Chromosomes Arise in the Absence of Condensin during Fast Replication in *B. subtilis*. *Curr Biol*.

References

72. Grunberg R, Burnier JV, Ferrar T, Beltran-Sastre V, Stricher F, van der Sloot AM, *et al.* **2013**. Engineering of weak helper interactions for high-efficiency FRET probes. *Nat Methods*; 10: 1021-1027.
73. Guerout-Fleury AM, Frandsen N, Stragier P. **1996**. Plasmids for ectopic integration in *Bacillus subtilis*. *Gene*; 180: 57-61.
74. Gustafsson C, Govindarajan S, Minshull J. **2004**. Codon bias and heterologous protein expression. *Trends Biotechnol*; 22: 346-353.
75. Hahne H, Mäder U, Otto A, Bonn F, Steil L, Bremer E, *et al.* **2010**. A comprehensive proteomics and transcriptomics analysis of *Bacillus subtilis* salt stress adaptation. *J Bacteriol*; 192: 870-882.
76. Halfmann A, Hakenbeck R, Bruckner R. **2007**. A new integrative reporter plasmid for *Streptococcus pneumoniae*. *FEMS Microbiol Lett*; 268: 217-224.
77. Harwood CR, Cutting SM. **1990**. *Growth, maintenance and general techniques. Chapter 1 and appendix 1*. Molecular biological methods for *Bacillus*. editors, Harwood CR, Cutting SM. Chichester, UK.: John Wiley & Sons, Inc.
78. Harwood CR, Cutting SM. **1990**. Molecular biological methods for *Bacillus*: John Wiley & Sons, Inc. Chichester, UK.
79. Hecker M, Pane-Farre J, Volker U. **2007**. SigB-dependent general stress response in *Bacillus subtilis* and related gram-positive bacteria. *Annu Rev Microbiol*; 61: 215-236.
80. Hecker M, Volker U. **2001**. General stress response of *Bacillus subtilis* and other bacteria. *Adv Microb Physiol*; 44: 35-91.
81. Heintzmann R, Ficz G. **2006**. Breaking the resolution limit in light microscopy. *Brief Funct Genomic Proteomic*; 5: 289-301.
82. Henkin TM, Grundy FJ, Nicholson WL, Chambliss GH. **1991**. Catabolite repression of alpha-amylase gene expression in *Bacillus subtilis* involves a trans-acting gene product homologous to the *Escherichia coli* *lacl* and *galR* repressors. *Mol Microbiol*; 5: 575-584.
83. Herzberg C, Weidinger LA, Dorrbecker B, Hubner S, Stülke J, Commichau FM. **2007**. SPINE: a method for the rapid detection and analysis of protein-protein interactions in vivo. *Proteomics*; 7: 4032-4035.
84. Holtmann G, Bakker EP, Uozumi N, Bremer E. **2003**. KtrAB and KtrCD: two K⁺ uptake systems in *Bacillus subtilis* and their role in adaptation to hypertonicity. *J Bacteriol*; 185: 1289-1298.
85. Hoper D, Volker U, Hecker M. **2005**. Comprehensive characterization of the contribution of individual SigB-dependent general stress genes to stress resistance of *Bacillus subtilis*. *J Bacteriol*; 187: 2810-2826.
86. Horstmann N, Seidel G, Aung-Hilbrich LM, Hillen W. **2007**. Residues His-15 and Arg-17 of HPr participate differently in catabolite signal processing via CcpA. *J Biol Chem*; 282: 1175-1182.
87. Hyde CC, Ahmed SA, Padlan EA, Miles EW, Davies DR. **1988**. Three-dimensional structure of the tryptophan synthase alpha 2 beta 2 multienzyme complex from *Salmonella typhimurium*. *J Biol Chem*; 263: 17857-17871.
88. Israelsen H, Madsen SM, Vrang A, Hansen EB, Johansen E. **1995**. Cloning and partial characterization of regulated promoters from *Lactococcus lactis* Tn917-lacZ integrants with the new promoter probe vector, pAK80. *Appl Environ Microbiol*; 61: 2540-2547.

89. Jones SE, Lennon JT. **2010**. Dormancy contributes to the maintenance of microbial diversity. *Proc Natl Acad Sci U S A*; 107: 5881-5886.
90. Kaern M, Elston TC, Blake WJ, Collins JJ. **2005**. Stochasticity in gene expression: from theories to phenotypes. *Nat Rev Genet*; 6: 451-464.
91. Kanjee U, Ogata K, Houry WA. **2012**. Direct binding targets of the stringent response alarmone (p)ppGpp. *Mol Microbiol*; 85: 1029-1043.
92. Kearns DB, Losick R. **2005**. Cell population heterogeneity during growth of *Bacillus subtilis*. *Genes Dev*; 19: 3083-3094.
93. Kentner D, Sourjik V. **2010**. Use of fluorescence microscopy to study intracellular signaling in bacteria. *Annu Rev Microbiol*; 64: 373-390.
94. Kentner D, Sourjik V. **2009**. Dynamic map of protein interactions in the *Escherichia coli* chemotaxis pathway. *Mol Syst Biol*; 5: 238.
95. Kenworthy AK. **2001**. Imaging protein-protein interactions using fluorescence resonance energy transfer microscopy. *Methods*; 24: 289-296.
96. Kerfeld CA, Sawaya MR, Tanaka S, Nguyen CV, Phillips M, Beeby M, *et al.* **2005**. Protein structures forming the shell of primitive bacterial organelles. *Science*; 309: 936-938.
97. Kiviet DJ, Nghe P, Walker N, Boulineau S, Sunderlikova V, Tans SJ. **2014**. Stochasticity of metabolism and growth at the single-cell level. *Nature*; 514: 376-379.
98. Klarenbeek JB, Goedhart J, Hink MA, Gadella TW, Jalink K. **2011**. A mTurquoise-based cAMP sensor for both FLIM and ratiometric read-out has improved dynamic range. *PLoS One*; 6: e19170.
99. Klein J, Leupold S, Biegler I, Biedendieck R, Munch R, Jahn D. **2012**. TLM-Tracker: software for cell segmentation, tracking and lineage analysis in time-lapse microscopy movies. *Bioinformatics*; 28: 2276-2277.
100. Knight T. **2003**. Idempotent Vector Design for Standard Assembly of Biobricks. <http://web.mit.edu/synbio/release/docs/biobricks.pdf>.
101. Kobayashi K, Ehrlich SD, Albertini A, Amati G, Andersen KK, Arnaud M, *et al.* **2003**. Essential *Bacillus subtilis* genes. *Proc Natl Acad Sci U S A*; 100: 4678-4683.
102. Koch AL, Higgins ML, Doyle RJ. **1982**. The role of surface stress in the morphology of microbes. *J Gen Microbiol*; 128: 927-945.
103. Kohlstedt M, Sappa PK, Meyer H, Maass S, Zapras A, Hoffmann T, *et al.* **2014**. Adaptation of *Bacillus subtilis* carbon core metabolism to simultaneous nutrient limitation and osmotic challenge: a multi-omics perspective. *Environ Microbiol*; 16: 1898-1917.
104. Konkol MA, Blair KM, Kearns DB. **2013**. Plasmid-encoded ComI inhibits competence in the ancestral 3610 strain of *Bacillus subtilis*. *J Bacteriol*; 195: 4085-4093.
105. Kotte O, Volkmer B, Radzikowski JL, Heinemann M. **2014**. Phenotypic bistability in *Escherichia coli*'s central carbon metabolism. *Mol Syst Biol*; 10: 736.
106. Kramer N, Hahn J, Dubnau D. **2007**. Multiple interactions among the competence proteins of *Bacillus subtilis*. *Mol Microbiol*; 65: 454-464.
107. Kunkel MT, Garcia EL, Kajimoto T, Hall RA, Newton AC. **2009**. The protein scaffold NHERF-1 controls the amplitude and duration of localized protein kinase D activity. *J Biol Chem*; 284: 24653-24661.

References

108. Kunst F, Ogasawara N, Moszer I, Albertini AM, Alloni G, Azevedo V, *et al.* **1997**. The complete genome sequence of the gram-positive bacterium *Bacillus subtilis*. *Nature*; 390: 249-256.
109. Kuster E, Luesink EJ, de Vos WM, Hillen W. **1996**. Immunological crossreactivity to the catabolite control protein CcpA *Bacillus megaterium* is found in many gram-positive bacteria. *FEMS Microbiol Lett*; 139: 109-115.
110. Kuster-Schock E, Wagner A, Volker U, Hillen W. **1999**. Mutations in catabolite control protein CcpA showing glucose-independent regulation in *Bacillus megaterium*. *J Bacteriol*; 181: 7634-7638.
111. Kuwada NJ, Traxler B, Wiggins PA. **2015**. Genome-scale quantitative characterization of bacterial protein localization dynamics throughout the cell cycle. *Mol Microbiol*; 95: 64-79.
112. Lakowicz JR. **2006**. Principles of fluorescence spectroscopy. Third ed. New York: Springer.
113. Lakowicz JR. **2006**. *Frequency-Domain Lifetime Measurements, Chapter 5*. Principles of fluorescence spectroscopy. New York: Springer. p. 157.
114. Lakowicz JR. **2006**. *Energy Transfer, Chapter 13*. Principles of fluorescence spectroscopy. New York: Springer. p. 443.
115. Lakowicz JR. **2006**. *Time-Domain Lifetime Measurements, Chapter 4*. Principles of fluorescence spectroscopy. New York: Springer. p. 97.
116. Laloux G, Jacobs-Wagner C. **2014**. How do bacteria localize proteins to the cell pole? *J Cell Sci*; 127: 11-19.
117. Lemon KP, Grossman AD. **1998**. Localization of bacterial DNA polymerase: evidence for a factory model of replication. *Science*; 282: 1516-1519.
118. Lewis K. **2010**. Persister cells. *Annu Rev Microbiol*; 64: 357-372.
119. Lewis P, Yang X. **2012**. *The organization of transcription and translation. Chapter 5*. *Bacillus. Cellular and Molecular Biology*. editor, Graumann P.: Caister Academic Press. p. 123-150.
120. Lewis PJ, Marston AL. **1999**. GFP vectors for controlled expression and dual labelling of protein fusions in *Bacillus subtilis*. *Gene*; 227: 101-110.
121. Lithwick G, Margalit H. **2003**. Hierarchy of sequence-dependent features associated with prokaryotic translation. *Genome Res*; 13: 2665-2673.
122. Locke JC, Young JW, Fontes M, Hernandez Jimenez MJ, Elowitz MB. **2011**. Stochastic pulse regulation in bacterial stress response. *Science*; 334: 366-369.
123. Long AD, Mangalam HJ, Chan BY, Toller L, Hatfield GW, Baldi P. **2001**. Improved statistical inference from DNA microarray data using analysis of variance and a Bayesian statistical framework. Analysis of global gene expression in *Escherichia coli* K12. *J Biol Chem*; 276: 19937-19944.
124. Ludwig H, Rebhan N, Blencke HM, Merzbacher M, Stülke J. **2002**. Control of the glycolytic gapA operon by the catabolite control protein A in *Bacillus subtilis*: a novel mechanism of CcpA-mediated regulation. *Mol Microbiol*; 45: 543-553.
125. Lulko AT, Buist G, Kok J, Kuipers OP. **2007**. Transcriptome analysis of temporal regulation of carbon metabolism by CcpA in *Bacillus subtilis* reveals additional target genes. *J Mol Microbiol Biotechnol*; 12: 82-95.
126. Maass S, Sievers S, Zuhlke D, Kuzinski J, Sappa PK, Muntel J, *et al.* **2011**. Efficient, global-scale quantification of absolute protein amounts by integration of targeted

- mass spectrometry and two-dimensional gel-based proteomics. *Anal Chem*; 83: 2677-2684.
127. Macnab RM. **2003**. How bacteria assemble flagella. *Annu Rev Microbiol*; 57: 77-100.
128. Mäder U, Schmeisky AG, Florez LA, Stülke J. **2012**. SubtiWiki--a comprehensive community resource for the model organism *Bacillus subtilis*. *Nucleic Acids Res*; 40: D1278-87.
129. Maisonneuve E, Gerdes K. **2014**. Molecular mechanisms underlying bacterial persisters. *Cell*; 157: 539-548.
130. Maisonneuve E, Castro-Camargo M, Gerdes K. **2013**. (p)ppGpp controls bacterial persistence by stochastic induction of toxin-antitoxin activity. *Cell*; 154: 1140-1150.
131. Marchadier E, Carballido-Lopez R, Brinster S, Fabret C, Mervelet P, Bessieres P, *et al*. **2011**. An expanded protein-protein interaction network in *Bacillus subtilis* reveals a group of hubs: Exploration by an integrative approach. *Proteomics*; 11: 2981-2991.
132. Marciniak BC, Pabijaniak M, de Jong A, Duhring R, Seidel G, Hillen W, *et al*. **2012**. High- and low-affinity *cre* boxes for CcpA binding in *Bacillus subtilis* revealed by genome-wide analysis. *BMC Genomics*; 13: 401-2164-13-401.
133. Margolin W. **2005**. FtsZ and the division of prokaryotic cells and organelles. *Nat Rev Mol Cell Biol*; 6: 862-871.
134. Marston AL, Errington J. **1999**. Dynamic movement of the ParA-like Soj protein of *B. subtilis* and its dual role in nucleoid organization and developmental regulation. *Mol Cell*; 4: 673-682.
135. Martin B, Granadel C, Campo N, Henard V, Prudhomme M, Claverys JP. **2010**. Expression and maintenance of ComD-ComE, the two-component signal-transduction system that controls competence of *Streptococcus pneumoniae*. *Mol Microbiol*; 75: 1513-1528.
136. Martin-Verstraete I, Stülke J, Klier A, Rapoport G. **1995**. Two different mechanisms mediate catabolite repression of the *Bacillus subtilis* levanase operon. *J Bacteriol*; 177: 6919-6927.
137. Merzlyak EM, Goedhart J, Shcherbo D, Bulina ME, Shcheglov AS, Fradkov AF, *et al*. **2007**. Bright monomeric red fluorescent protein with an extended fluorescence lifetime. *Nat Methods*; 4: 555-557.
138. Meyer FM, Gerwig J, Hammer E, Herzberg C, Commichau FM, Völker U, *et al*. **2011**. Physical interactions between tricarboxylic acid cycle enzymes in *Bacillus subtilis*: evidence for a metabolon. *Metab Eng*; 13: 18-27.
139. Meyer H, Weidmann H, Mäder U, Hecker M, Völker U, Lalk M. **2014**. A time resolved metabolomics study: the influence of different carbon sources during growth and starvation of *Bacillus subtilis*. *Mol Biosyst*; 10: 1812-1823.
140. Mika JT, van den Bogaart G, Veenhoff L, Krasnikov V, Poolman B. **2010**. Molecular sieving properties of the cytoplasm of *Escherichia coli* and consequences of osmotic stress. *Mol Microbiol*; 77: 200-207.
141. Milde S, Brown J, Schmidt H, Boettger L, Chapart M, Cheng K, *et al*. **2008**. Team:Cambridge/Improved GFP - 2008.igem.org. partsregistry.org Part:BBa I746909.
142. Miwa Y, Nakata A, Ogiwara A, Yamamoto M, Fujita Y. **2000**. Evaluation and characterization of catabolite-responsive elements (*cre*) of *Bacillus subtilis*. *Nucleic Acids Res*; 28: 1206-1210.

References

143. Moller BL. **2010**. Plant science. Dynamic metabolons. *Science*; 330: 1328-1329.
144. Moreno MS, Schneider BL, Maile RR, Weyler W, Saier MH, Jr. **2001**. Catabolite repression mediated by the CcpA protein in *Bacillus subtilis*: novel modes of regulation revealed by whole-genome analyses. *Mol Microbiol*; 39: 1366-1381.
145. Moszer I, Rocha EP, Danchin A. **1999**. Codon usage and lateral gene transfer in *Bacillus subtilis*. *Curr Opin Microbiol*; 2: 524-528.
146. Msadek T. **1999**. When the going gets tough: survival strategies and environmental signaling networks in *Bacillus subtilis*. *Trends Microbiol*; 7: 201-207.
147. Munster vEB, Gadella TWJ. **2005**. *Fluorescence Lifetime Imaging Microscopy (FLIM)*, Chapter 5. *Advances in Biochemical Engineering/Biotechnology*. editor, Scheper T. p. 143-175.
148. Nagai T, Ibata K, Park ES, Kubota M, Mikoshiba K, Miyawaki A. **2002**. A variant of yellow fluorescent protein with fast and efficient maturation for cell-biological applications. *Nat Biotechnol*; 20: 87-90.
149. Nagy P, Vamosi G, Bodnar A, Lockett SJ, Szollosi J. **1998**. Intensity-based energy transfer measurements in digital imaging microscopy. *Eur Biophys J*; 27: 377-389.
150. Newman JA, Rodrigues C, Lewis RJ. **2013**. Molecular basis of the activity of SinR protein, the master regulator of biofilm formation in *Bacillus subtilis*. *J Biol Chem*; 288: 10766-10778.
151. Nguyen AW, Daugherty PS. **2005**. Evolutionary optimization of fluorescent proteins for intracellular FRET. *Nat Biotechnol*; 23: 355-360.
152. Nicolas P, Mäder U, Dervyn E, Rochat T, Leduc A, Pigeonneau N, *et al.* **2012**. Condition-dependent transcriptome reveals high-level regulatory architecture in *Bacillus subtilis*. *Science*; 335: 1103-1106.
153. Nobis M, McGhee EJ, Morton JP, Schwarz JP, Karim SA, Quinn J, *et al.* **2013**. Intravital FLIM-FRET imaging reveals dasatinib-induced spatial control of src in pancreatic cancer. *Cancer Res*; 73: 4674-4686.
154. Norholm MH. **2010**. A mutant Pfu DNA polymerase designed for advanced uracil-excision DNA engineering. *BMC Biotechnol*; 10: 21-6750-10-21.
155. Overkamp W, Beilharz K, Detert Oude Weme R, Solopova A, Karsens H, Kovacs AT, *et al.* **2013**. Benchmarking various GFP variants in *Bacillus subtilis*, *Streptococcus pneumoniae* and *Lactococcus lactis* for live cell imaging. *Appl Environ Microbiol*; 79: 6481-6490.
156. Ozbudak EM, Thattai M, Kurtser I, Grossman AD, van Oudenaarden A. **2002**. Regulation of noise in the expression of a single gene. *Nat Genet*; 31: 69-73.
157. Padilla-Parra S, Tramier M. **2012**. FRET microscopy in the living cell: different approaches, strengths and weaknesses. *Bioessays*; 34: 369-376.
158. Padilla-Parra S, Auduge N, Lalucque H, Mevel JC, Coppey-Moisan M, Tramier M. **2009**. Quantitative comparison of different fluorescent protein couples for fast FRET-FLIM acquisition. *Biophys J*; 97: 2368-2376.
159. Pedelacq JD, Cabantous S, Tran T, Terwilliger TC, Waldo GS. **2006**. Engineering and characterization of a superfolder green fluorescent protein. *Nat Biotechnol*; 24: 79-88.
160. Piston DW, Kremers GJ. **2007**. Fluorescent protein FRET: the good, the bad and the ugly. *Trends Biochem Sci*; 32: 407-414.

161. Poyales DA, Goldstein A, Ward G, Hughes Jr AJ. **1994**. TEV-protease, recombinant: a site-specific protease for efficient cleavage of affinity tags from expressed proteins. *Focus*; 16: 1-5.
162. Prax M, Bertram R. **2014**. Metabolic aspects of bacterial persisters. *Front Cell Infect Microbiol*; 4: 148.
163. Puigbo P, Guzman E, Romeu A, Garcia-Vallve S. **2007**. OPTIMIZER: a web server for optimizing the codon usage of DNA sequences. *Nucleic Acids Res*; 35: W126-31.
164. Quisel JD, Burkholder WF, Grossman AD. **2001**. In vivo effects of sporulation kinases on mutant Spo0A proteins in *Bacillus subtilis*. *J Bacteriol*; 183: 6573-6578.
165. Rajapakse HE, Gahlaut N, Mohandessi S, Yu D, Turner JR, Miller LW. **2010**. Time-resolved luminescence resonance energy transfer imaging of protein-protein interactions in living cells. *Proc Natl Acad Sci U S A*; 107: 13582-13587.
166. Remington SJ. **2011**. Green fluorescent protein: a perspective. *Protein Sci*; 20: 1509-1519.
167. Rizzo MA, Springer GH, Granada B, Piston DW. **2004**. An improved cyan fluorescent protein variant useful for FRET. *Nat Biotechnol*; 22: 445-449.
168. Rojas E, Theriot JA, Huang KC. **2014**. Response of *Escherichia coli* growth rate to osmotic shock. *Proc Natl Acad Sci U S A*; 111: 7807-7812.
169. Rudner DZ, Losick R. **2010**. Protein subcellular localization in bacteria. *Cold Spring Harb Perspect Biol*; 2: a000307.
170. Salis HM, Mirsky EA, Voigt CA. **2009**. Automated design of synthetic ribosome binding sites to control protein expression. *Nat Biotechnol*; 27: 946-950.
171. Sambrook J, Fritsch EF, and Maniatis T. **1989**. Molecular Cloning: A Laboratory Manual. 2nd ed. New York: Cold Spring Harbor Laboratory Press.
172. Scheu PD, Witan J, Rauschmeier M, Graf S, Liao YF, Ebert-Jung A, *et al.* **2012**. CitA/CitB two-component system regulating citrate fermentation in *Escherichia coli* and its relation to the DcuS/DcuR system in vivo. *J Bacteriol*; 194: 636-645.
173. Schmutz J, Wheeler J, Grimwood J, Dickson M, Yang J, Caoile C, *et al.* **2004**. Quality assessment of the human genome sequence. *Nature*; 429: 365-368.
174. Scholz O, Thiel A, Hillen W, Niederweis M. **2000**. Quantitative analysis of gene expression with an improved green fluorescent protein. p6. *Eur J Biochem*; 267: 1565-1570.
175. Schreiber G, Barberis M, Scolari S, Klaus C, Herrmann A, Klipp E. **2012**. Unraveling interactions of cell cycle-regulating proteins Sic1 and B-type cyclins in living yeast cells: a FLIM-FRET approach. *FASEB J*; 26: 546-554.
176. Schumacher MA, Sprehe M, Bartholomae M, Hillen W, Brennan RG. **2011**. Structures of carbon catabolite protein A-(HPr-Ser46-P) bound to diverse catabolite response element sites reveal the basis for high-affinity binding to degenerate DNA operators. *Nucleic Acids Res*; 39: 2931-2942.
177. Schumacher MA, Seidel G, Hillen W, Brennan RG. **2007**. Structural mechanism for the fine-tuning of CcpA function by the small molecule effectors glucose 6-phosphate and fructose 1,6-bisphosphate. *J Mol Biol*; 368: 1042-1050.
178. Schumacher MA, Seidel G, Hillen W, Brennan RG. **2006**. Phosphoprotein Crh-Ser46-P displays altered binding to CcpA to effect carbon catabolite regulation. *J Biol Chem*; 281: 6793-6800.

References

179. Schumacher MA, Allen GS, Diel M, Seidel G, Hillen W, Brennan RG. **2004**. Structural basis for allosteric control of the transcription regulator CcpA by the phosphoprotein HPr-Ser46-P. *Cell*; 118: 731-741.
180. Seidel G, Diel M, Fuchsbaauer N, Hillen W. **2005**. Quantitative interdependence of coeffectors, CcpA and cre in carbon catabolite regulation of *Bacillus subtilis*. *FEBS J*; 272: 2566-2577.
181. Seidenari S, Arginelli F, Dunsby C, French PM, Konig K, Magnoni C, *et al.* **2013**. Multiphoton laser tomography and fluorescence lifetime imaging of melanoma: morphologic features and quantitative data for sensitive and specific non-invasive diagnostics. *PLoS One*; 8: e70682.
182. Shaner NC, Steinbach PA, Tsien RY. **2005**. A guide to choosing fluorescent proteins. *Nat Methods*; 2: 905-909.
183. Shaner NC, Campbell RE, Steinbach PA, Giepmans BN, Palmer AE, Tsien RY. **2004**. Improved monomeric red, orange and yellow fluorescent proteins derived from *Discosoma sp.* red fluorescent protein. *Nat Biotechnol*; 22: 1567-1572.
184. Shapiro L, McAdams HH, Losick R. **2009**. Why and how bacteria localize proteins. *Science*; 326: 1225-1228.
185. Shcherbo D, Souslova EA, Goedhart J, Chepurnykh TV, Gaintzeva A, Shemiakina II, *et al.* **2009**. Practical and reliable FRET/FLIM pair of fluorescent proteins. *BMC Biotechnol*; 9: 24-6750-9-24.
186. Shimomura O. **1995**. A short story of aequorin. *Biol Bull*; 189: 1-5.
187. Shimomura O, Johnson FH, Saiga Y. **1962**. Extraction, purification and properties of aequorin, a bioluminescent protein from the luminous hydromedusan, *Aequorea*. *J Cell Comp Physiol*; 59: 223-239.
188. Singh KD, Schmalisch MH, Stülke J, Görke B. **2008**. Carbon catabolite repression in *Bacillus subtilis*: quantitative analysis of repression exerted by different carbon sources. *J Bacteriol*; 190: 7275-7284.
189. Sleator RD, Hill C. **2002**. Bacterial osmoadaptation: the role of osmolytes in bacterial stress and virulence. *FEMS Microbiol Rev*; 26: 49-71.
190. Sliusarenko O, Heinritz J, Emonet T, Jacobs-Wagner C. **2011**. High-throughput, subpixel precision analysis of bacterial morphogenesis and intracellular spatio-temporal dynamics. *Mol Microbiol*; 80: 612-627.
191. Smits WK, Kuipers OP, Veening JW. **2006**. Phenotypic variation in bacteria: the role of feedback regulation. *Nat Rev Microbiol*; 4: 259-271.
192. Soetaert W, Vandamme E. **2006**. The impact of industrial biotechnology. *Biotechnol J*; 1: 756-769.
193. Solopova A, van Gestel J, Weissing FJ, Bachmann H, Teusink B, Kok J, *et al.* **2014**. Bet-hedging during bacterial diauxic shift. *Proc Natl Acad Sci U S A*; 111: 7427-7432.
194. Solov'yev V, Salamov A. **2011**. BPROM - Prediction of bacterial promoters. <http://linux1.softberry.com/berry.phtml?topic=bprom&group=programs&subgroup=gfindb>.
195. Sonenshein AL, Hoch JA, Losick R. **1993**. *Bacillus subtilis* and other Gram-positive bacteria: Biochemistry, Physiology, and Molecular Genetics. 1st ed. Washington D.C.: American Society for Microbiology.
196. Sonenshein AL. **2007**. Control of key metabolic intersections in *Bacillus subtilis*. *Nat Rev Microbiol*; 5: 917-927.

197. Southward CM, Surette MG. **2002**. The dynamic microbe: green fluorescent protein brings bacteria to light. *Mol Microbiol*; 45: 1191-1196.
198. Sprehe M, Seidel G, Diel M, Hillen W. **2007**. CcpA mutants with differential activities in *Bacillus subtilis*. *J Mol Microbiol Biotechnol*; 12: 96-105.
199. Strachotova D, Holoubek A, Kucerova H, Benda A, Humpolickova J, Vachova L, *et al.* **2012**. Ato protein interactions in yeast plasma membrane revealed by fluorescence lifetime imaging (FLIM). *Biochim Biophys Acta*; 1818: 2126-2134.
200. Stryer L. **1978**. Fluorescence energy transfer as a spectroscopic ruler. *Annu Rev Biochem*; 47: 819-846.
201. Stülke J, Hillen W. **2000**. Regulation of carbon catabolism in *Bacillus* species. *Annu Rev Microbiol*; 54: 849-880.
202. Subtiwiki. **2014**. CcpA regulon. http://subtiwiki.uni-goettingen.de/wiki/index.php/CcpA_regulon.
203. Sun Y, Rombola C, Jyothikumar V, Periasamy A. **2013**. Forster resonance energy transfer microscopy and spectroscopy for localizing protein-protein interactions in living cells. *Cytometry A*; 83: 780-793.
204. Sun Y, Day RN, Periasamy A. **2011**. Investigating protein-protein interactions in living cells using fluorescence lifetime imaging microscopy. *Nat Protoc*; 6: 1324-1340.
205. Tabone M, Lioy VS, Ayora S, Machon C, Alonso JC. **2014**. Role of toxin zeta and starvation responses in the sensitivity to antimicrobials. *PLoS One*; 9: e86615.
206. Thattai M, van Oudenaarden A. **2001**. Intrinsic noise in gene regulatory networks. *Proc Natl Acad Sci U S A*; 98: 8614-8619.
207. Tsien RY. **2009**. Indicators based on fluorescence resonance energy transfer (FRET). *Cold Spring Harb Protoc*; 2009: 57.
208. Tsien RY. **1998**. The green fluorescent protein. *Annu Rev Biochem*; 67: 509-544.
209. Uetz P, Giot L, Cagney G, Mansfield TA, Judson RS, Knight JR, *et al.* **2000**. A comprehensive analysis of protein-protein interactions in *Saccharomyces cerevisiae*. *Nature*; 403: 623-627.
210. Valdivia RH, Cormack BP, Falkow S. **2006**. The uses of green fluorescent protein in prokaryotes. *Methods Biochem Anal*; 47: 163-178.
211. van den Bogaart G, Hermans N, Krasnikov V, Poolman B. **2007**. Protein mobility and diffusive barriers in *Escherichia coli*: consequences of osmotic stress. *Mol Microbiol*; 64: 858-871.
212. van der Krogt GN, Ogink J, Ponsioen B, Jalink K. **2008**. A comparison of donor-acceptor pairs for genetically encoded FRET sensors: application to the Epac cAMP sensor as an example. *PLoS One*; 3: e1916.
213. van Gestel J, Weissing FJ, Kuipers OP, Kovacs AT. **2014**. Density of founder cells affects spatial pattern formation and cooperation in *Bacillus subtilis* biofilms. *ISME J*; 8: 2069-2079.
214. van Hijum SA, de Jong A, Baerends RJ, Karsens HA, Kramer NE, Larsen R, *et al.* **2005**. A generally applicable validation scheme for the assessment of factors involved in reproducibility and quality of DNA-microarray data. *BMC Genomics*; 6: 77.
215. van Hijum SA, Garcia de la Nava J, Trelles O, Kok J, Kuipers OP. **2003**. MicroPreP: a cDNA microarray data pre-processing framework. *Appl Bioinformatics*; 2: 241-244.
216. Van Munster EB, Gadella TW, Jr. **2004**. phiFLIM: a new method to avoid aliasing in frequency-domain fluorescence lifetime imaging microscopy. *J Microsc*; 213: 29-38.

References

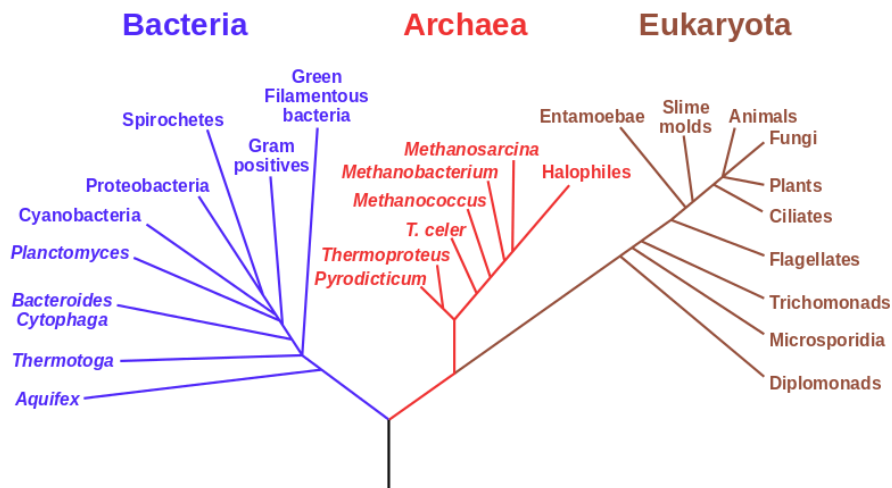
217. van Rheenen J, Langeslag M, Jalink K. **2004**. Correcting confocal acquisition to optimize imaging of fluorescence resonance energy transfer by sensitized emission. *Biophys J*; 86: 2517-2529.
218. Veening JW, Smits WK, Kuipers OP. **2008**. Bistability, epigenetics, and bet-hedging in bacteria. *Annu Rev Microbiol*; 62: 193-210.
219. Veening JW, Smits WK, Hamoen LW, Jongbloed JD, Kuipers OP. **2004**. Visualization of differential gene expression by improved cyan fluorescent protein and yellow fluorescent protein production in *Bacillus subtilis*. *Appl Environ Microbiol*; 70: 6809-6815.
220. Vlamakis H, Chai Y, Beauregard P, Losick R, Kolter R. **2013**. Sticking together: building a biofilm the *Bacillus subtilis* way. *Nat Rev Microbiol*; 11: 157-168.
221. W.M. Keck Center for Cellular Imaging. **2011**. Seven images required for FRET data process. <http://www.kcci.virginia.edu/FRET/process/seven.php>.
222. Wade JT, Struhl K, Busby SJ, Grainger DC. **2007**. Genomic analysis of protein-DNA interactions in bacteria: insights into transcription and chromosome organization. *Mol Microbiol*; 65: 21-26.
223. Waldo GS, Standish BM, Berendzen J, Terwilliger TC. **1999**. Rapid protein-folding assay using green fluorescent protein. *Nat Biotechnol*; 17: 691-695.
224. Wendrich TM, Marahiel MA. **1997**. Cloning and characterization of a *relA/spoT* homologue from *Bacillus subtilis*. *Mol Microbiol*; 26: 65-79.
225. Whatmore AM, Chudek JA, Reed RH. **1990**. The effects of osmotic upshock on the intracellular solute pools of *Bacillus subtilis*. *J Gen Microbiol*; 136: 2527-2535.
226. Whatmore AM, Reed RH. **1990**. Determination of turgor pressure in *Bacillus subtilis*: a possible role for K⁺ in turgor regulation. *J Gen Microbiol*; 136: 2521-2526.
227. Williamson MP, Sutcliffe MJ. **2010**. Protein-protein interactions. *Biochem Soc Trans*; 38: 875-878.
228. Wood JM. **2011**. Bacterial osmoregulation: a paradigm for the study of cellular homeostasis. *Annu Rev Microbiol*; 65: 215-238.
229. Wood JM, Bremer E, Csonka LN, Kraemer R, Poolman B, van der Heide T, *et al.* **2001**. Osmosensing and osmoregulatory compatible solute accumulation by bacteria. *Comp Biochem Physiol A Mol Integr Physiol*; 130: 437-460.
230. Wu F, Minteer S. **2015**. Krebs cycle metabolon: structural evidence of substrate channeling revealed by cross-linking and mass spectrometry. *Angew Chem Int Ed Engl*; 54: 1851-1854.
231. Yeates TO, Crowley CS, Tanaka S. **2010**. Bacterial microcompartment organelles: protein shell structure and evolution. *Annu Rev Biophys*; 39: 185-205.
232. Yoshida K, Kobayashi K, Miwa Y, Kang CM, Matsunaga M, Yamaguchi H, *et al.* **2001**. Combined transcriptome and proteome analysis as a powerful approach to study genes under glucose repression in *Bacillus subtilis*. *Nucleic Acids Res*; 29: 683-692.
233. Young JW, Locke JC, Elowitz MB. **2013**. Rate of environmental change determines stress response specificity. *Proc Natl Acad Sci U S A*; 110: 4140-4145.
234. Young JW, Locke JC, Altinok A, Rosenfeld N, Bacarian T, Swain PS, *et al.* **2011**. Measuring single-cell gene expression dynamics in bacteria using fluorescence time-lapse microscopy. *Nat Protoc*; 7: 80-88.

235. Zacharias DA, Violin JD, Newton AC, Tsien RY. **2002**. Partitioning of lipid-modified monomeric GFPs into membrane microdomains of live cells. *Science*; 296: 913-916.
236. Zeigler DR, Pragai Z, Rodriguez S, Chevreux B, Muffler A, Albert T, *et al.* **2008**. The origins of 168, W23, and other *Bacillus subtilis* legacy strains. *J Bacteriol*; 190: 6983-6995.
237. Zellmeier S, Zuber U, Schumann W, Wiegert T. **2003**. The absence of FtsH metalloprotease activity causes overexpression of the sigmaW-controlled *pbpE* gene, resulting in filamentous growth of *Bacillus subtilis*. *J Bacteriol*; 185: 973-982.
238. Zhao Q, Schelen B, Schouten R, van den Oever R, Leenen R, van Kuijk H, *et al.* **2012**. Modulated electron-multiplied fluorescence lifetime imaging microscope: all-solid-state camera for fluorescence lifetime imaging. *J Biomed Opt*; 17: 126020.
239. Zhao X, Norris SJ, Liu J. **2014**. Molecular architecture of the bacterial flagellar motor in cells. *Biochemistry*; 53: 4323-4333.
240. Zimmer C. **2009**. Origins. On the origin of eukaryotes. *Science*; 325: 666-668.

Nederlandse Samenvatting voor de Leek

“Als je niet van bacteriën houdt, dan ben je op de verkeerde planeet.” Vrij vertaald, Stewart Brand.

Het Life Science gebouw van de Universiteit van Groningen, *de Linnaeusborg*, is vernoemd naar Carolus Linnaeus. Hij is de grondlegger van de indeling van organismen in groepen op basis van morfologie. Organismen kunnen worden ingedeeld in drie domeinen: Archaea (ook wel oerbacteriën), Bacteriën en Eukaryoten (o.a. bakkersgist, planten en dieren) zie afbeelding 1. Archaea en bacteriën zijn organismen zonder celkern en eukaryoten zijn organismen met celkern.



Afbeelding 1. Fylogenetische stamboom om de evolutionaire geschiedenis van soorten weer te geven. De drie domeinen zijn weergegeven in blauw, rood en bruin. De knooppunten in deze boom verwijzen naar de meest recente gemeenschappelijke voorouder. Bron: http://nl.wikipedia.org/wiki/Fylogenetische_stamboom

Bacteriën waren waarschijnlijk de eerste vorm van leven op aarde. Later tijdens de evolutie zorgde een symbiose tussen eukaryote cellen en een bacterie ervoor dat eukaryoten nu mitochondriën (de verbrandingsmotor die voor energie zorgt) hebben.

Bacteriën zijn voor het eerst ontdekt rond 1670 door de Nederlandse opticien en bioloog Antonie van Leeuwenhoek. Hij deed zijn ontdekking met een zelfgemaakte microscoop en hij noemde ze *beesjes*, *kleijne schepsels* of *animalcules*.

Veel mensen denken als het over bacteriën gaat alleen aan de negatieve aspecten, zoals infecties (bijvoorbeeld van *Streptococcus pneumoniae* en *Staphylococcus aureus*) en bederving van voedsel (bijvoorbeeld door *Bacillus cereus*). Maar bacteriën zijn juist ook ontzettend nuttig voor ons! In het menselijk lichaam zitten ongeveer 10x zoveel bacteriën dan het aantal cellen waaruit we bestaan. Deze bacteriën zitten bijvoorbeeld op onze huid, maar vooral in onze darmen (onze darmflora). Hier helpen ze ons met de vertering van voedsel, om vitamines voor ons te maken en om ons te beschermen tegen ziekteverwekkers. De groei van de goede bacteriën in onze darmen zorgt ervoor dat de ziekteverwekkers niet kunnen groeien.

Bacteriën worden ook gebruikt voor de fermentatie van voedsel, waardoor het voedsel een andere (vaak betere) textuur, smaak, geur en houdbaarheid krijgt. Denk bijvoorbeeld aan de productie van zuurkool of kaas en yoghurt. Terwijl (melkzuur)bacteriën in de melk groeien scheiden ze melkzuur uit wat zorgt voor een smaakverandering en een langere houdbaarheid van het voedsel.

Een ander voorbeeld van nuttig gebruik van bacteriën is dat sommige bacteriën worden gebruikt om de antibiotica te maken waarmee we ziekteverwekkende bacteriën kunnen bestrijden.

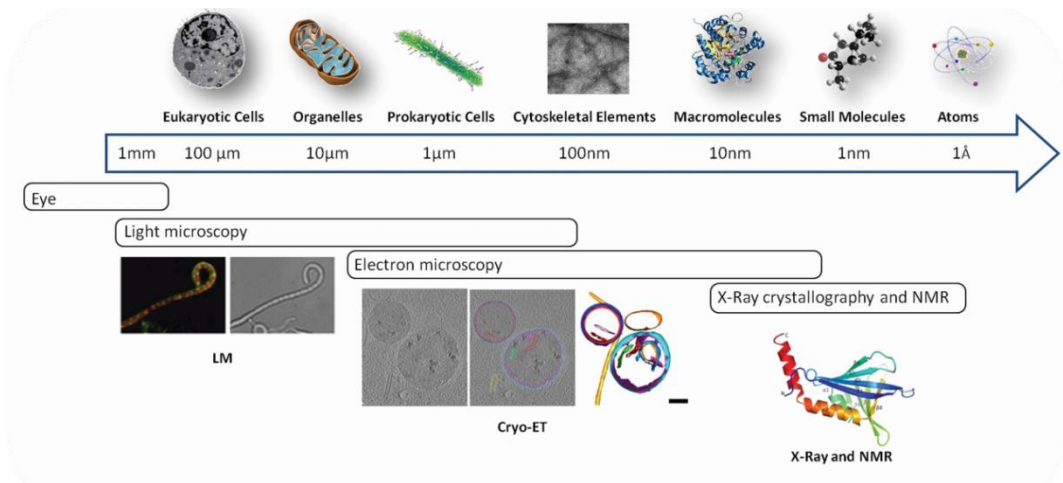
Het genoom, ook wel het DNA, van een bacterie is ongeveer 1000x kleiner dan dat van mensen. DNA bevat de genetische informatie en is de bouwtekening van leven. Sinds de jaren 80 van de vorige eeuw slagen mensen er steeds beter in om het DNA te veranderen. Dankzij deze genetische modificatie kunnen we bacteriën steeds beter voor ons laten werken. Denk hierbij aan eiwitproductie voor wasmiddelen of aan productie van bioplastics voor een beter milieu.

Het voordeel van werken met bacteriën is dat ze snel groeien (verdubbelingstijd van 30-60 minuten) en dat veel genen, zoals voor suikermetabolisme, ook bij veel andere organismen voorkomen, zelfs ook bij mensen. We zijn dus sterker verwant aan bacteriën dan we denken! De kennis die is opgedaan met bacteriën kan dan ook worden gebruikt om andere organismen te bestuderen.

Bacillus subtilis

In dit proefschrift is de bacterie *Bacillus subtilis* gebruikt. *B. subtilis* komt veel voor in de grond en op de wortels van planten, maar kan ook voorkomen in onze darmflora. *B. subtilis* wordt wereldwijd als model-organisme gebruikt, d.w.z. dat veel onderzoekers deze bacterie als studie object kiezen en de kennis die met deze bacterie is opgedaan kan weer worden ingezet om andere bacteriën te bestuderen. Voordat vanaf de jaren 1950 antibiotica op grote schaal werden gebruikt werd *B. subtilis* ook gebruikt

als voedingssupplement om het menselijk immuunsysteem te stimuleren. Dit hielp tegen infecties in het spijsverteringskanaal en in de urinewegen.



Afbeelding 2. Weergave van de grootte van verschillende cellen en onderdelen van cellen. Bacteriële cellen zijn bijna honderd keer zo klein als eukaryote cellen. Ook is weergegeven wat de resolutie is van verschillende technieken om cellen of onderdelen daarvan te bestuderen. Bron: Katherine Celler, Journal of Bacteriology 2013 [28].

Organisatie in bacteriën

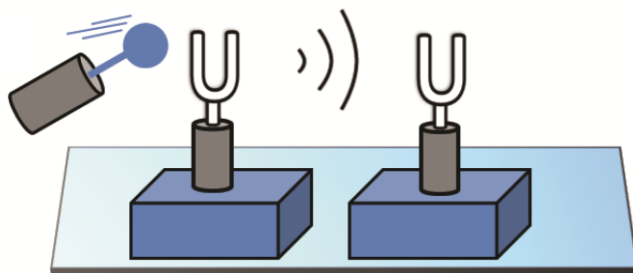
Lange tijd werd gedacht dat bacteriën aan de binnenkant slechts een ongeorganiseerd zootje waren, omdat ze geen organellen hebben. Maar bacteriën hebben ook een 'skelet': het cytoskelet. Dit is een ringvormige structuur die tegen hun celmembraan aanzit. Er is ook steeds meer bekend over de organisatie binnenin bacteriën en het blijkt dat veel eiwitten een specifieke locatie in de cel hebben. Eiwitcomplexen in bacteriën zijn misschien wel het bacteriële equivalent van eukaryote organellen.

Eerder onderzoek suggereert dat deze eiwitcomplexen tijdelijk van aard zijn; ze vormen wanneer nodig en vallen daarna weer uit elkaar. In dit onderzoek wilden we van een paar eiwitten weten wat de dynamiek van deze complexvorming is.

We hebben de eiwitten die betrokken zijn bij de vertering van suiker bestudeerd om meer te weten te komen over de interacties van die eiwitten. Dit is onderzocht in levende cellen met behulp van een microscoop.

Methodie om eiwit-eiwit interacties te onderzoeken

De methode die wij gebruiken hebben om eiwit-eiwit interacties mee te onderzoeken heet FRET (dat staat voor Förster Resonantie Energie Transfer (*overdracht*)). FRET kun je vergelijken met twee stemvorken (afbeelding 3). Wanneer je één van de stemvorken aanslaat begint deze te trillen; deze verspreidt een geluidsgolf. Een tweede stemvork kan deze geluidsgolf absorberen als die dichtbij is en daardoor begint deze ook te trillen met dezelfde frequentie. Dit natuurkundige verschijnsel heet resonantie.



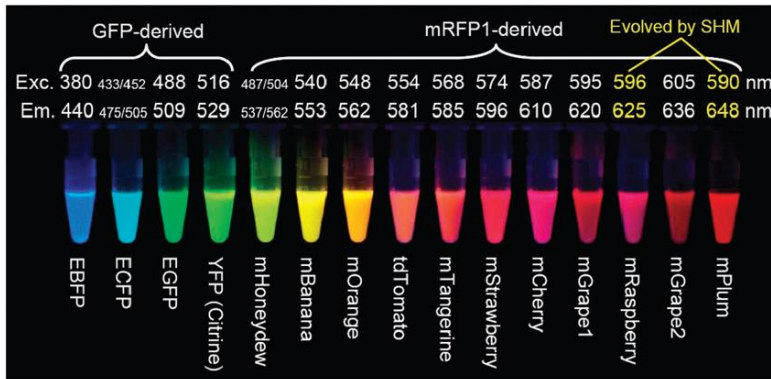
Afbeelding 3. Het principe van FRET kan worden uitgelegd aan de hand van stemvorken. Een aangeslagen stemvork kan door middel van resonantie (trilling met gelijke frequentie) zijn energie overdragen aan een tweede stemvork. Bron: <http://www.photobiology.info/Experiments/Biolum-Expt.html>

Groen Fluorescerend Protein (*eiwit*, GFP) is in 1962 ontdekt in kwallen en in 1994 voor het eerst gebruikt in bacteriën. Fluorescente eiwitten zijn lichtgevende eiwitten. Sindsdien hebben onderzoekers wereldwijd dit eiwit aangepast om het feller te maken en om het andere kleuren te geven (zie afbeelding 4 en hoofdstuk 2). In ons onderzoek hebben we groene en rode fluorescente eiwitten gebruikt voor FRET. Het groen fluorescerende eiwit absorbeert lichtblauw licht met een golflengte van 490 nm (490 miljardste meter), en straalt vervolgens groen licht uit met een golflengte van 525 nm. Een rood fluorescerend eiwit kan juist groen licht absorberen en daarna rood licht (585 nm) uitstralen. Maar het rood fluorescerende eiwit kan ook worden ‘aangeslagen’ door de trilling van het groen fluorescerende eiwit: als dat gebeurt is er sprake van FRET.

In hoofdstuk 3 is getest welke combinaties van fluorescerende eiwitten het meest efficiënt hun energie kunnen overdragen. Het blijkt dat GFP (groen) en tagRFP (rood) het beste werken.

Voor mijn onderzoek hebben we deze groene en rode eiwitten vastgemaakt aan eiwitten die we willen onderzoeken in *B. subtilis*. Als we het groen fluorescerende eiwit aanslaan en we zien daarna rood licht, dan is dat

het bewijs dat deze eiwitten een interactie met elkaar hebben. We zijn vooral geïnteresseerd in de dynamiek van deze interactie: wanneer vindt die interactie plaats en gebeurt het in alle cellen op dezelfde manier?



Afbeelding 4. Een greep uit de verschillende fluorescerende eiwitten die nu beschikbaar zijn. Bron: lezing van Nobelprijswinnaar Roger Tsien, 2008. www.nobelprize.org

Eiwit-eiwit interacties in levende bacterie cellen

De vertering van suikers en koolhydraten heet koolstofmetabolisme en is een belangrijke bron van energie en bouwstoffen voor bacteriën (en mensen).

Er zijn veel verschillende koolhydraten (suikers) beschikbaar en bacteriën hebben voor elke suiker unieke genen. Het is belangrijk dat alleen de genen die op dat moment nodig zijn ook 'aan' staan, want het aanzetten van andere genen is energieverspilling. CcpA en HPr zorgen voor deze regulatie ('aan- of uitzetten') van genen voor koolstofmetabolisme. Het fluorescente eiwitpaar dat als beste uit de test kwam in hoofdstuk 3 is in hoofdstuk 4 vastgemaakt aan de regulatie eiwitten CcpA en HPr.

Bacteriën groeien het snelst wanneer ze maar één koolstofsoort tegelijkertijd gebruiken. Snelle groei is goed voor hun voortbestaan. Het omzetten van DNA naar RNA naar eiwit kost energie en cellen moeten zuinig zijn op hun energie, o.a. door alleen de noodzakelijke eiwitten te maken. De favoriete koolstofbronnen van *B. subtilis* zijn glucose en fructose. Wanneer de favoriete koolstoffen niet aanwezig zijn is CcpA vrijwel niet actief. Maar wanneer een van deze aanwezig is zetten CcpA en HPr de genen voor de verwerking hiervan aan en genen voor de verwerking van andere koolhydraten worden onderdrukt. De eiwitten CcpA en HPr zorgen hiervoor door aan DNA te binden. Alle genen hebben een promotor (een startplaats voor de vertaling van DNA naar RNA naar eiwit). Wanneer CcpA vóór deze startplaats op het

DNA bindt zet het een gen 'aan' en als CcpA ná deze startplaats op het DNA bindt zorgt het voor een blokkade, een wegversperring, waardoor het gen 'uit' blijft.

Het was al bekend dat CcpA en HPr een interactie aangaan. In hoofdstuk 4 hebben we onderzocht wanneer ze dat precies doen en of alle cellen in een bacterie cultuur hetzelfde gedrag vertonen. De fusie van de *ccpA* en *HPr* genen met de genen voor de fluorescente eiwitten (op DNA-niveau) zorgde ervoor dat de eiwitten fluorescent gelabeld waren. De labeling van CcpA met een groen eiwit en HPr met een rood eiwit ging goed, maar het is niet gelukt om de energie overdracht van het groen- naar het rood fluorescerende eiwit te meten. Een reden hiervoor kan zijn dat maar een klein deel van de CcpA en HPr eiwitten een complex met elkaar vormen; het interactie signaal gaat dan verloren in de achtergrondruis. Of de groen- en rood fluorescerende eiwitten waren te ver weg van elkaar. Dit zou getest kunnen worden door de eiwitten op veel verschillende manieren aan CcpA en HPr vast te maken, maar dat is erg tijdrovend werk. Mijn advies voor de toekomst is: gebruik een directere methode om interacties te meten, zoals het meten van de fluorescente levensduur. De fluorescente levensduur is de tijd dat het groen fluorescerende eiwit groen licht kan uitstralen. De aanwezigheid van een rood fluorescerend eiwit verkort deze levensduur. Deze levensduur hebben we ook gemeten in hoofdstuk 3 en 4, maar deze methode bleek nog niet gevoelig genoeg voor gebruik op bacteriële cellen. Toepassing op eukaryote cellen is in het werk van anderen wel gelukt. Dit komt mede omdat eukaryote cellen veel groter zijn en dus veel meer kopieën van een eiwit hebben waardoor het lichtsignaal veel sterker wordt. Men kan ook andere methoden zoeken om eiwit-eiwit interacties te bestuderen.

Functie van individuele aminozuren van CcpA

De bouwstenen van eiwitten heten aminozuren. Uit eerder werk met CcpA is bekend welke aminozuren betrokken zijn bij DNA binding, bij vorm veranderingen van CcpA (het eiwit is flexibel) ten behoeve van de functie en bij de binding van HPr. In hoofdstuk 5 hebben we onderzocht wat het effect op gen regulatie is als CcpA in zijn geheel is verwijderd en wanneer drie van de aminozuren zijn veranderd (gemuteerd). De verandering van gen regulatie is over het hele *B. subtilis* genoom onderzocht. Daarvoor is DNA transcriptoom analyse gebruikt. Met deze techniek meet je de hoeveelheid RNA die per gen aanwezig is. RNA is het intermediair in de omzetting van DNA naar eiwit en de hoeveelheid RNA varieert per gen. We willen de veranderingen in gen regulatie weten en daarvoor is RNA uit de *B. subtilis* stam met het gemuteerde CcpA vergeleken met een controle, namelijk RNA uit *B. subtilis* met de

originele, natuurlijke CcpA variant. Wanneer de hoeveelheid RNA hetzelfde is als in de controle dan is er niets veranderd, maar als de hoeveelheid RNA in de mutant meer of minder is dan in de controle dan wordt het interessant, want dat laat zien dat de gen regulatie door de CcpA mutant veranderd is. Het blijkt dat CcpA-M17R (CcpA waarin aminozuur 17 is veranderd) een deel van zijn regulatie functie verloren heeft, want de onderdrukking van alle koolstofmetabolisme genen die niet bij glucose horen is zwakker. CcpA-T62H is juist een sterkere regulator geworden. CcpA-R304W is een mutant die de regulatie van genen ook kan doen zonder de hulp van HPr. Verder laten we in detail zien hoe de regulatie van genen veranderd is. Deze kennis kan worden ingezet bij de productie van interessante eiwitten (voor bijvoorbeeld wasmiddelen).

De reactie van *Bacillus subtilis* op zoutstress

Zoals gezegd komt *B. subtilis* vooral veel voor in de grond. Daar heeft de bacterie te maken met regen en droogte waardoor de osmotische druk (zoutstress) nogal varieert. Wanneer de grond droog is heeft *B. subtilis* te maken met een hoge osmotische druk en wanneer de grond door regen nat is heeft *B. subtilis* te maken met een lage osmotische druk. Osmose zorgt ervoor dat water naar die kant van het celmembraan stroomt waar de zoutconcentratie het hoogst is. In het geval van hoge osmotische druk in de omgeving van de bacterie stroomt het water de cel uit. Dit heeft gevolgen voor alle processen in de cel (zoals functioneren van eiwitten of celdeling). In hoofdstuk 6 hebben we op het niveau van individuele cellen bestudeerd hoe *B. subtilis* reageert op zoutstress. Het blijkt dat niet alle cellen bij een bepaalde hoeveelheid zout op dezelfde manier reageren, terwijl ze wel genetisch identiek zijn! Sommige cellen weten zich aan te passen en kunnen verder groeien en sommige cellen kunnen zich niet aanpassen en kunnen dus niet verder groeien. De cellen die zich aanpasten maakten zelf een zogenaamde osmobeschermer aan: het aminozuur proline. Proline kan door de cel in hoge concentratie worden opgehoopt en verhoogd daarmee de osmotische druk in de cel waardoor het water ook weer terug de cel in stroomt.

Dit verschijnsel van heterogeniteit (verschillend gedrag in een genetisch gelijke celcultuur) is interessant: lang werd gedacht dat alle cellen precies hetzelfde doen, maar dat is dus niet altijd zo. Het begrijpen van deze variatie kan belangrijk zijn bij de industriële productie van eiwitten want als niet alle cellen hetzelfde doen dan gaat dat ten koste van de opbrengst. Ook bij de bestrijding van infecties kan deze kennis bruikbaar zijn.

Dankwoord

The research done in this thesis was of a fundamental nature. That is very nice because of the large degree of freedom to decide the research direction and the opportunity to explore a subject in great detail. On the other hand, it is a bit more difficult to define clear goals.

I had to start 'the MolGen train' on protein-protein interactions studies, where it was already more or less decided to use FRET to study these interactions in live cells. My project was an exciting journey full of exciting moments, but also with many frustrations and unfortunately the train never reached its full speed. However, the train has reached some important stations: publications of my work in scientific journals, improving many skills (presenting, writing, setting up and performing research) and most of all: this PhD-thesis! I want to take the opportunity to thank the people who helped me along this journey.

Oscar. Allereerst bedankt dat je me hebt aangenomen op dit project. Het internationale karakter van het project is interessant en nuttig vanwege alle contacten. Bedankt voor het vertrouwen dat je altijd hebt gehad (Ja dat is een cliché, maar het is belangrijk op de momenten dat het project niet zo goed loopt). Bedankt ook voor de manier van denken over risicovolle projecten. Verder ben je altijd in voor een grap. Helaas is de beste grap niet uitgekomen, de nisine N20D mutant die je hebt gepresenteerd op een Europees congres tijdens het EK voetbal in 2012. Het werd 12, in nisine de K van ... kansloos? Verder heb je er altijd veel lol in gehad om te vragen wie de snelste wielrenner is: Martijn, Katrin, Robin of ik.

Oscar, Jan en Jan-Willem jullie hebben samen een fantastische groep om in te werken.

Jeroen Siebring – bedankt voor alle hulp bij de microscoop, het advies en de discussies over van alles en nog wat: van dit proefschrift tot en met voetbal en van de microscoop tot en met muziek. En de bijdrage aan hoofdstuk 3! En bedankt dat je mijn paranimf wilt zijn.

Ákos Kovács you were a daily base of knowledge in the first year. I learned a lot from your advice and knowledge, thanks a lot! After two years you left our group to start your own group in Jena. Good luck with your scientific career. I am sure that you can and will run a nice and excellent research group. Bedankt en succes!

Dankwoord

Jan-Willem Veening voor alle tips, trucs en weetjes omtrent bacteriën, fluorescente eiwitten en microscopen. Veel succes als professor, jij gaat het ver schoppen! Jouw zelfvertrouwen is bewonderenswaardig!

Katrin: je promotie was eerder begonnen, maar de dingen waar je tegenaan bent gelopen, heb ik altijd goed onthouden voor als ik ze zelf had. Bedankt ook voor de samenwerking met het GFP paper. Bedankt voor alle fietstochten! Tijdens de gitaarlessen hebben we misschien nog iets geleerd van elkaar, maar in elk geval hebben we er allebei een mooie hobby aan, veel plezier ermee! Vielen dank.

Martijn voor alle discussies en het wielrennen. In het begin lachte ik je uit als je weer een grote tocht wilde maken van een hele dag, maar nu zie ik er zelf ook de lol van in om lange tochten te maken. De fietselfstedentocht en de Amstel Gold Race hebben we mooi gedaan. Wie weet wat de volgende tocht wordt...LBL of La Marmotte?

Ard Jan bedankt voor alle gezelligheid en dat je mijn paranimf wilt zijn! Succes met je onderzoek!

Sjoerd, Jelle, Lieke, Marielle, Auke bedankt voor alle gezelligheid binnen en buiten het lab en de tips voor experimenten.

Maarten Mols, bedankt voor de discussies en het sparren over experimentele opzet en resultaat analyse en alle mooie gesprekken op het lab.

Luiza, thanks a lot for continuing the work on chapter 6! Good luck with your projects! Elrike, thanks for the discussions and proofreading chapter 4! Maïke, thanks for the discussions and proofreading chapter 5!

Jan voor de discussies op feestjes. Mirjam, je bent een geweldige persoon om mee te discussiëren en het eerste onderwerp waar we het over eens zijn moet nog gevonden worden, als we ons microbiologische werk buiten beschouwing laten. Ook moet je vaker taarten bakken! Robin bedankt voor alle fietstochten en leuke praatjes! Robyn bedankt voor de pub quiz waar we met een MolGen team altijd mooie avonden hebben gehad. Wout, bedankt voor de samenwerking in het GFP paper! Manolo, always in for a joke. Good to see that you like it in The Netherlands and that you bring some of the Spanish culture to our group. Enjoy your stay in Groningen! Afzal, we had a nice time in the party committee of the group! Good luck with everything! Ana, thanks for the collaboration that resulted in the GFP paper. You are always in for a joke

and also in your case it is nice to see that you like it so much in Groningen. Good luck with in your future career. Anne-Stephanie, thanks for all the comparisons between France and The Netherlands. Dongdong, it is nice to learn more about China. I will never forget the cola-chicken that you made on international dinners.

Siger voor alles om het lab draaiende te houden. En voor het samen opruimen van de -80 vriezers, kost wat tijd maar dan heb je ook wat! Ik hoop dat het nu lang netjes blijft. Anne voor alles om het lab draaiende te houden en de bio-informatica tools die ik heb gebruikt. Anne H. voor alles om het lab draaiende te houden en de leuke praatjes over van alles. Zonder jullie (Siger, Anne en Anne) zou MolGen niet zo efficiënt zijn geweest!

Peter, Mozes, Jannet, Mirelle, Klazien voor alle ondersteuning om het lab soepel te laten draaien. Mirelle sterkte en beterschap!

Tomas, Harma, Jimmy, Tonia, Irfan, Andrius, Renske, Morten, Mikkell, Li, Yi, Rieza, Barbara, Liang, Haojie, Andrius, Yoshi, Clement, and Yi for the nice atmosphere in the group, in the lab and during drinks and lab outings.

Eliene Timmer. Bedankt voor je inzet en enthousiasme bij hoofdstuk 6, ik vond het leuk om je te begeleiden tijdens je onderzoeksstage.

Patricia Razquin Navas. Thanks for your enthusiasm and help on chapter 6. Also for comparing the Spanish and Dutch culture. It was nice to supervise you during your research project. Good luck with your own PhD-project!

Anna Lauxen. Bedankt voor je inzet en enthousiasme bij hoofdstuk 4! Ik vond het leuk om je te begeleiden.

Verder wil ik Ben bedanken voor de gitaarlessen en Hanneke voor de zanglessen. Dit is een mooie hobby die heel ontspannend werkt!

Natuurlijk wil ik ook alle vrienden bedanken voor alle vakanties, feesten, discussies over van alles en nog wat en de bieren die we zelf gebrouwen hebben!!

Dankwoord

Pa en Ma, bedankt voor alles! Jullie hebben altijd vertrouwen in mij gehad. Het belangrijkste moment was in het eerste jaar van mijn scheikunde studie toen ik twijfelde over mijn studiekeuze. Dankzij jullie ben ik doorgedaan en al snel wist ik zeker dat scheikunde wel mijn studie is!

Martijn en Stefan bedankt voor alle gezelligheid en grappen over mijn studentenleven!

Anne, Marijke, Rodger ook bedankt voor alle gezelligheid.

Petra, mijn lief;) We hebben tegelijkertijd promotieonderzoek gedaan en we verdedigen ons proefschrift allebei op dezelfde dag: hoe mooi is dat! Voor alle dingen die we tegen gekomen zijn, waren we mooi elkaars klankbord. Ik vind het superfijn om bij jou te zijn: laten we samen nog heel veel meemaken, zoals bijvoorbeeld mooie vakanties, stedentrips, feesten en concerten.

Dikke zoen;)

Ruud

Groningen, december 2015.